CHARGE TRANSPORT IN MOLECULAR JUNCTIONS WITH NOVEL TWO-DIMENSIONAL CONTACTS

Ph.D. Dissertation in Chemistry

A DISSERTATION SUBMITTED TO THE DEPARTMENT OF CHEMISTRY AND THE COMMITTEE ON GRADUATE STUDIES OF UNIVERSITY OF LIVERPOOL IN PARTIAL FULFILLMENT OF THE REQUIREMENTS FOR THE DEGREE OF DOCTOR OF PHILOSOPHY

Shuhui Tao

01/DEC/2020

CONTENTS

Abstract

The final goal of molecular electronics is completing electronic devices by using individual molecules as the basic building blocks. To achieve such a goal, a good understanding of charge transport through individual molecule bridged into electrodes is essential. Despite continuing experimental success in building single molecular wire even single molecular devices, the widespread implementation has yet to occur, more basic research is required.

The research presented in this thesis investigates three major questions. The first is a study into the effect of electrode/molecule contact and the conjugation degree of the bridged molecule in the conductance of molecular junction. Here, we have systematically determined the electrical properties of amine and thiol terminated poly(p-phenylene) molecular wires bound either between two gold electrode contacts (Au/Au) or between a gold contact and a graphene electrode (Au/graphene) using STM-*I*(s) method. We also compared the conductivity of 1,4-benezenedithiol and 1,4-benzene dimethanethiol with Au/Au and Au/graphene contact to explain the effect of molecular conjugation. The experimental results showed that the junction formed with Au/Au electrodes have higher conductance than those formed with Au/graphene electrodes. The measured conductance decays exponentially with an increase in the number of phenyl rings, giving a decay constant that is similar for amine and thiol terminated molecular junctions with Au/graphene system. This work reveals that poly(p-phenylene) chains are similarly coupled to either gold or graphene electrodes, independently of the anchoring group, and that the transport properties are essentially dominated by the intrinsic molecular properties.

After discussing the effect of a series of intrinsic factors, such as anchoring group, electrode materials, and molecular conjugation degree to the conductivity of (single) molecular junctions, the focus was moved to evaluate the stochastic nature of measuring the electronic properties of (single) molecular junctions, which requires to collect large data sets to obtain the full detail of a molecular system. Using the unsupervised data sorting algorithm, the multiple conductance behaviors of chain shape and phenyl based molecular junctions, which are Au/DBDT/Au, Au/TBDT/Au, Au/6MHI/Au and

Au/8MOI/Au, have been observed.

With more understanding the principle in construction of (single) molecular junction, the attempts were made to a higher goal of molecular electronics, namely using a single molecule to work as an active electronic component, such as molecular switch and molecular diode, to perform a series of controllable functions. In this study, an electrochemical gating was applied to modulate the current flow through the molecular junction. Here, the conductance behavior of 6V6 has been investigated as a function of potential in an ionic liquid medium with both of Au/Au and Au/graphene contact. A clear "off-on-off" conductance switching behavior was achieved through gating of the redox state when the electrochemical potential was swept. Au/6V6/graphene junctions showed a single-molecule conductance maximum centered close to the equilibrium redox potential.

This research has shown that graphene could be used as a promising electrode material to construct stable (single) molecular junction in both ambient and ionic liquid environments. In addition, this project has shown that when performing molecular electronics measurements among the electrode material, electrode/molecule contacts, conjugation degree of bridged molecules, and the data analysis method are important. At last, the successful electrochemical gating effect indicated the true three terminal molecular electronics can be realized based on our experimental equipment. Based on this, our group members will further explore the approach of electrostatic 'gating' from a third electrode to realize the practical three terminal electronic devices.

Acknowledgements

I firstly would like to take this opportunity to express my sincere thanks to supervisor Dr. Li Yang for her strong support, kind encouragement and warm consideration over the past four years. I met her in my last year of undergraduate study, for me, she is the enlightenment and the shining example.

I would also like to extend my appreciation to my supervisor, Prof. Richard Nichol. He gave me lot of valuable suggestions and encouragement in research over my PhD study. I also would like to thank my co-supervisor Prof. Cezhou Zhao for his kind help.

Much appreciation goes to our collaborators, Dr. Yannick J. Dappe and his group for their excellent theoretical work. In personal, I would like to express my heartfelt gratitude to Dr. Yannick J. Dappe, he replied hundreds of emails to help me understand the theoretical background of computer simulation.

I am also grateful indebted to Prof. Kim Lau, who always answered me electrochemistry and PhD learning strategy questions. He really instructed me a lot in the past years. I also would like to thank Dr. Eric Amigues for his strong help in organic synthesis and his inspired advices.

I also wish to thank all the staff at Chemistry Department especially Mrs. Jianfang Wu, Mrs Peipei Wang and Miss Tong ji for their strong technical support. I am also grateful to our research members, with special mentions going to Miss Yinqi Fan, Mr. Ruowei Yi and Mr. Chunhui He.

On a personal note, I would like to thank my friend Jingyi Yang for her fantastic photographic technique. I also would like to thank my friend Jie and Lu for their long-distance companionship.

Special thanks should go to Dr. Qian Zhang, thanks for the communication, understanding, persistence and company, and thanks for always being there for me.

Finally, I am indebted to my parents and my grandparent for their continuous supporting and unconditional love.

List of Abbreviations

6MHI	6-(methylthio) hexyl isothiocyanate
6V6	N,N'-Di-(6-(thioacetyl)hexyl)-4,4'-bipyridinium bis(hexafluorophosphate)
8MOI	8-(methylthio) octyl isothiocyanate
BDMT	1,4-benzene dimethanethiol
BDT	benzenedithiol
BMIM-OTf	1-Butyl-3-methylimidazolium triflate
CV	cyclic voltammetry
DBDT	biphenyl-4,4′-dithiol
DFT	density functional theory
FWHM	full width at half maximum
HOMO	Highest occupied molecular orbital
IL	ionic liquid
ITO	Indium tin oxide
KSAc	potassium thioacetate
LB	Langmuir-Blodgett
LUMO	Lowest unoccupied molecular orbital
MCBJ	controlled break junction
OMBE	organic molecular beam epitaxial growth
Ossac	Os bisterpyridine complex
SAM	self-assembly
SPM	scanning probe microscopy
STM	scanning tunneling microscopy
STM-BJ	STM break junction
STM-*I*(s)	STM-current distance
TDBT	p-terphenyl-4,4″-dithiol
THF	tetrahydrofuran
TTFdT	dithiolated tetrathiafulvalene derivatives

List of Figures

List of Tables

1 Chapter 1: Introduction

1.1. Molecular electronics

In recent years, there has been a dramatic growth of the electronic industry, however the development of conventional bulk silicon electronics components is reaching a bottleneck. The size of devices is hard to further decrease as Moore's Law, which has been proposed in 1965 and specifically predicted that the number of transistors on per affordable CPU would double every 18 to 24 months.[1]

The non-stopping efforts have been seen in various communities to tackle this challenge. Among them, the proposal of using single molecules even single atoms to work as a controllable electronic component opened up new horizons for electronic industry. The revolutionary idea of single molecular electronics can be traced back to 1950's. In1956, a German physicist Arthur von Hippel proposed the basic idea of a bottom-up approach which he called molecular engineering.[2] Then, Richard Feynman gave a legendary and famous lecture "There's plenty of room at the bottom" at the end of 1950's.[3] This idea is not only a vital basis of scientific spirit but also that of philosophy spirit. People realized that the "space" is not only obtained by increasing the size, but also could be obtained by decreasing the size. He discussed the possibility of manipulating matter from bottom to top and suggested constructing matters starting from molecules or atoms. Based on this idea, the size of electronic device can be further minimized.

In the sense of a potential technology, the field of building electronic devices through the "bottom-up" approach is known as molecular electronics and rises to prominence. Recently, molecular electronics has become a true field of science where many basic mechanisms and techniques have been discussed and proved. The first breakthrough of molecular electronics took place in 1974, Aviram and Ratner discussed the charge transfer in single molecule and proposed the creative idea that a single molecule could act as a molecular rectifier.[4] They firstly proposed a potential single organic molecular rectifier which was constructed by connecting the electron donor tetrathiofulvalene to the electron acceptor tetracyanoquinodimethane by a sigma

bonded (methylene) tunnelling bridge. Their publication is probably the first specific proposal to use an individual molecule as a functionable electronic component. Although this idea had not been materialized experimentally during a long time, it still occupies an important place in the history of the development of molecular electronics. Soon after, a series of experiments on the structure and conductance properties of molecular devices were carried out. In the 1980s, Kuhn et al. firstly experimentally demonstrated the possibility of molecular rectification.[5] They fabricated Langmuir-Blodgett film, and further sandwiched them into metals to measure the electronic properties of conducting molecular components. Relying on these further experimental technologies, such as Langmuir-Blodgett (LB)[5] membrane, self-assembly (SAM) technology,[6] organic molecular beam epitaxial growth (OMBE)[7] and scanning probe microscopy (SPM),[8,9] the development of molecular electronics has been greatly promoted.

1.2. Construction of molecular junctions

In molecular electronics, building a stable and repeatable single molecular junction is the first and the most important step. For a single molecular junction, the basic structure is left electrode/single molecule/right electrode. The linked molecule can be considered as a wire which is able to transfer electrons. A specific molecular junction can be formed successfully when there is a single molecule linked into two electrodes by the binding force of the electrodes and anchoring groups. At the beginning, only metal materials are used as the electrodes to form the metal/molecule/metal junction, as shown in the Figure 1.

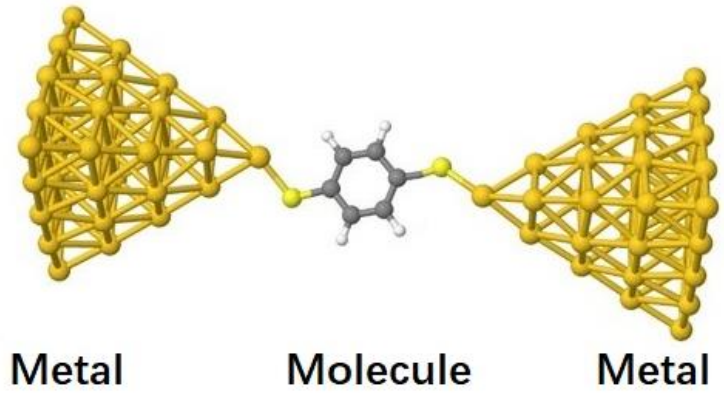

Figure 1: An example of metal/molecule/metal junction (Au/1,4-benzenedithiol/Au).

Au/1,4-benzenedithiol (BDT)/Au was the first measured system in 1997. Reed et al. reported the building of Au/BDT/Au single molecular junctions by a mechanically controlled break junction (MCBJ) in ambient condition.[10] The single molecule was linked into two gold electrodes by the effect of Au-S covalent bond. Based on this molecular junction, they further reported a direct observation of charge transport through the molecules. Till now, a stable single molecular junction can be fabricated with various techniques. This development and the subsequent introduction of several other techniques for studying small groups of molecules and even single molecules have provided significant motivation towards the recent development of molecular electronics. For example, effective approaches have been developed to construct and characterize single molecular junctions such as the scanning tunneling microscope,[11,12] mechanically controlled break junction technique,[10] conductive probe atomic force microscopy (C-AFM).[13]

1.2.1. Scanning tunneling microscope (STM) technique

The technological breakthrough of molecular electronics started in 1980's with the invention and application of scanning tunneling microscopy (STM) by Binnig and Rohrer.[8] The development of equipment provided a practical way to manipulate matter at the atomic scale as shown in Figure 2.[14] In addition, STM technique provides a realistic way to "see" and "touch" even to "move" single molecules for human beings.[15] Scientists have showed great interests in manipulating an individual molecules or even atom, in other words, single molecules or atoms can be moved to assigned stations, and specific structures can be built atom-by-atom.[16] Meyer et al. showed several excellent examples of atomic manipulation using STM technique,[17] such as the successful sliding of molecules (CO, C_2H_4 and Pt) along the Cu (211) surface.

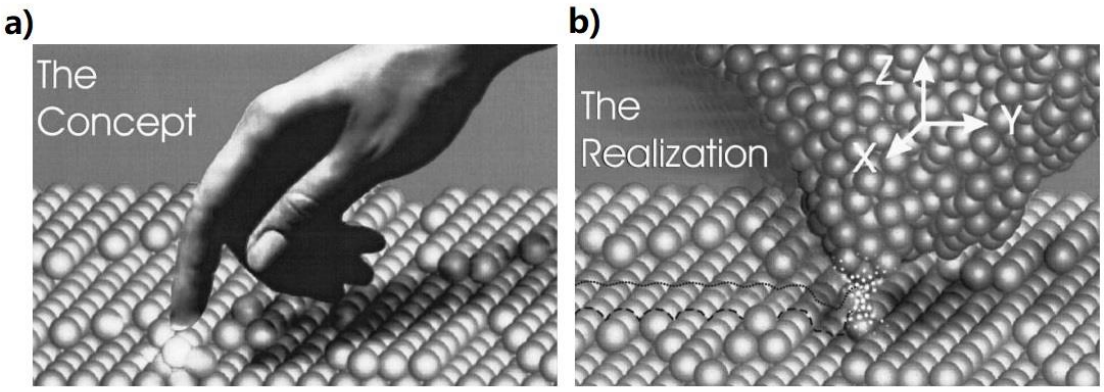

Figure 2: The principle of a STM probe: the gentle touch of a nanofinger. [Copyright, Review of Modern Physics, Ref. 14]

The ability of STM in which provide both geometric and electronic information lead to a new way of studying the electron transport properties in an individual molecule. This leap forward in micro technology lays a key foundation for the advanced molecular electronics. Based on the powerful feature of STM, in 2003, there are two significant breakthroughs happened in molecular electronics. In that year, STM break junction (STM-BJ) technique[11] and STM-*I*(s)[12] (*I* is current, s is distance) technique[12] emerged.

1.2.1.1.STM-break junction (STM-BJ) method

The STM-BJ method was firstly reported by Xu and Tao in 2003.[11] The procedure of forming a (single) molecular junction was shown in Figure 3. In this method, The STM tip is first placed at a preset position controlling by the measured tunneling current feedback. Then the STM tip approaches to the substrate to form a tip-substrate (in their experiment is gold-gold) contact as shown in Figure 3a. The STM tip then retracted from the substrate, with the retracting of the tip, the metal–metal contact breaks, and molecular junctions can be formed. During this stage, the conductance decreased in a stepwise fashion, with each step occurring preferentially at an integer multiple of conductance quantum G_0, where $G_0 = 2e^2/h$, as shown in Figure 3b.

Upon further pulling, by choosing proper experimental conditions one may end up with a single molecule junction before the contacts break completely, as shown in Figure 3c. During the retraction of the tip, a current–distance curve is recorded to represent the conductance behavior. In this stage, the measured statistic conductance showed peaks around $0.01G_0$, $0.02\ G_0$, and $0.03\ G_0$, which is two orders of magnitude lower than those that arose through the conductance quantization, as shown in figure 3d. Upon further pulling, the metal/molecule/metal junction would break when the distance between tip and substrate is longer than the maximum size of bridged molecules as shown in Figure 3e. In this stage, there is no such steps or peaks are observed within the same conductance range as shown in Figure 3f.

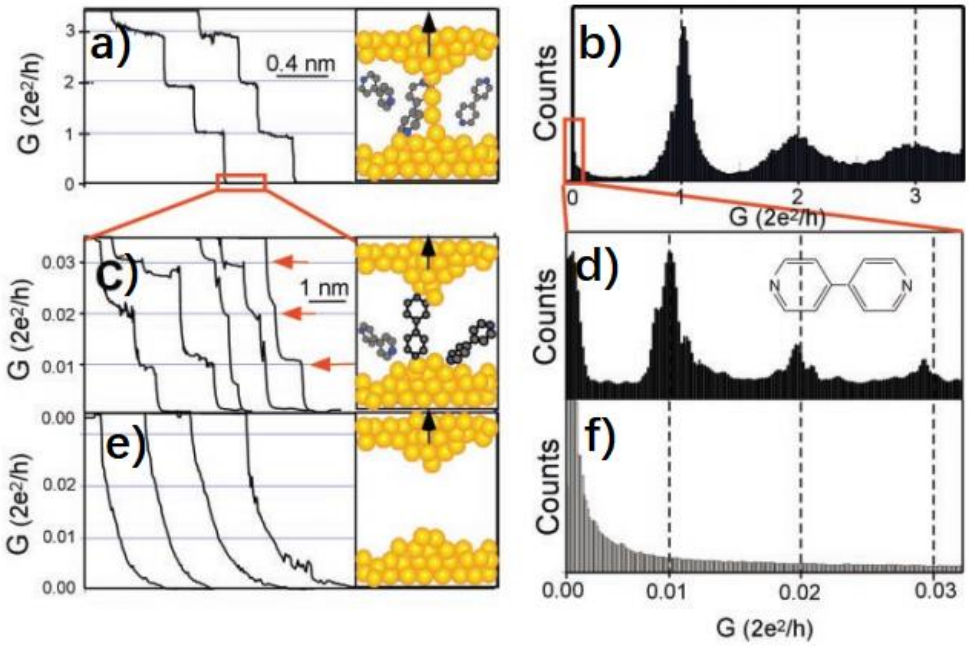

Figure 3: Illustration of STM-BJ technique where, (a) The STM tip approach to the gold substrate to form a gold-gold contact; (b) A corresponding conductance histogram constructed from 1000 conductance curves as shown in (a) ;(c) When the contact shown in (a) is completely broken, the molecule bridged into tip-substrate to form metal/molecule/metal junction . (d) A conductance histogram obtained from 1000 measurements as shown in (c); e) With the further pulling of STM tip, the metal/molecule/metal junction is completely broken, f) the corresponding conductance histogram shows no obvious peaks. [Copyright, American Association for the Advancement of Science, Ref. 11]

1.2.1.2. STM-*I*(s) method

The STM-*I*(s) method was developed by Haiss et al. in 2003,[12] where *I* represents the current, s is the relative tip-sample distance. The biggest difference compared with STM-BJ method is that there is no contact between tip and substrate in the STM- *I*(s) method.[18] The avoiding of tip-substrate contact can protect the substrate surface. It is important when the substrate is very thin or soft. However, comparing with STM-BJ method, STM-*I*(s) has the limitation of the relative low rate of successful building molecular junction.

By controlling the set-point current feedback, the STM tip is brought extremely close to the substrate, but avoiding the tip-substrate contact, as shown in Figure 4a. then

the STM tip is retracted to its original position at a pre-set speed until the molecular junction is completely cleaved, as shown in Figure 4a-4c, while the current versus distance *I*-s curves is recorded.

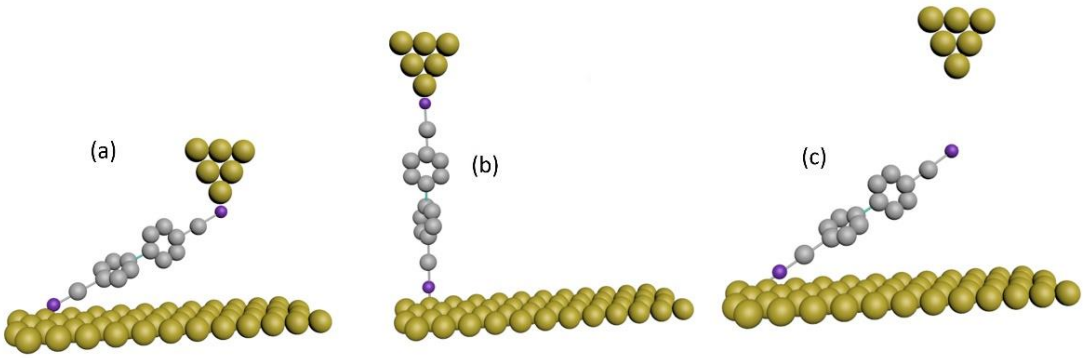

Figure 4: An illustration of the STM *I*-(s) method. Thiol terminated molecules were bridged into gold STM tip and gold substrate, where (a) The tip approaches to the substrate surface extremely, but without contact. (b) Retraction of the STM tip pulling the molecular by the binding force between tip and anchoring group, the bridged molecule wire upright in the junction. (c) The STM tip/molecule/substrate junction cleaved when STM tip continues leaving the substrate.

Plateau characteristic *I*-(s) curves represent the success of building (single) molecular junctions. Here, two *I*-s curves from Au/6-methylthiohexyl isothiocyanate/Au system (Figure 5) worked as example to explain the plateau characteristics. The red curve, which contained an obvious plateau, is identified the forming of electrode/molecule/electrode junction, while the black curve shows an exponential conductance decay for an empty junction. Through statistical analysis of many *I*-(s) curves, the electronic properties of the target molecular junction could be obtained. Both these two STM based methods reply on the collection of many hundreds of such junction stretching traces and statistical analysis of the data.

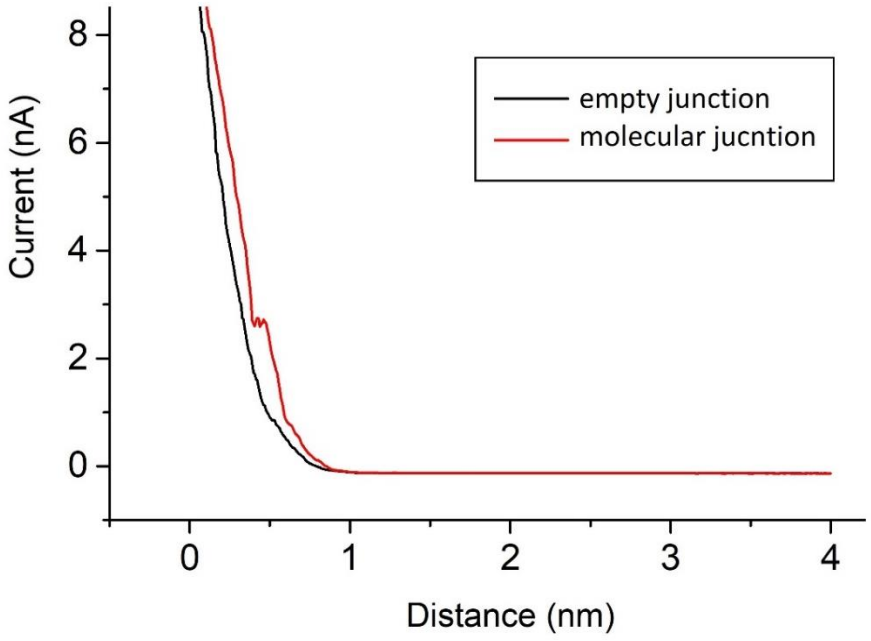

Figure 5: The typical *I*-(s) curves in measurements, the black curve shows an exponential conductance decay for an empty junction. While the red curve shows a characteristic plateau for a successful forming of (single) molecular junction.

1.2.1.3. Electrochemical controlled STM (EC-STM) technique

Both of STM-BJ and STM-*I*(s) methods are propitious to measurements of conductance of (single) molecular junctions with a wide range of environments, especially, they can be applied in electrolyte solution and provided the electrochemical control to the bridged molecules.[19] The EC-STM technique could be considered as adding an external electrochemical gating to the molecular junction that linked between STM tip and substrate.

As seen in the Figure 6, a liquid cell is used to provide the electrolyte solution environment to the molecular junction. There are four electrodes in the EC-STM set-up, including two working electrodes (STM tip and substrate), a counter electrode, and a reference electrode, as shown in the inset of Figure 6. This four-electrode bipotentiostat configuration allows independent electrochemical potential control and the STM tip and substrate bias voltage. In measurements, the STM tip should be coated with non-conductive material to minimize the Faradic current. In experiments, the electrochemical gating is considered as the "electrolyte gating" which relies on the formation of electrochemical double layers along the STM tip-substrate channel.

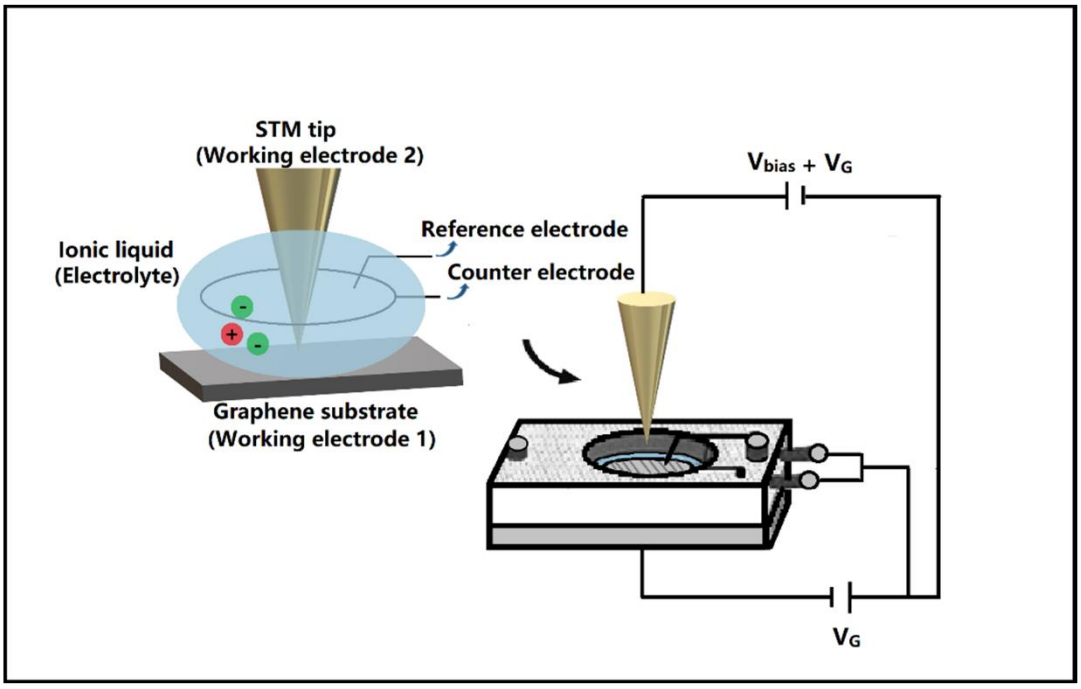

Figure 6: Schematic diagram of the electrochemical STM-based *I*-(s) technique, the inset shows four electrodes system with two working electrodes (STM tip and substrate), Pt counter electrode and Pt reference electrode. The counter and reference electrodes provide.

This technique can be applied in electrolytes and with full electrochemical control of both contacting electrodes which is an inspiring development in both of electrochemistry and molecular electronics. In this EC-STM configuration, current transport through the bridged molecule can be monitored as the electrode potential of the STM tip and substrate are changed.[12]

1.2.2. Mechanically controlled break junction (MCBJ) technique

The MCBJ method was developed by Muller and coworkers.[20] The working principle is depicted in Figure 7. The most basic principle of MCBJ method consists a stretching a thin metal wire by bending the substrate with an extremely precise mechanical control until the metal wire snaps providing two separate electrodes. The positions of the pushing rod and the two counter supports were controlled by the piezo drive or motor. The elastic substrate is deflected by the pushing rod in a three-point bending configuration. After breaking with appropriate size (d), it is possible for (single)molecules to bridge this gap, resulting in the production of conductance plateaus. In measurements, the collected voltage versus current signal can represent the conductance of the bridged molecule.

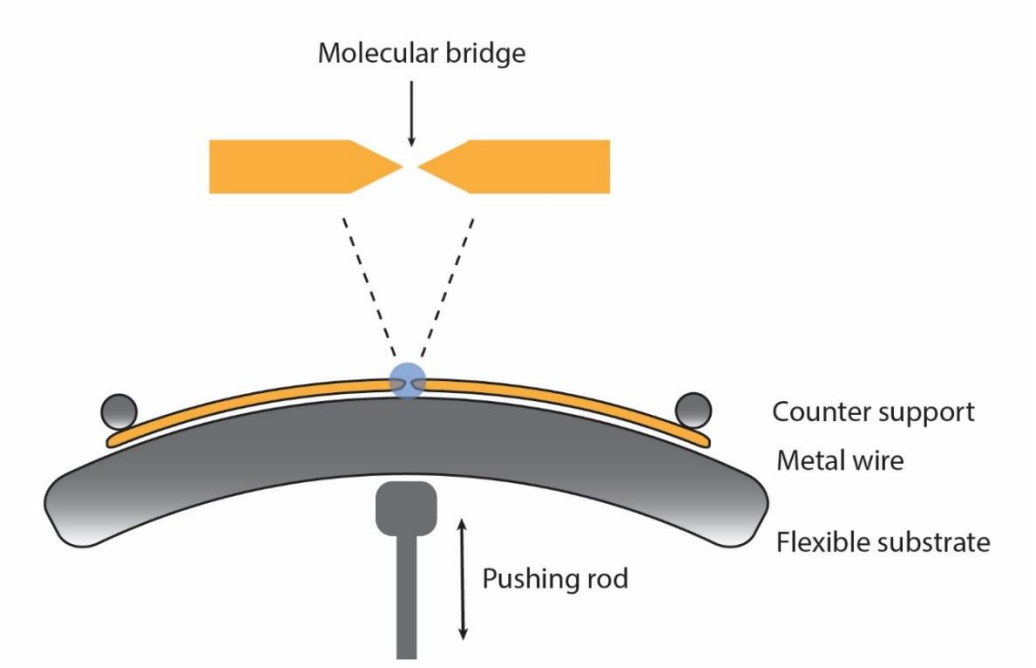

Figure 7: Working principle of the MCBJ method to build (single) molecular junction.

1.2.3. Conducting-atomic force microscope (C-AFM) technique

C-AFM is another important technique to build and identify the (single) molecular junction. This technique was introduced by Leatherman et al. in 1999.[22] In order to explain the reliability of C-AFM method and the effect of chemically bonded contact in C-AFM measurements, Cui et al. have measured a well studied octanethiol monolayer system.[23] The principle of C-AFM technique is shown in the inset of Figure 8, which is using a conducting AFM probe to locate and contact individual particles bonded to the self-assembled monolayer (SAM). Different from STM method, which is controlled by the tunneling current feedback, AFM is controlled by a force feedback loop. In the measurements, the relative current versus voltage (*I*-V) curves, as shown in Figure 8, were recorded to present the conductance behavior of the bridged molecules.

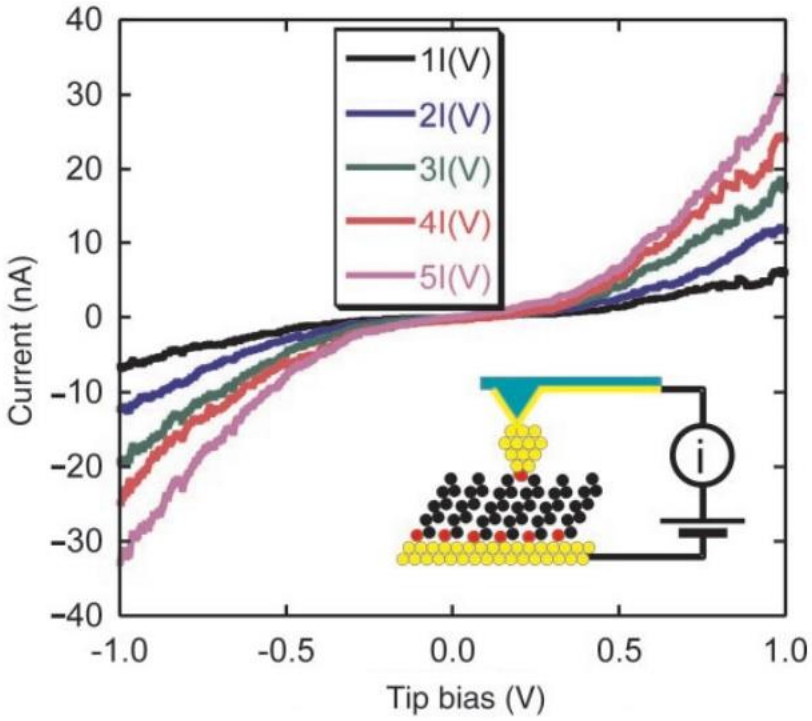

Figure 8: The characteristic *I*-V curves in C-AFM measurements. Inset: schematic representation of the C-AFM measurements. [Copyright, American Association for the Advancement of Science, Ref. 23]

1.3. The conductance of single molecular junction

A good understanding of how electron transport through a single molecule is important for building controllable molecular devices. For conventional metallic wires, their conductivity can be expected by the Ohm's law. Based on the Ohm's Law the resistance of a wire can be calculated as:

$$R = \frac{V}{I} \quad (1)$$

Where, *R* is resistance, *V* is voltage, while *I* is current. The relative conductance is defined as the potential for a wire to conduct electricity. For a conventional metallic wire, conductance is the measure of how easily electrical current can pass through a material, it is expected as:

$$C = \frac{I}{V} = \frac{1}{R} \quad (2)$$

Where C is conductance, which is the inverse (or reciprocal) of electrical resistance.

In atomic scale, Sharvin had described an idea for an experiment which produce inside a metal single crystal.[24] They considered that if the potential difference between the two half-spaces is eV, the conduction electrons passing through the orifice should change their velocity by the amount

$$\Delta v = \pm eV/P_F \quad (3)$$

Where P_F is the Fermi momentum. The further conductance (G) for a circular ballistic point-contact can be obtained by

$$G = \frac{2e^2}{h}\left(\frac{\pi R}{\lambda_F}\right)^2 \quad (4)$$

Where πR^2 is the contact area, $\frac{2e^2}{h}$ is a proportionality constant with quantum nature. It is worth to notice that, for ballistic point contacts the conductance is proportional to the contact area, like in Ohm's Law.

When size of the contact becomes small that the wave nature of an electron can not be neglected. Rolf Lamdauer[25] proposed that in order to get the conductance of a molecular junction, one should find the current-carrying eigenmodes, calculate their transmission values and sum up their contributions. Mathematically, the conductance

of the single molecule junction is calculated using the Landauer formula, shown below in Equation 5.

$$G = \frac{2e^2}{h}\sum_{n=1}^{N} T_n \quad (5)$$

This formula sum over all available modes of conduction, T_n are the transmission coefficients. When the transmission is perfect, $\sum_{n=1}^{N} T_n$=1, it contributes one quantum unit of conductance, where $G = G_0 = \frac{2e^2}{h}$=77400nS.

Experimentally, the conductance of a molecular junction could be measured by the current/voltage characters, where

$$G = \frac{I}{V} \quad (6)$$

Where G is the measured conductance, I is the current through the (single) molecular junction, while V is the applied bias in experiments.

1.4. Factor of conductance of molecular junction

The conductance of a (single) molecular junction is mainly composed of three parts: electrode, electrode-molecule contact, and the linked molecule. In other words, the conductance of molecular junction can be tuned with the selection of the anchoring groups and electrode materials.

1.4.1. Anchoring group

Anchoring group plays an essential role in building (single) molecular junctions. An ideal anchoring group is expected to possess following three characteristics: long stretching distance with sufficiently high junction formation probability; small conductance variation in molecular junction; and relatively high conductance.

Over the last decades a large library of anchoring groups has been amassed, including, but not limited to: thiol (-SH),[10,26-34] amine(-NH_2),[34-37] carboxylic acid, (-COOH)[38-41] isocyanide (-NC),[31,42,43] cyano (-CN),[44,45] trimethylsilylethynyl (-CCSiMe),[46] pyridine[47], isothiocyanate (-NCS)[48], methyl thiol (-SCH_3)[49]. methyl selenide(-$SeCH_3$)[49], nitro (-NO_2),[50-52] selenol (-SeH),[53] hydroxy(-OH),[37] even some of carbon-based group such as fullerene. [54-56]

The effect of different anchoring group in (single) molecular junctions has been discussed in significant amount of previous researches. Chen et al.[38] have systematically compared the conductance of aromatic molecular wires with -SH, NH_2, and -COOH anchoring groups. Their study showed that the conductance of a same molecular junction (Au/molecule/Au) system is decreased with the following sequence: -SH>-NH_2>-COOH. They explained their experimental observations to different molecule-electrode coupling and the alignment of the molecular energy levels relative to the Fermi energy level of the electrodes which was introduced by different anchoring groups.

Tan et al.[31] have designed a series of experiments to study the effect of contact coupling strength and contact chemistry through systematically varying the anchoring groups (-SH, -NC) of the aromatic molecules. They have modeled the transport properties of thiol and isocyanide terminal junctions to analyze the sign dependence of

the thermopower on the contact, as shown in Figure 9. The transmission function showed that transport in thiol terminal junctions is dominated by HOMO channel, while isocyanide junctions was dominated by the LUMO channel. Their study further indicated that the thermopower of thiol-terminated junctions is positive in sign, while the thermopower of isocyanide-terminated junction is negative in sign.

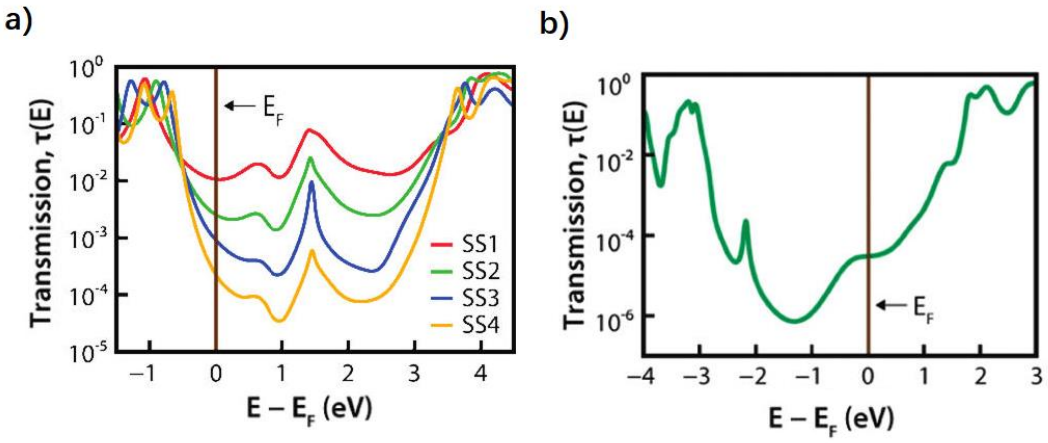

Figure 9: a) Computed transmission functions for the Au/aromatic dithiol/Au junction. b) Computed transmission functions for the Au/aromatic diisocyanide/Au junction. [Copyright, American Chemical Society. Ref. 31]

1.4.2. Binding geometry

For a given molecular structure, multiple conductance values are frequently observed and ascribed to distinct binding modes of the contact at each of the molecular terminal. Different binding geometries can produce different conductance behavior even to the same molecule/electrode contact. In molecular junction, among the tilt-angle of the molecule to the surface, the site of binding on flat terraces or step edges, and adjacent neighboring adatoms could affect the conductance behavior.[57,58] For example, the Au/SH contact always produces variable conductance. Especially, 1,4-benzene dithiol (BDT) with Au/Au contacts attracts widely interests as it has been a long-studied model junction,[10, 26, 27,32, 33,59-61] the reported conductance value ranges from 10^{-4} G_0 to around 10^{-1} G_0 (7.7nS to 7740nS), where $G_0 = 2e^2/h$, while most of these studies demonstrated a broad peak in 1D conductance histogram. Ulrich et al.[26]

have compared the conductance behavior of Au/BDT/Au system that measured under room temperature (293K) and low temperature (30K). Their experimental results showed that there was a broad distribution of conductance, while no one unambiguous conductance peak could be observed in 1D histogram in either at room temperature or low temperature as shown in Figure 10. They further attributed this conductance behavior of Au/BDT/Au system to the variation of junction's geometry. Kim et al.[32] have predicted that the large variation occurs because the BDT molecule may adopt several conformations. Sergueev et al.[33] have concluded that the conductance of the BDT junction depends strongly on both the separation between the contacts and the trapping configuration of the BDT molecule, and the stretching of the junction results from pulling the gold atom out of the electrode accompanied by a sudden rise in the conductance.

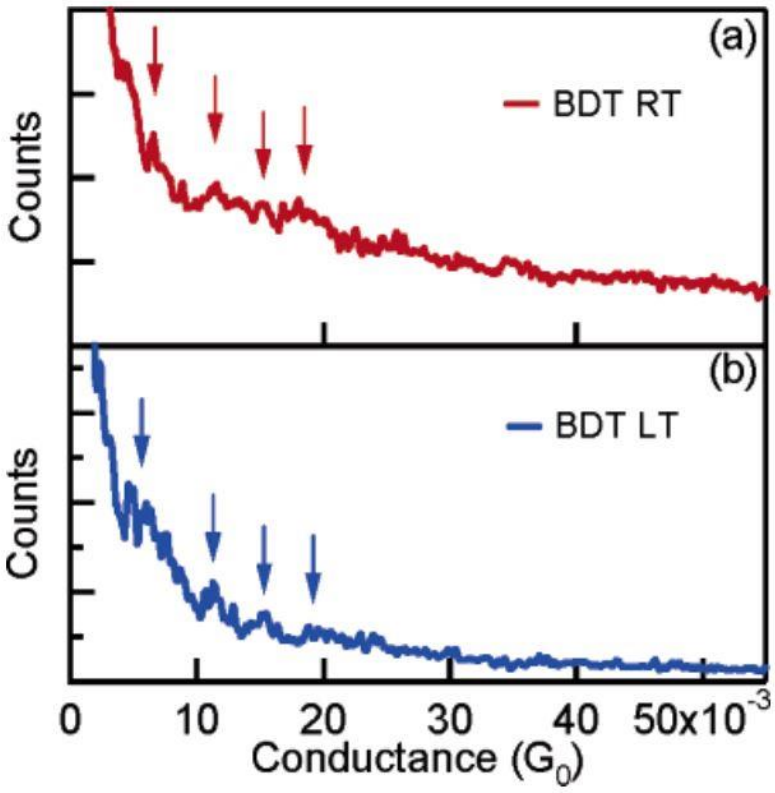

Figure 10: The 1D conductance histograms of Au/BDT/Au system that measured under room temperature (a) and low temperature (b). [Copyright, ACS Publications, Ref.26]

1.4.3. Electrode materials

1.4.3.1. Metal electrode in molecular junction

The electrode material can directly affect conductance of (single) molecular junctions through molecule-electrode coupling effect. So far, in molecular electronics, well studied molecular junction systems mainly use metal electrodes to build metal−molecule−metal (MMM) junctions. Gold is the most widely used electrode material for the assembly of molecular junctions because of its good chemical stability, good electrical conductivity, ease of fabrication, and absence of a surface oxide under most ambient measurement conditions. Moreover, gold can form strong metal−molecule covalent bonding such as in Au−S, Au−N(H)x, and Au−(OOC−) to contribute stable molecular jucntions.[10,38]

The possibility of using Ag,[62,63] Pt,[48,64] Pd,[48] Cu[62] and Ni[64,65] as electrode material to form (single) molecular junctions have been explored in many previous studies. Peng et al.[62] have studied the conductances of dicarboxylic acid terminated alkane (HOOC−(CH_2)n−COOH, where n is the number of methylene (n=1,2,3,4,5), binding to Cu and Ag electrodes respectively using STM-BJ method. They found that the different electrode could contributed the different decay constant as shown in Figure 11. They explained that this difference could be attribute to the different electronic coupling efficiencies between molecules and electrodes.

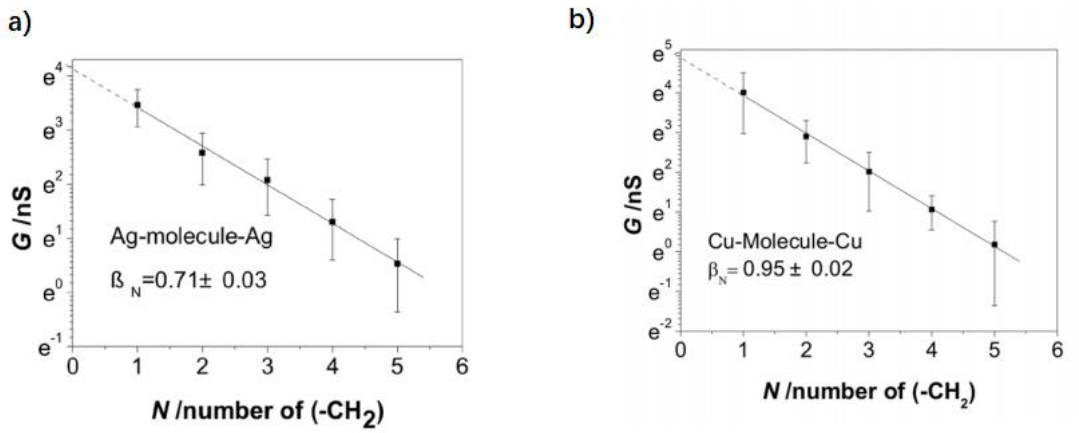

Figure 11: Natural logarithmic plots of single-molecule conductance vs number of (−CH_2) units for molecular junctions formed with a) Ag and b) Cu electrodes. [Copyright, ACS Publications, Ref.62]

1.4.3.2. Non-metal electrode material in molecular junction

Although gold is the most used and studied electrode material to build (single) molecular junction, the drawbacks of gold electrodes in practical devices are also apparent including their noncompatibility with complementary metal-oxide-semiconductor (CMOS) technologies as well as their surface mobility and the rising price. To tackle these issues, there is an increasing trend in the community to establish the use of nonmetallic electrodes. To date, the measurements of individual molecular junctions using nonmetallic electrodes, such as indium−tin oxide (ITO),[66,67] semiconductors such as gallium arsenide[68,69] and silicon[70-74] and carbon-based materials,[75−82] have been demonstrated.

These previous studies provided the possibility and the reliability of using of non-metal material as the electrode component. Among these non-metal materials, carbon-based materials are the most common but also the most fathomless materials in the world, which could form the hardest diamond to the soft graphite. The discoveries of fullerene,[83] carbon nanotube,[84] and graphene[85] have inspired a new wave of research at the time, especially the graphene. In 2004, two Russian scientists found that the carbon atoms form monoatomic layer material through sp^2 hybridization with a stable hexatomic ring unit. This kind of material that possessed perfect two-dimensional (2D) structure was named as graphene. Till now, zero-dimensional fullerene, one-

dimensional carbon nanotube, two-dimensional graphene, and the three-dimensional graphite have made the carbon materials become an integrated system. Graphene is the thinnest 2D material in the world with the thickness is only 0.35nm. As the most promising 2D material so far, graphene shows many advanced physical and chemical properties. For example, graphene has super high strength which could achieved 130 GPa.[86] It also has high carrier mobility of $15000 cm^2 \cdot V^{-1} \cdot s^{-1}$,[5] which is twice higher than indium antimonide and ten times higher than commercial silicon slice. Under a specified condition, such as ultra-low temperature, the carrier mobility of graphene even can up to $250000\ cm^2 \cdot V^{-1} \cdot s^{-1}$.[87] The thermal conductivity of graphene can attain $5000\ W \cdot m^{-1} \cdot K^{-1}$, which is three times higher than diamond.[88] In addition, graphene still has some special properties, such as room-temperature quantum hall effect,[89] and room-temperature ferromagnetism.[90]

Based on this novel graphene electrode material, Zhang et al.[76,77] have demonstrated the conductance properties of thiol, amine and carboxylic acid terminated alkane chain in the asymmetry Au/molecule/graphene junctions using STM-*I*(s) technique in air condition. The configuration of this kind of Au/molecule/graphene junction was shown in the inset of Figure 12. Their studies presented that graphene material could have a good performance in building molecular junction. Their research has given rise to some interesting findings that amine terminated group showed higher conductance than thiol terminated group in Au/graphene contact, which is opposed to their conductance properties in Au/Au contact. In addition, there is a big difference compared with Au/molecule/Au system, where the resulting attenuation factor of Au/molecule/graphene is much lower, as shown in Figure 12. This effect was considered by the asymmetric coupling of the molecule through strong chemisorption at the molecule-gold contact, and weak van der Waals contact at molecule-graphene contact.

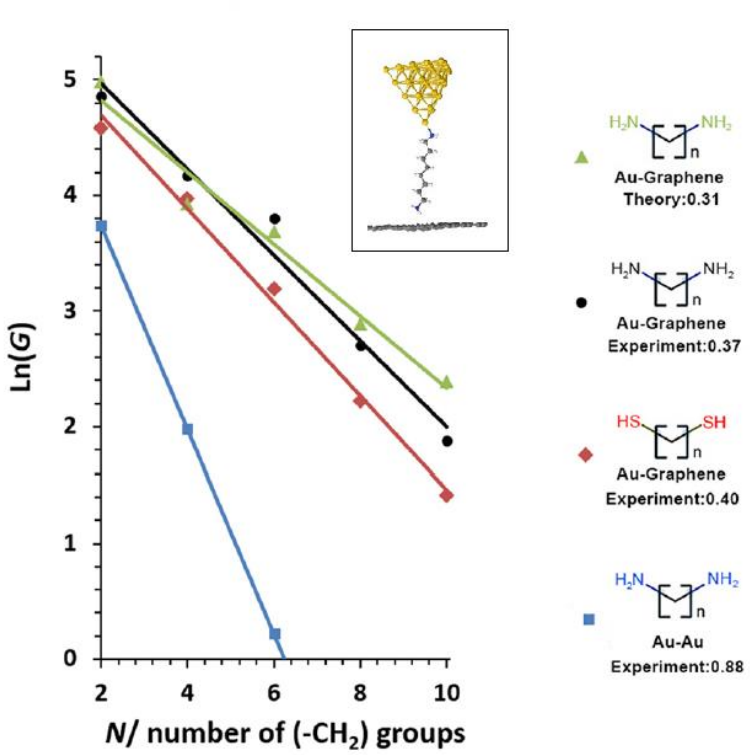

Figure 12: The measured and theoretical calculated conductance behavior of Au/thiol terminated alkane/graphene, Au/thiol terminated alkane/Au, Au/amine terminated alkane/graphene and Au/amine terminated alkane/Au junctions. The inset illustrated the construction of Au/molecule/graphene using STM-*I*(s) technique. [Copyright, ACS Publications, Ref.76]

1.5. Charge transport mechanisms

A main challenge in molecular electronics is the understanding of how does the electron transport through the single molecular junction. There is also a major research question in molecular electronics that how to identify the charge transport mechanism from the experimental measurements results. In general, the charge mechanism could be represented by *I*-V characteristics, and the temperature dependence and voltage dependence.

Five most possible of charge transfer mechanisms are listed in Table 1. They are, respectively, tunneling, Fowler-Nordheim tunneling, thermionic emission, Poole-Frankel emission and hopping mechanisms, which are identified by their temperature and the voltage dependence. Here we can find that only conductance by direct tunnelling and Fowler-Nordheim tunneling does not requires thermal activation.[91]

Table 1: The possible conduction mechanism in molecular junction, where *I* is the current, V is the bias voltage, φ is the barrier height, d is the barrier length, while T is the measurement temperature.

Mechanism	Conduction Behavior	Temperature dependence	Voltage dependence
Direct tunneling[92]	$I \propto Vexp(-\frac{2d}{h}\sqrt{2m\varphi})$	none	$I \propto V$
Fowler-Nordheim tunneling[92]	$I \propto Vexp(-\frac{4d\sqrt{2m}\varphi^{2/3}}{3qhV})$	none	$\ln(\frac{I}{V^2}) \propto \frac{1}{V}$
Thermionic emission[92,93]	$I \propto T^2 exp(-\frac{\varphi - q\sqrt{qV/4\pi\epsilon d}}{k_B T})$	$\ln(\frac{I}{T^2}) \propto \frac{1}{T}$	$\ln(I) \propto V^{1/2}$
Poole-Frankel Emission[94]	$I \propto T^2 exp(-\frac{q(\varphi - \sqrt{qV/\pi\epsilon d}}{k_B T})$	$\ln(I) \propto \frac{1}{T}$	$\ln(\frac{I}{V}) \propto V^{1/2}$
Hopping[92]	$I \propto Vexp\left(-\frac{\varphi}{k_B T}\right)$	$\ln(\frac{I}{V}) \propto \frac{1}{T}$	$I \propto V$

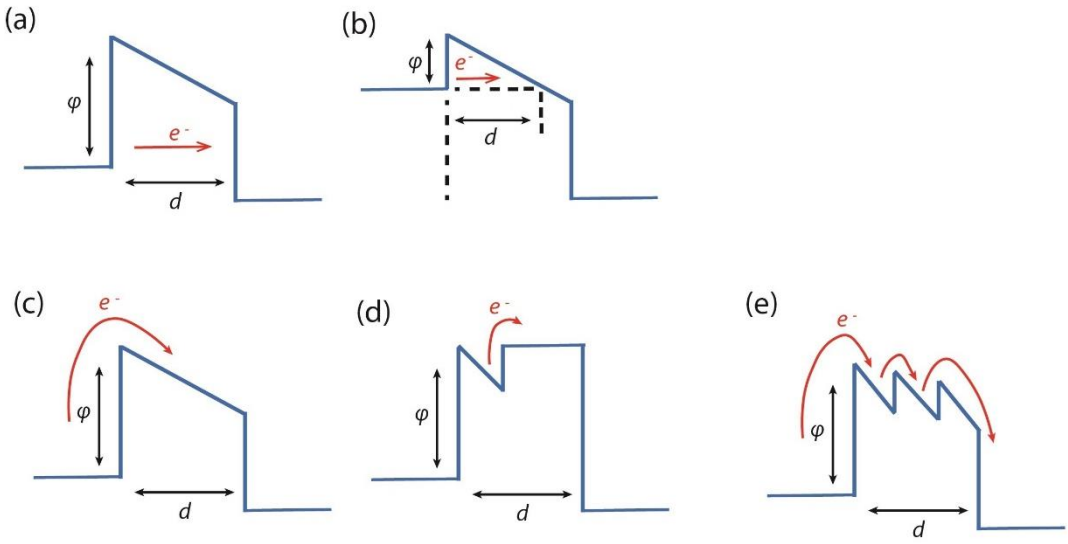

Figure 13: The illustration of these five different charge transport mechanisms: (a) Direct tunneling, (b) Fowler-Nordheim tunneling, (c) Thermionic emission, (d) Poole-Frankel Emission and (d) Hopping.

The more visualized charge transport mechanisms are shown in Figure 13, where φ is the barrier height while *d* is the barrier length. The explicit voltage and temperature dependence are coming from Simmons model,[95] which identified a general current

tunneling density of a molecular junction as an arbitrary barrier, as shown below in Equation.

$$J = J_0\{\varphi \exp(-A\sqrt{\varphi}) - (\varphi + eV)\exp(-A\sqrt{\varphi + eV})\} \quad (7)$$

where J is the zero-temperature net current density, with

$$J_0 = \frac{e}{2\pi h\alpha^2 d^2} \quad (8)$$

and A is identified as:

$$A = \frac{2\alpha d}{\hbar}\sqrt{2m} \quad (9)$$

Where α is the dimensionless correction factor, that can be further simplified in Equations depending on the applied bias voltage. The first two mechanisms, tunneling and Fowler-Nordheim tunneling are coherent tunneling through a potential barrier. When the charge transport was dominated by tunnelling, electrons are transmitted from one electrode to the other electrode often without any charge residing on the bridged, and without the need for thermal activation.[92,96] The first direct tunneling (Figure 13a) happens at low bias range, where the applied bias between two electrodes is much lower than the barrier height (φ). Correspondently, the Fowler-Nordheim tunneling (Figure 13b) occurs when the applied bias is higher than the average barrier height. Both of these two tunneling mechanism are independent with temperature, so the relative *I*-V curves are insensitive to the change of temperature. It is worth noticing that, in tunneling process, there is an important exponential dependence with distance (molecular length) and conductance.[32] This characteristic can be quantified by the attenuation factor (β):

$$G = G_0(-\beta L) \quad (10)$$

Where G is the conductance. *L* is the length of the bridged molecule tween two electrodes that could be also considered as the barrier width. Chen et al. have measured the conductance behavior of thiol, amine, and carboxylic acid terminated alkanes with gold/gold contact, they summarized that, for this Au/terminal alkane/Au system, among the characteristic *I*-V traces (Figure 14a), temperature independence (Figure 14b), and exponential decay of the conductance with the molecular length indicated tunneling is the dominated conduction mechanism (Figure 14c).

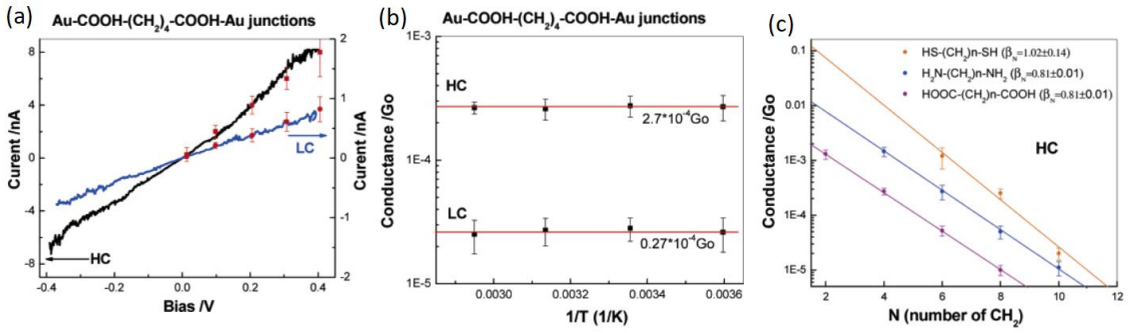

Figure 14: *I*-V characteristic traces of Au/COOH-$(CH_2)_4$)-COOH/Au junction, (b) Conductance vs temperature plots for Au/COOH-$(CH_2)_4$)-COOH/Au, (c) Logarithmic plots of conductance versus molecular length for Au/terminal alkane/Au systems. [Copyright, ACS Publications, Ref. 38]

The thermionic emission charge transport mechanism occurs when the electrons are excited over the potential barrier rather than tunneling through the potential barrier, as shown in Figure 13c. In this process, the charge obtained extra energy by thermal activation. This thermionic emission process is strong dependent with temperature. This kind of thermionic emission generally occurs when the barrier potential is relatively low. Chen et al.[93] have reported this thermionic emission mechanism by measuring the conductance behavior of metal/1,4-phenylenediisocyanide/metal junctions, as shown in Figure 15a. They discovered a distinct linear relationship between $\ln(\frac{I}{T^2})$ and $\frac{1}{T}$, as shown in Figure 15b, which is the characteristic of thermionic emission.

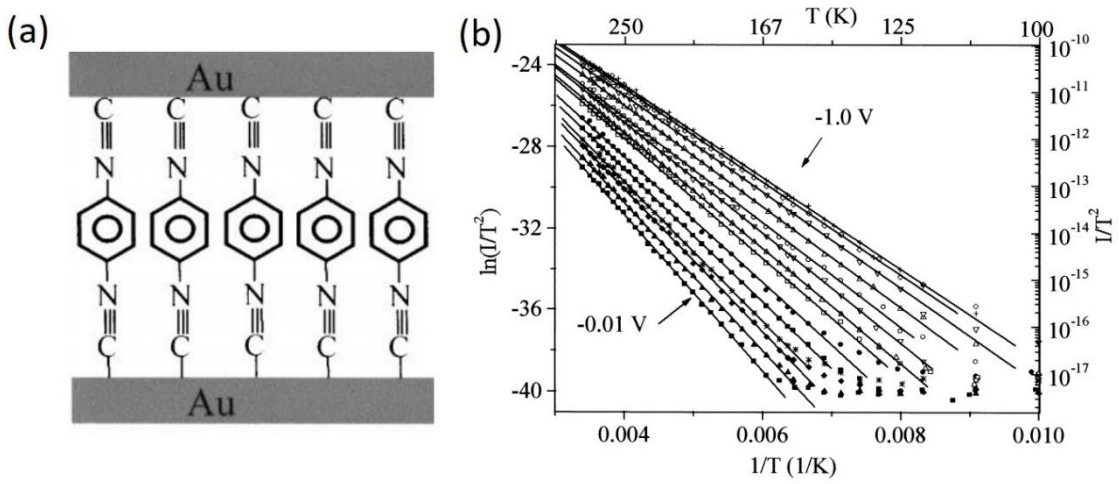

Figure 15: Illustrate of Au/1,4-phenylenediisocyanide/Au junction, (b) The slopes of $\ln\left(\frac{1}{T^2}\right) vs. \frac{1}{T}$, which measured in -0.01V bias to -1 V bias, showed a clear linear dependence. [Copyright, Elsevier, Ref. 93]

There is another thermally active transport mechanism called Poole-Frankel Emission, as shown in Figure 13d. This kind of charge transport conduction mechanism occurs in semi-conductor systems, which is reported by Sharma et al. in 1991.[94] They have measured and plotted the current density versus square root of the field across AI-Y_2O_3 -Si, which showed a linear relationship. Their study confirmed that Poole-Frankel emission was the dominant conduction mechanism in Y_2O_3 films at higher fields.

Hopping conduction is also an important charge transport mechanism. In hopping conduction, when electrons transmit from one side electrode to another electrode, they can localize at certain points within the bridged molecular wire, and hop through the points, as shown in Figure 13e. This kind of charge transport mechanism often seen for relative longer and complicated molecules in junction, such as redox active metal centre complex,[97,98] DNA,[98-100] and some of oligomers.[101-105] Because the electrons would resident on the bridged molecule, the path of the transporting is multiple. It is makes sense that there is a weak relation between conductance and molecular length.

For a redox active bridged molecule, the hopping mechanism has been further explained by a Kuznetsov-Ulstrup two step charge transmission model,[106] when measured by STM technique with an electrochemical control. It is worthy to notice that, in this model the interaction of the redox group with both metals is weak, corresponding to totally nonadiabatic electronic transitions. Under the totally adiabatic limit, the electron transfers from the redox centre of bridged molecule to the right electrode Fermi level before the redox molecular level has fully relaxed, the molecular level then returns to the energy of the oxidised species allowing the next electron to move onto the point which increased the current. The electric current through the contact following this two-step hopping mechanism can be described with Kuznetsov -Ulstrup model as Equation.[107]

$$j = e\frac{k_1 k_2 - k_{2'} k_{1'}}{k_1 + k_2 + k_{1'} + k_{2'}} \qquad (11)$$

Where k_1 is the rate constant for electron transport from left electrode to the redox centre of bridged molecule, while k_2 is the rate constant for the electron transport from redox centre to the right electrode. $k_{1'}$ and $k_{2'}$ is the relative reverse transition. e is the elementary charge. And on this basis, Zhang et al.[108] updated the Equation 11 through neglecting the weak dependence of the reorganization energy on the redox centre within the tunnel gap to describe the enhanced current (J_{enh}) following across the molecular junction as a result of charge transport following the two-step adiabatic model.

$$J_{enh} \approx J_0 \exp\left(-\frac{\lambda}{4kT}\right) \frac{\exp\left(e|V_{bias}|4kT\right.}{\cosh\left(\frac{e(0.5-\gamma)V_{bias}-e\xi\eta}{2kT}\right)} \qquad (12)$$

Where λ is the reorganization energy, k is the Boltzmann constant, T is the temperature, γ is the fraction of the bias drop at the redox site, and ξ is the electrochemical gating parameter.

1.6. Research aim

After viewing the development of molecular electronics, we realized that there are many factors can affect the conductivity of an individual molecular junction. A good understanding of theses complex conductance effects is important for building a controllable true molecular device. In order to realize the practical application of single molecular devices in the future, systematic exploring research are needed.

In general, the research in this project focus on the determining factors of conductivity of (single) molecular junctions, such as electrode material, anchoring group, the intrinsic properties of the bridged molecule, the electrode/molecule coupling, the data analysis method, and the environments.

In previous studies, gold was the most used electrode material to form (single) molecular junctions. However, there are many challenges of building molecular junctions with Au/Au contact, such as the non-compatibility with complementary metal-oxide-semiconductor (CMOS) technologies, the surface mobility and the high cost. The first focus of study was aimed at using carbon based 2D graphene as a potential material to replace one side of metal electrode to construct robust and repeatable (single) molecular junctions with STM-*I*(s) technique.

The conductance of series of alkane based molecular junctions has been system systematically studied in our previous researches.[76-78] The experimental results showed that conductivity of these saturated chain shape molecular wire is relatively low, especially for longer alkanes, such as the conductance of Au/1,12-dodecanedithiol/graphene measured as low as 2.4nS.[76] Therefore, in this study, we hope to find a molecular junctions system that has higher conductivity. Molecules with

conjugated structure were considered have better performance in electron transport. Therefore, the conductance behavior of a series of poly(p-phenylene) based molecules with different anchoring group has been systematically investigated.

Based on STM-*I*(s) technique, we obtain the conductance value of each molecular junction relied on a data selection process to remove the noisy *I*(s) traces. An accurate evaluating of the stochastic nature of electronic properties of (single) molecular junctions required large conductance traces data sets to obtain the full detail of a molecular system. In order to avoiding the bias that happened in manual selection, an unsupervised MATLAB algorithm was used in this research to analysis the most possible conductance value.

In molecular electronics, the final challenge is realizing a true three-terminal single molecular devices. In this research, we aim to achieve the controllable molecular three terminal devices through an electrochemical gating. Here, a redox active 6V6 molecule was synthesised, and ionic liquid was used as the electrolyte to provide a stable measurements environment. Both the electrochemical properties and conductivity of the 6V6 wire are attractive. We aim at investigating the conductance behaviors of Au/6V6/Au and Au/6V6/graphene were measured as a function of electrochemical potentials to reveal the electrochemical gating effect in (single) molecular junction.

2 Chapter 2: Conductance of conjugated molecular wire

2.1. Preface

This research was carried out in collaboration with the theoretical calculation by Dr. Yannic J Dappe (CEA, CNRS, France). I will present my experimental work on the conductance measurements of series of molecular junctions. This research was published with the title is, "Graphene-Contacted Single Molecular Junctions with Conjugated Molecular Wires", and reproduced with permission from ACS Applied Nano Material, 2019 (DOI: 0.1021/acsanm.8b01379).

In this study, we have determined the electrical properties of amine and thiol terminated poly(p-phenylene) molecular wires bound either between two gold electrode contacts (Au/Au) or between a gold contact and a graphene electrode (Au/graphene). These different junctions were studied using a STM-*I*(s) technique. We show that for these molecular targets, junctions formed with Au/Au electrodes have higher conductance than those formed with Au/graphene electrodes. The measured conductance decays exponentially with an increase in the number of phenyl rings, giving a decay constant that is similar for amine and thiol terminated molecular junctions with Au/graphene system. This work reveals that poly(p-phenylene) chains are similarly coupled to either gold or graphene electrodes, independently of the anchoring group, and that the transport properties are essentially dominated by the intrinsic molecular properties.

2.2. Introduction

In the previous studies of our group,[76-78] there is a systematically explored the deployment of graphene electrodes for the formation of hybrid Au/"alkane"/graphene junctions with various anchoring groups being employed, namely thiol, amine, and carboxylic acid. It was found that the decay constant of hybrid Au/"alkane"/graphene junctions is much lower than that of the symmetric Au/"alkane"/Au junctions. Consequently, we showed that using graphene as one of the electrodes may lead to more-conductive molecular junctions at longer lengths for saturated molecules with polymethylene backbones. Having developed the methodology for single molecule electrical measurements with graphene, we now move our focus from polymethylene ("alkane") to poly(pphenylene) (PPP)-based compounds, since molecular junctions with polymethylene backbones are fairly benign, as they act as rather resistive and passive molecular bridges. Such use of a more-conductive PPP bridge can be seen as a step toward developing more highly conducting molecular electronic junctions down to the single molecular level with graphene/ molecule junctions, which might inspire future functional hybrid molecular/solid-state technologies.

There is also a great interesting to research the role of a conjugated effect in a molecular junction. To describe this conjugation effect, Venkataraman et al.[109] have designed a series of experiments which measured the conductance of biphenyl molecules by STM-BJ method. They modified the substituent group to further control the angle between the two phenyl rings, as shown in Figure 16a. The conjugated effect of the molecule (named as 2, 4, 6, 8) decreased with the increasing of the twist angle (from 0° to 88°). They found that the relative conductance increased with the conjugated effect obviously (Figure 16b).

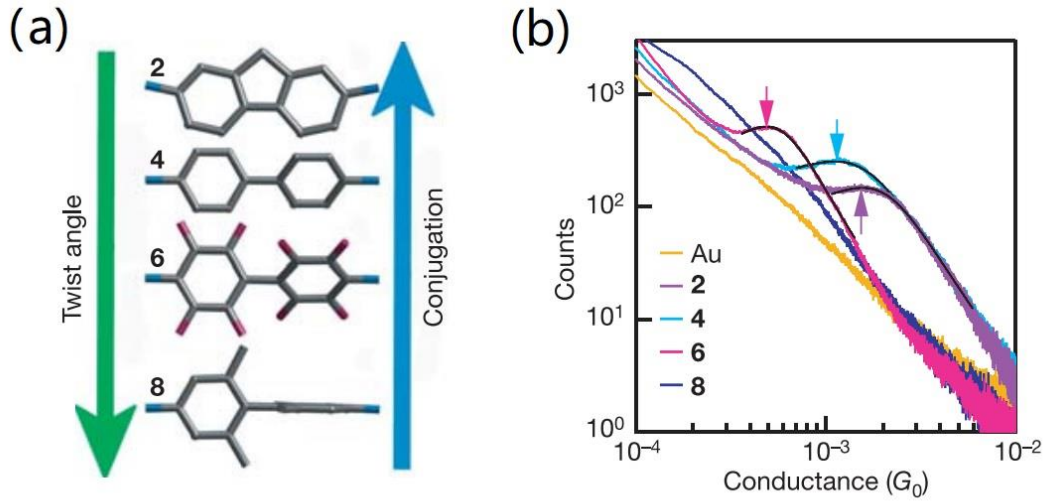

Figure 16: (a) Illustrating the target biphenyls, shown in order of increasing twist angle with decreasing conjugation. (b) Conductance value obtained from measurements. [Copyright, Springer Nature, Ref. 109]

Till now, there are many significant previous studies have shown that conjugated molecular wires with delocalized π electrons, such as oligophenyls[110], oligothiophenes,[111] tetrathiafulvalene (TTF)[112] are better candidates for long-distance charge transport studies because of the lower attenuation factor compared to saturated molecular bridges in metal/metal contacts.[113-115] Moreover, for MMM junctions, molecular conductance measurements using both saturated and conjugated compounds have clearly shown that the electrical properties of the individual molecular junctions are not only strongly determined by the chemical and electronic properties of the target molecules but also critically dependent on the terminal group, binding geometry, and the electrode materials.[10,62-85,] Therefore, research into how the graphene electrode affects the conductance and the attenuation factor of the conjugated molecular junction is of fundamental importance in the field of molecular electronics.

2.3. Research Aim

In this study, systematic measurements and comparison of the conductances of four different series of conjugated molecular junctions has been undertaken. This includes Au/(amine-terminated PPP)/Au, Au/(amine-terminated PPP)/graphene, Au/(thiol-terminated PPP)/Au, and Au/(thiol-terminated PPP)/graphene systems. Note that the graphene electrode has been chosen for its weaker interaction with the molecule, through van der Waals interactions between the thiol (−SH) terminal group and graphene, contrary to the strong chemisorption interaction through Au-thiolate (−S, the hydrogen atom being removed during the chemisorption process) bonding at the gold electrode contact. We show that the molecular junction conductance falls exponentially with the length of the molecular backbone for these four series of molecular junctions. More importantly, similar decay constant values have been obtained for Au/(thiol-terminated PPP)/ graphene and Au/(amine-terminated PPP)/graphene junctions. Density functional theory (DFT) calculations reveal that the symmetry characteristics of the molecular wave function are similar whether using gold−gold or gold−graphene electrode pairs. As a result, the electronic transport properties of the PPP are dominated by the intrinsic molecular properties with little impact of the coupling to the electrode or the anchoring group.

2.4. Experimental

2.4.1. Sample preparation

All the studied compounds are commercially available and were used as received. The molecular structures of 1,4-benzenedithiol (1a), biphenyl-4,4'-dithiol (2a), p-terphenyl-4,4″-dithiol (3a), 1,4-diaminobenzene (1b), biphenyl-4,4'-diamine (2b), and p-terphenyl-4,4″- diamine (3b) and 1,4-benzene dimethanethiol (BDMT) are shown in Figure 17 a, b, and c. Figure 17d shows the expected gold/molecule/graphene junction that forming by STM-*I*(s) technique.

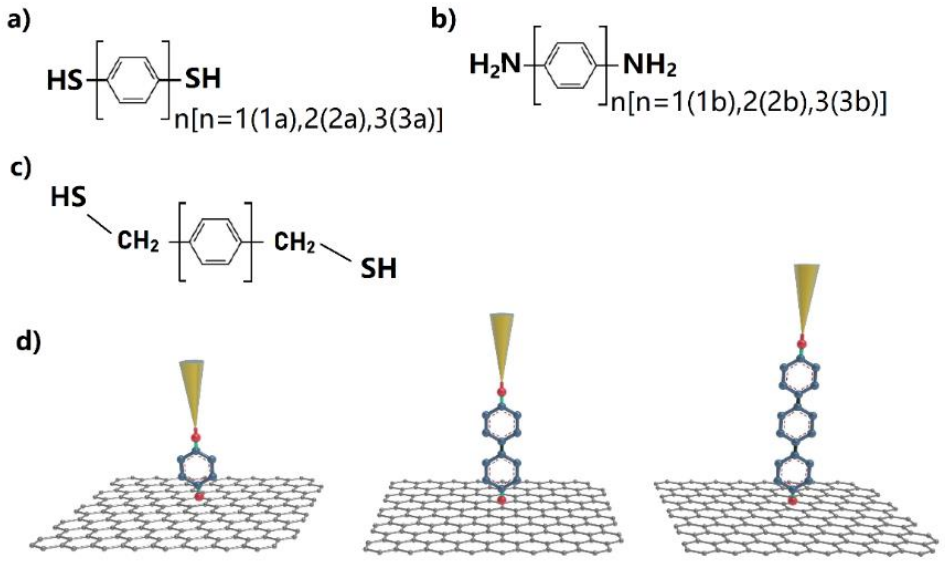

Figure 17: a) Molecular structures of 1,4-benzenedithiol (1a), biphenyl-4,4'-dithiol (2a), p-terphenyl-4,4″-dithiol (3a), b) 1,4-diaminobenzene (1b), biphenyl-4,4'-diamine (2b), and p-terphenyl-4,4″- diamine (3b) and c) 1,4-benzene dimethanethiol (BDMT). d) Illustrating of the expected gold/molecule/graphene junction that forming by STM-*I*(s) technique.

Mesitylene (99%) was used as the solvent to provide a stable liquid environment, which was purchased from Aladdin. In each measurement, mesitylene was degassed by repeatedly sparging with nitrogen gas followed by an ultrasonic treatment to assist the degassing process. Then, a 1 mM solution of the compound in mesitylene was prepared. As shown in the Figure 18, there is no obvious peak during our maximum measurements range indicating the suitability of mesitylene as a solution.

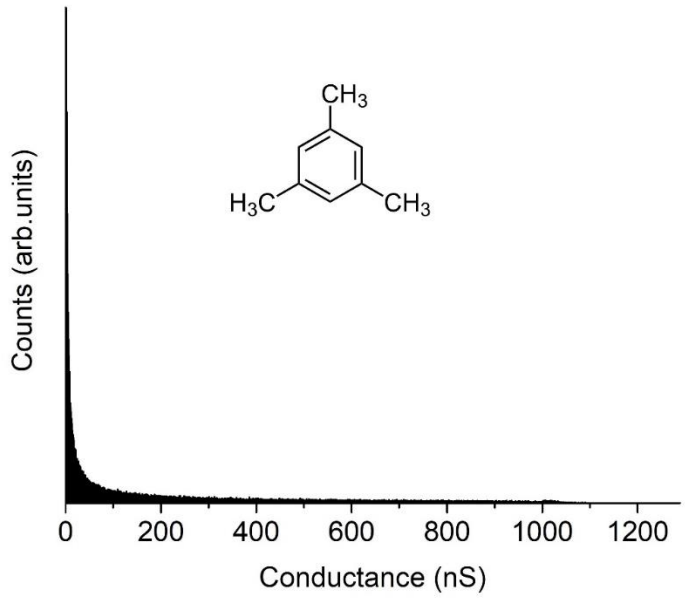

Figure 18: Conductance measurements of mesitylene with gold STM tip and gold substrate with STM *I*-(s) technique.

2.4.2. STM tip preparation

The gold STM tips were fabricated by an electrochemical etching method reported in 2004 by Ren et al.[116] The involving electrochemical etching processes are shown as:[116]

$$Au + 4Cl^- \rightarrow AuCl_4^- + 3e^-, E_0 = 1.002\ V$$

$$Au + 2Cl^- \rightarrow AuCl_2^- + e^-, E_0 = 1.154\ V$$

$$AuCl_2^- + 2Cl^- \rightarrow AuCl_4^- + 2e\text{-}, E_0 = 0.926\ V$$

For preparing the STM tip a gold wire with a 0.25 mm diameter was electrochemically etched using a mixture of hydrochloric acid and ethanol (volume ratio = 1:1) as etching solution, while an etching voltage of 5 V was applied constantly. The quality of the fabricated gold STM tip was checked by scanning electron microscope (SEM) with 15kV operating as shown in Figure 19.

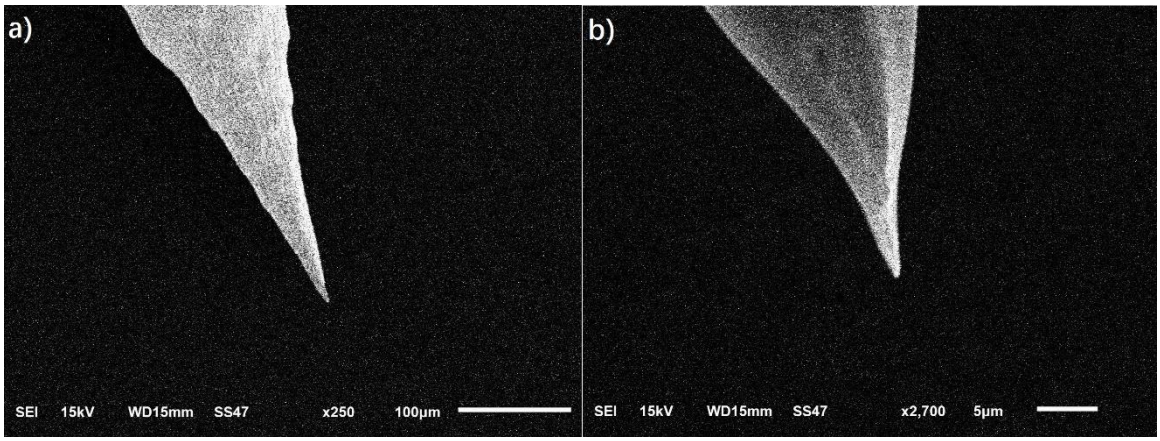

Figure 19: The SEM images of fabricated gold STM tips with the scan range of (a) 100 μm, (b) 5 μm.

2.4.3. Substrates

The 1 × 1 cm size graphene substrates were purchased from Graphene Supermarket (US). Before the conductance measurement, the used graphene substrate was examined by the Raman spectroscopy. For the graphene spectrum, as shown in the Figure 20a, the major bands can be assigned to the sp^2 in-plane vibration of carbon atoms (1580 cm^{-1}), which is referred as G peak. Another major band called G' peak or 2D peak appears at 2700 cm^{-1}, which is associated to the disorder vibration peaks of graphene. The electron dispersion of multilayer and monolayer graphene is different, which leads to the obvious difference of Raman spectrum. The G' peak strength of single-layer graphene is greater than G peak, and with the increase of layers, the full width at half maximum (FWHM) of G' peak gradually increases and moves towards the high wave digit. In addition, the intensity of G peak increases approximately linearly with the increase in the number of graphene layers (within 10 layers), because more carbon atoms could be detected in the multilayer graphene.[117-119] Through comparing the intensity and shape of G peak and G' peak, the graphene substrates used in our experiments were high quality multilayer graphene.

In addition, the STM technique was used to describe the surface of the graphene surface. The 3D STM surface image of the graphene substrate was shown in Figure 20b, the height information was recorded. This 3D image showed that height difference in this graphene substrate is around 0.3nm. This height difference is similar with the height of a single layer of graphene.

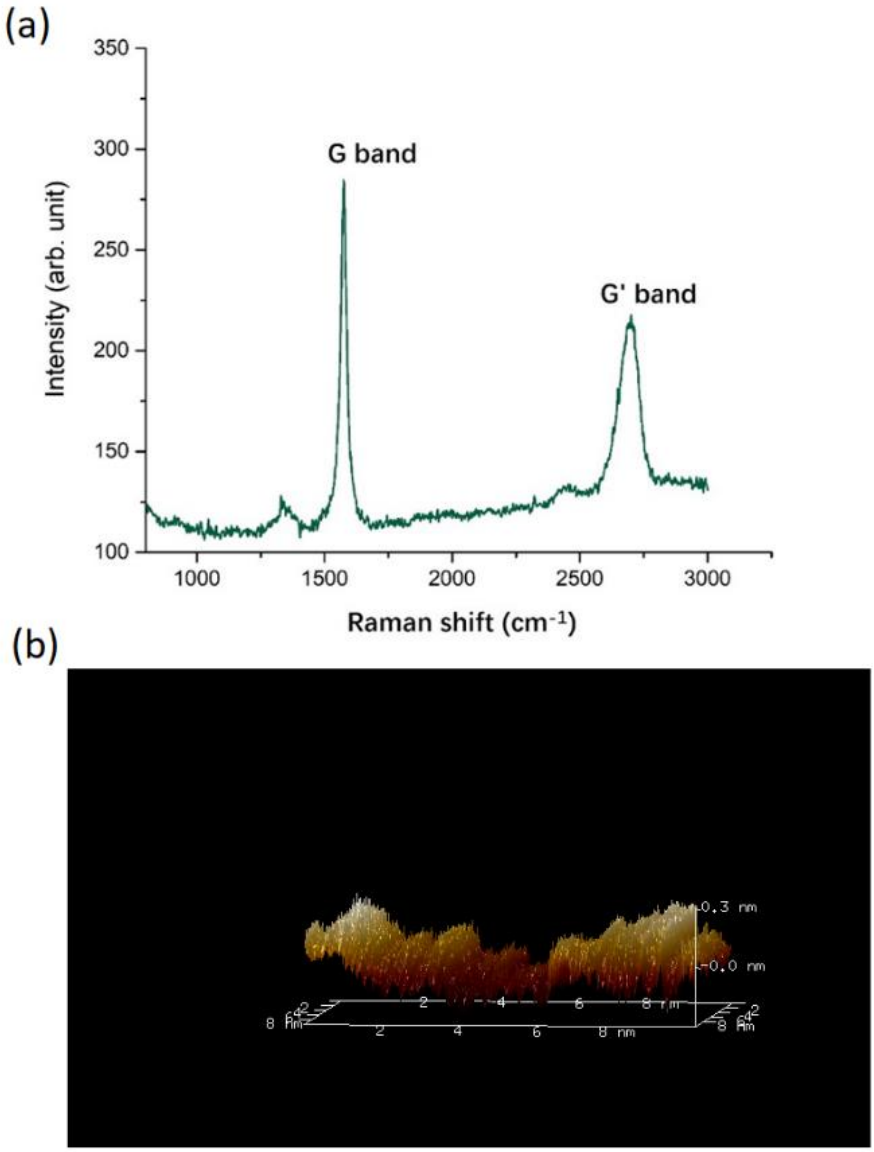

Figure 20: (a) Raman spectrum of a typical graphene substrate (laser: 532nm); (b)3D STM image of graphene substrate (scan range:10nm×10nm, V_{bias}=300mV).

The 1 × 1 cm size gold substrate was purchased from Arrandee in Germany. Before building molecular junctions by STM *I*(s) technique, the gold substrate was annealed under a butane flame to obtain regular Au (111) surface. The Au (111) surface was detected by STM technique as shown in Figure 21. The ideal annealed gold substrate was shown in Figure 21a, that identified by the regular triangle patterns. Figure 21b showed a gold substrate surface with mixed crystal surface. This kind of mixed crystal gold surface is not accepted in building molecular junction because it is difficult to estimate the gold/molecule binding geometry.

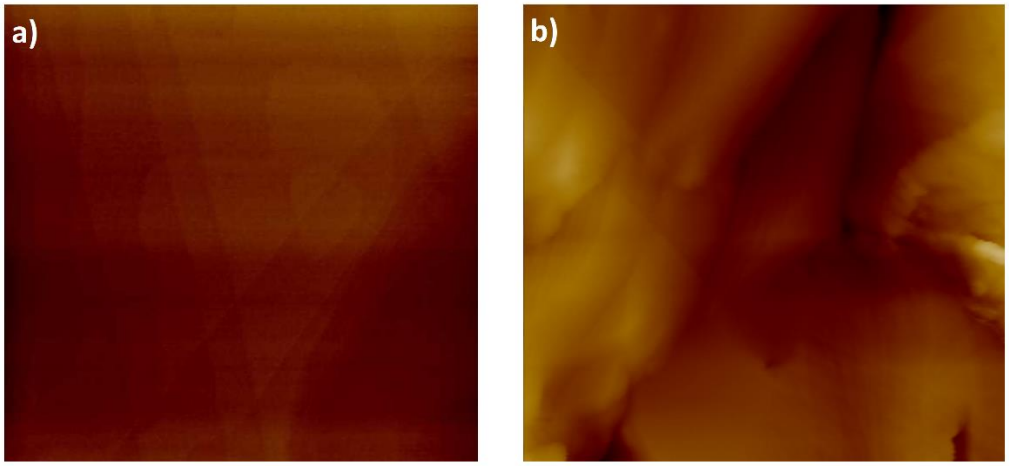

Figure 21: STM image of gold substrate ($200nm \times 200nm$) where (a) regular Au (111) substrate with clear triangle pattern, (b) mixed gold crystal surface.

2.4.4. Conductance measurements

In this study, the STM noncontact *I*(s) technique was used to form single molecular junctions. Because of the non-contact nature between STM tip and substrate, the STM *I*(s) technique better protects the graphene (substrate) surface from tip intruded indentation and damage. A liquid cell filled with mesitylene was used to provide a stable environment for the substrate and molecular adsorbates. In this research, all the conductance measurements were performed under ambient air conditions. In the process of measurement, the gold tip was brought into close proximity with the graphene substrate surface with an STM set point current of 1 nA. Then, the tip was approached and retracted to a given distance (4 nm) from the substrate surface. The tip bias in each experiment was set at +0.3 V. Over 10 000 *I*(s) traces were collected during each measurement of the molecular junction. To select molecular junction forming retraction curves, a manual group sieving method was employed here. At first, noisy and pure decay *I*(s) traces were removed. The Y-axis (current) of remaining plateaus containing *I*(s) trace was divided into a few equal bins. The number of bins was normally set to 5 to 10 depending on the current measurement range (a large measurement range corresponds to a greater number of bins). The bins with the greatest number of *I*(s) traces indicated the most probable position of plateaus. After the *I*(s) traces were sieved, over 500 *I*(s) curves (which came from the bins with the most *I*(s) traces) were combined to make one-dimensional (1D) and 2D conductance histograms.

2.5. Results and discussion

The conductances of Au/(amine-terminated PPP)/Au, Au/(amine-terminated PPP)/graphene, Au/(thiol-terminated PPP)/Au, Au/(thiol-terminated PPP)/graphene, and Au/BDMT/Au have been measured. For all these molecular junctions studied, 1D and 2D conductance histograms have been plotted. For each 1D conductance histogram, a clear peak dominates. In Figure 22a, we show 1D conductance histograms of Au/(thiol-terminated PPP)/graphene junctions. Each histogram reveals a broad and nonperfect Gaussian distribution peak indicating the most probable conductance values of 68.0 (Au/1a/graphene), 18.5 (Au/2a/graphene), and 5.00 nS (Au/ 3a/graphene). The conductance is clearly highly dependent on the number of phenyl rings in the target compound. In addition, there is a broad peak in the 1D histogram of the Au/ 1a/graphene junction with a FWHM value of 18.2 nS after the Gaussian peak fitting. The corresponding 2D histogram (shown in inset of Figure 22a) also reveals a broad distribution of conductance values, as indicated by the white ring.

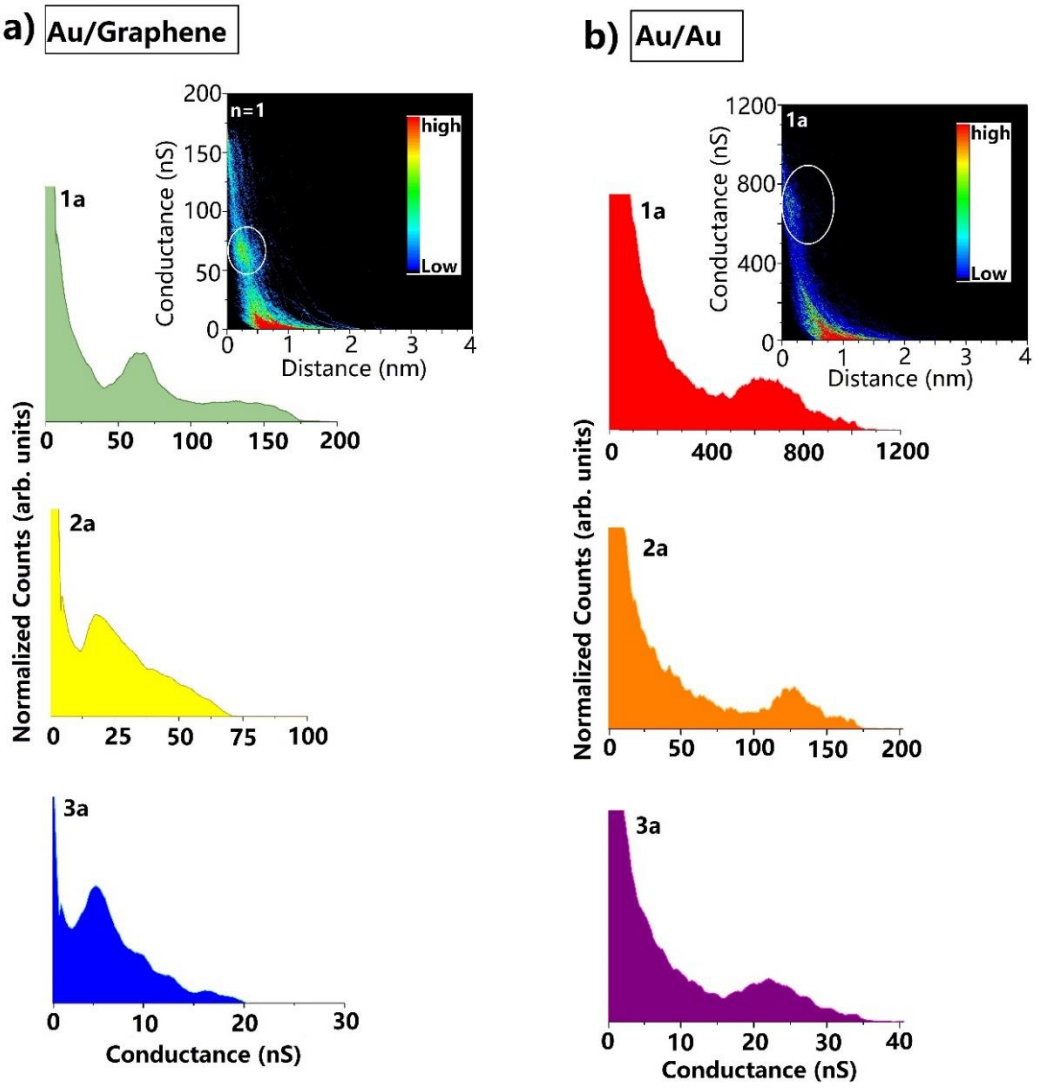

Figure 22: (a) Normalized 1D conductance histograms of Au/1a/ graphene, Au/2a/graphene, and Au/3a/graphene (the inset shows the 2D conductance histogram of Au/1a/graphene, where the white ring indicates the distribution of conductance of the molecular junctions). (b) The normalized 1D conductance histograms of Au/1a/Au, Au/ 2a/Au, and Au/3a/Au (the inset shows the 2D conductance histogram of Au/1a/Au, where the white ring indicates the distribution of conductance of the molecular junctions).

In order to get a rigorous comparison with standard metallic junctions, we have also measured the thiol-terminated PPP molecules bound to a pair of Au electrodes. The 1D conductance histograms of Au/(thiol-terminated PPP)/Au are shown in Figure 22b, and the inset shows the corresponding 2D histogram of Au/1a/Au junctions. Each of the 1D conductance histograms shows a very broad peak with nonperfect Gaussian distribution. This kind of broad peak is likely to arise from a combination of several individual peaks resulting from the flexible configuration of Au/(thiolterminated PPP)/Au systems, which agrees well with a previously reported statement of Ulrich et al.[28] They found that the Au/(thiol-terminated PPP)/Au system has a high degree of static disorder (each manifestation of the junction is different from the previous one) and dynamic disorder (the junctions can switch spontaneously between different configurations). We have listed here the most probable conductance values of Au/(thiol-terminated PPP)/Au in Table 2, which are 645 nS for Au/1a/Au, 126 nS for Au/2a/Au, and 23.2 nS for Au/3a/Au. These conductance values correspond to the most likely molecular junction configuration being formed under our experimental conditions. The conductance value of 1a bound between gold electrode pairs has also been widely discussed in previous studies.[10,26-29,120-123] However, on the basis of the diversity in the reported conductance values for 1a, it is clear that there is no a universal consensus. The reported conductance of 1,4-benzenedithiol (BDT) linked with Au electrodes ranges from 31 nS ($4 \times 10{-}4G_0$)[10] to 7740 nS ($0.1G_0$),[29] and most of these studies displayed a broad peak in the 1D conductance histogram. Bürkle et al.[124] have reported the conductance of Au/2a/Au junctions. They found the torsion angle between each phenyl ring could affect the conductance value of the molecular junction. Clearly, it is not straightforward to compare the conductance values for thiol-terminated PPP molecules in Au/ Au configurations reported from different research groups.

In order to further explain the effect of conjugated effect, we measured the conductance of Au/BDMT/graphene and Au/BDMT/Au junctions to compared with BDT based molecular junctions. The measurement results of BDMT were showed in Figure 23a, that is 17.7nS for Au/BDMT/graphene and Figure 23b that is 91.2nS for

Au/BDMT/Au. The measured conductance value of BDMT is obviously lower than 1a in both of Au/Au and Au/graphene contacts. These results showed that the adding methylene units could decrease the conductance of the molecular junction by decreasing the degree of conjugation. These experimental are agrees well with a previously reported measurements from Xiao et al.[27] They showed the conductance value of BDT is much higher than BDMT in Au/Au contact that measured by STM-BJ method.

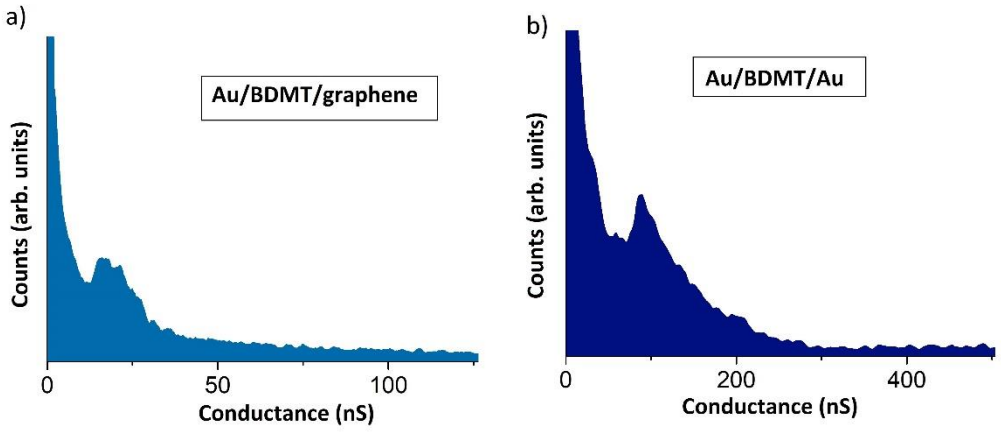

Figure 23: Normalized 1D conductance histogram of (a) Au/BDMT/graphene, (b) Au/BDMT/Au.

We further explored the dependence of the conductance of single molecular junctions on the anchoring group and electrode material by considering also amine-terminated PPP molecules in both Au/Au and Au/graphene configurations. The measured 1D conductance histograms are shown in Figure 24a (Au/(amine-terminated PPP)/graphene) and Figure 24b (Au/(amine-terminated PPP)/Au). The inset pictures in Figure 24a, b represent the individual *I*(s) traces of Au/1b/graphene (gray) and Au/1b/Au (dark yellow) junctions. These curves highlight the similarities and key differences between the Au electrode and graphene electrode. A clear plateau is seen around 58 nS for the formation of stable Au/1b/graphene junctions. In the case of using gold electrodes, we see a plateau appearing at a much higher conductance close to 500 nS, which is attributed to the formation of Au/1b/Au junctions.

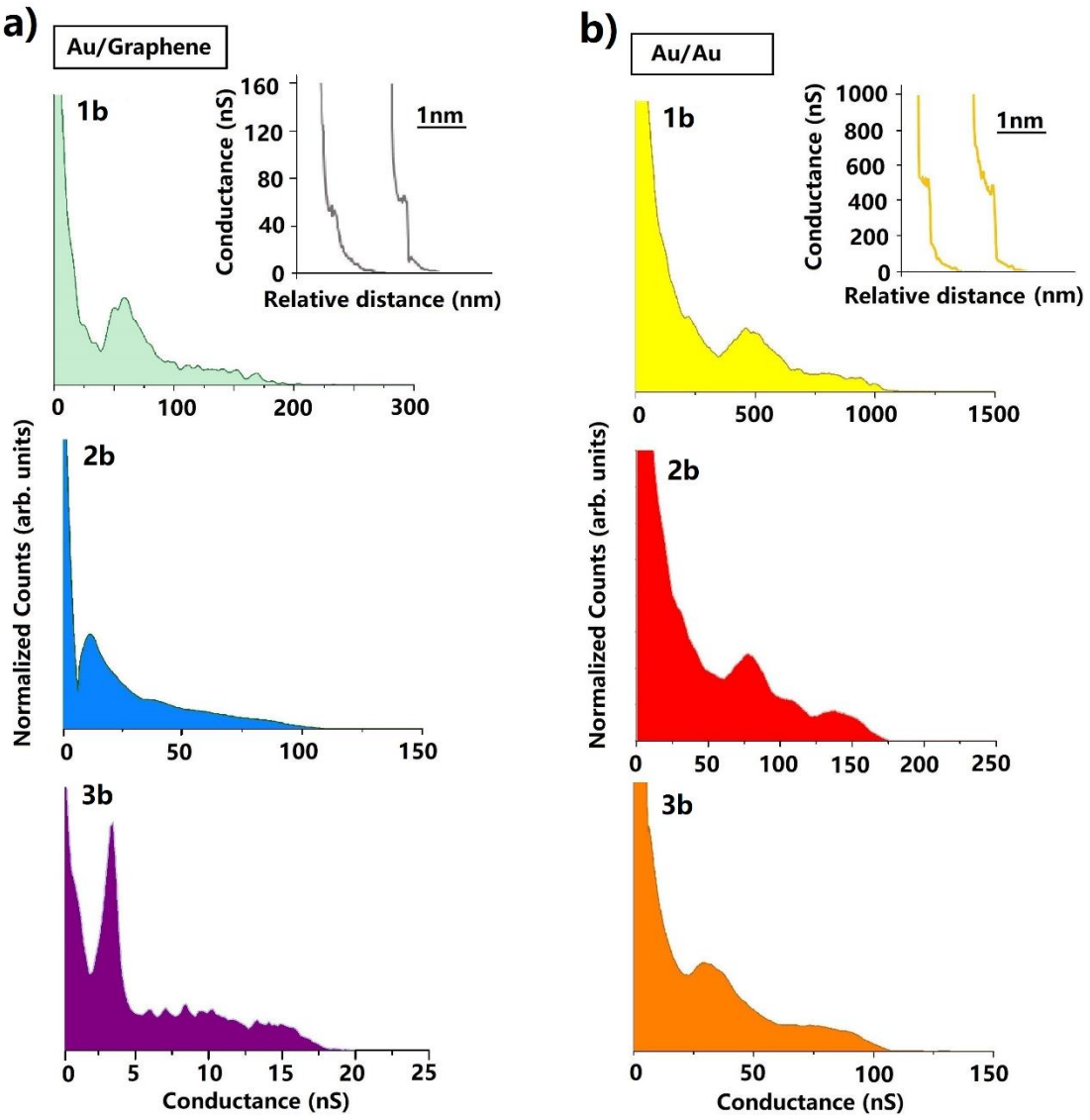

Figure 24: (a) Normalized 1D conductance histograms for Au/1b/graphene, Au/2b/graphene and Au/3b/graphene molecular junctions (the inset shows 2 individual I(s) traces for Au/1b/graphene junctions) (b). Normalized 1D conductance histograms for Au/1b/Au, Au/2b/Au and Au/3b/Au.

Each 1D conductance histogram reveals the predominant peak corresponding to the most likely junction configuration, and it is clear that the conductance decreases exponentially with the number of phenyl rings in both systems. The measured details are listed in Table 2, and the following conductance values have been recorded: 478 (Au/1b/Au), 82.0 (Au/2b/Au), and 30.0 nS (Au/3b/Au) as well as 58.2 (Au/1b/graphene), 13.5 (Au/2b/graphene), and 3.50 nS (Au/ 3b/graphene), respectively.

The corresponding conductance values are obviously much higher for Au/Au systems when compared to Au/graphene systems, which we attribute to contact resistance. In addition, when comparing the Au/(thiolterminated PPP)/graphene system with the Au/(amineterminated PPP)/graphene system, it can be seen that the conductance values of the latter are slightly lower.

Table 2: Conductance value and tunneling decay value for five types of molecular junction (The decay constant is per phenyl group).

Molecular junctions	Conductance (nS)		Decay constant β	
	Experiment	Theory	Experiment	Theory
Au/1a/graphene	68.0	57.8		
Au/2a/graphene	18.5	22.7	1.31	1.10
Au/3a/graphene	5.00	6.40		
Au/1b /graphene	58.2	69.2		
Au/2b/graphene	13.5	12.0	1.40	1.17
Au/3b/graphene	3.50	6.60		
Au/1a/Au	645			
Au/2a/Au	126		1.64	
Au/3a/Au	23.2			
Au/1b /Au	478			
Au/2b/Au	82.0		1.38	
Au/3b/Au	30.0			
Au/BDMT/graphene	17.7			
Au/BDMT/Au	91.2			

Similarly, Venkataraman et al. have studied the length dependence of the conductance using the STM-BJ method for a range of amine-terminated molecules, including alkanes[43] and oligophenyls.[63, 79] In Figure 25a, we compare the natural logarithmic conductance plots of our experimental measurements with the ones reported by the Venkataraman group. The attenuation trend satisfies the equation $G = Aexp(-\beta L)$, where $\beta$is the decay constant, L is the number of phenyl groups, and A is a constant related to the interaction between the molecular target and the electrode, which reflects the contact resistance. The βvalue is readily calculated from the slope of the plot of $\ln(G)$versus L. For Au/(amine-terminated PPP)/Au junctions, our experimental results (red) are in good agreement with the results presented by the Venkataraman group (green), which indicates that both the STM-BJ and STM-*I*(s) methods are effective for forming these gold contacted molecular junctions. More importantly, the measurements on Au/amine-terminated PPP/graphene junctions yield $\beta = 1.40$per phenyl group, which is essentially the same as Au/ amine-terminated PPP/Au junctions ($\beta = 1.38$ phenyl group). These experimental results show that the decay constant is essentially the same for amine-terminated PPP measured between Au/graphite (Figure 25a, blue, Venkataramn result) and Au/Au (Figure 25a, green) electrodes, which is in good agreement with the results reported in the literature.[63,79] Hence, we find that the decay constant β of PPP-based molecular junctions is independent of the electrode material, contrary to alkane-based molecular junctions, where, importantly, the use of a graphene electrode reduces this decay.[76,77]

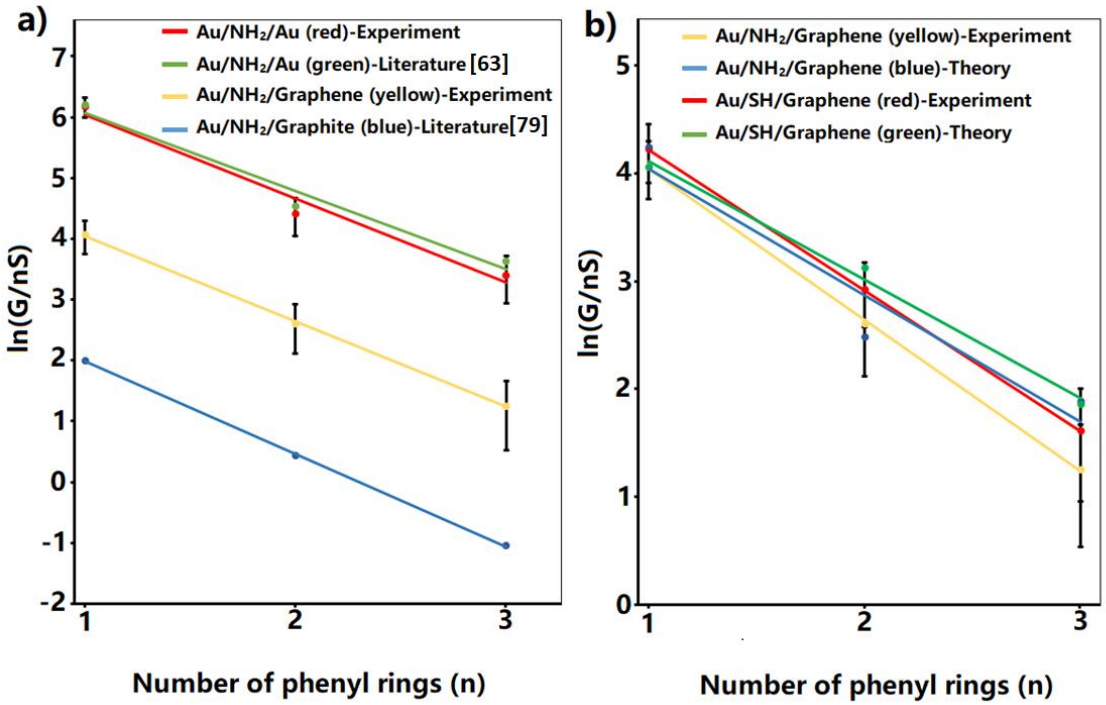

Figure 25: (a) Natural logarithmic plots of the conductance as a function of the number of phenyl rings for amine terminated PPP, experimentally measured for the Au/Au system (red) and in Au/graphene system (yellow). The green line shows literature data for Au/Au system,[63] and the blue line shows literature data for Au/graphite system.[79] (b) Natural logarithmic plot of the conductance as a function of the number of phenyl rings. The amine and thiol terminal groups have been compared in Au/graphene system. The yellow (blue) lines represent the experimental (theoretical) decay values of Au/(amine terminated PPP)/graphene junctions. The red (green) lines represent the experimental (theoretical) decay values of Au/(thiol terminated PPP)/graphene junctions.

To provide further insight into the experimental results, we have performed DFT calculations to model these molecular junction systems. In Figure 25b, we compare the experimental and theoretical attenuation trends of amine terminated PPP molecular junctions (experimental=yellow, theoretical=blue) and thiol terminated PPP molecular junctions (experimental=red, theoretical=green) for the Au/graphene system. The present experimental and theoretical results are consistent with each other. Moreover, both experimental and theoretical results produce similar attenuation factors for thiol and amine terminated molecular junctions in the Au/graphene case. For example, we note that the experimental measured conductance decay constant β is almost the same for Au/amine terminated PPP/graphene (1.40 per phenyl ring, or 0.33 $Å^{-1}$) and Au/thiol terminated PPP/graphene (1.31 per phenyl ring, or 0.31 $Å^{-1}$). This phenomenon is similar to our previous studies where we have obtained a similar decay constant for Au/alkanedithiol/graphene and Au/alkanediamine/graphene junctions.[76.77] Table 2 compares the details of experimental and theoretical electronic properties of these four series of molecular junctions. The corresponding calculated transmissions for Au/(thiol terminated PPP)/graphene and Au/(amine terminated PPP)/graphene are presented in Figure 26a and Figure 27a, respectively.

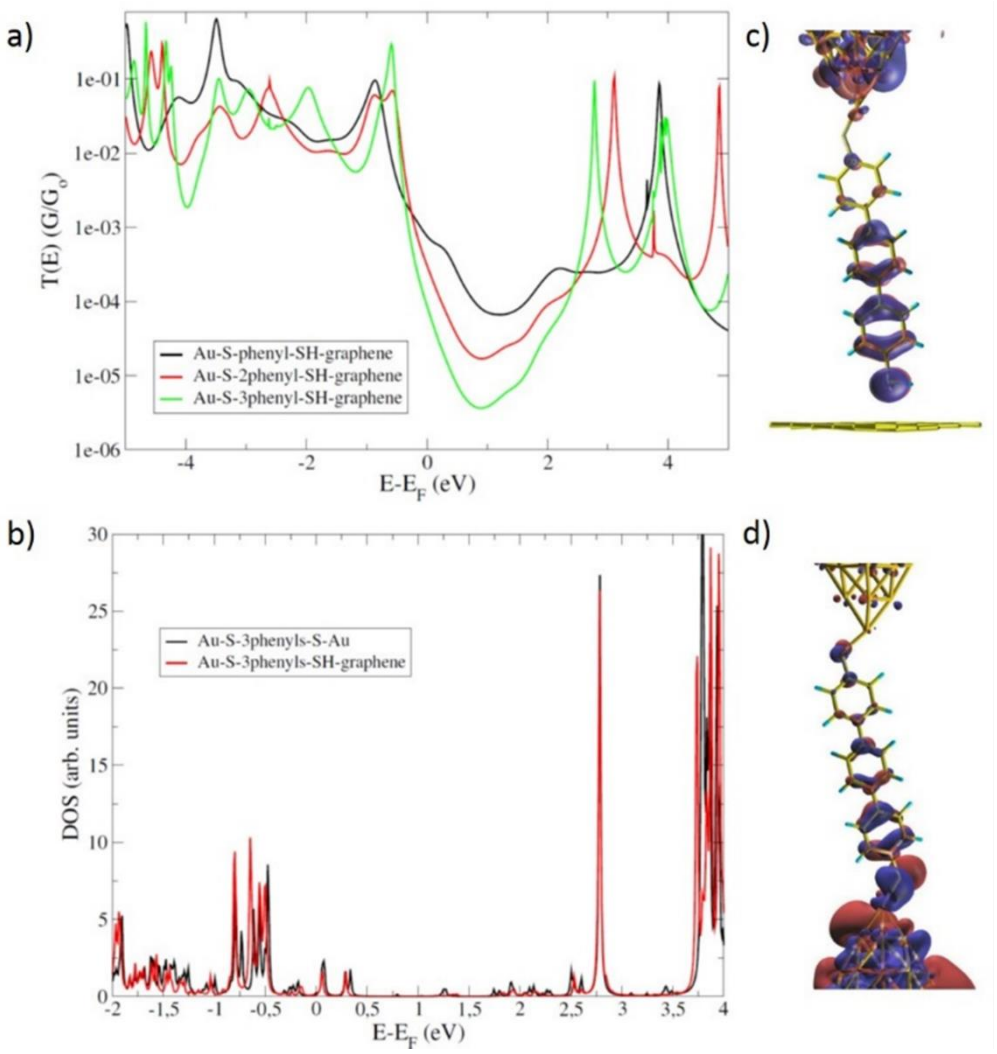

Figure 26: Calculated transmissions for the Au/(thiol terminated PPP)/graphene junctions (n=1, 2 and 3). (b) DOS comparison for Au/3a/Au and Au/3a/graphene junctions. (c) and (d) representations of the Au/3a /graphene and Au/3a/Au junctions, showing the respective HOMO wavefunctions.

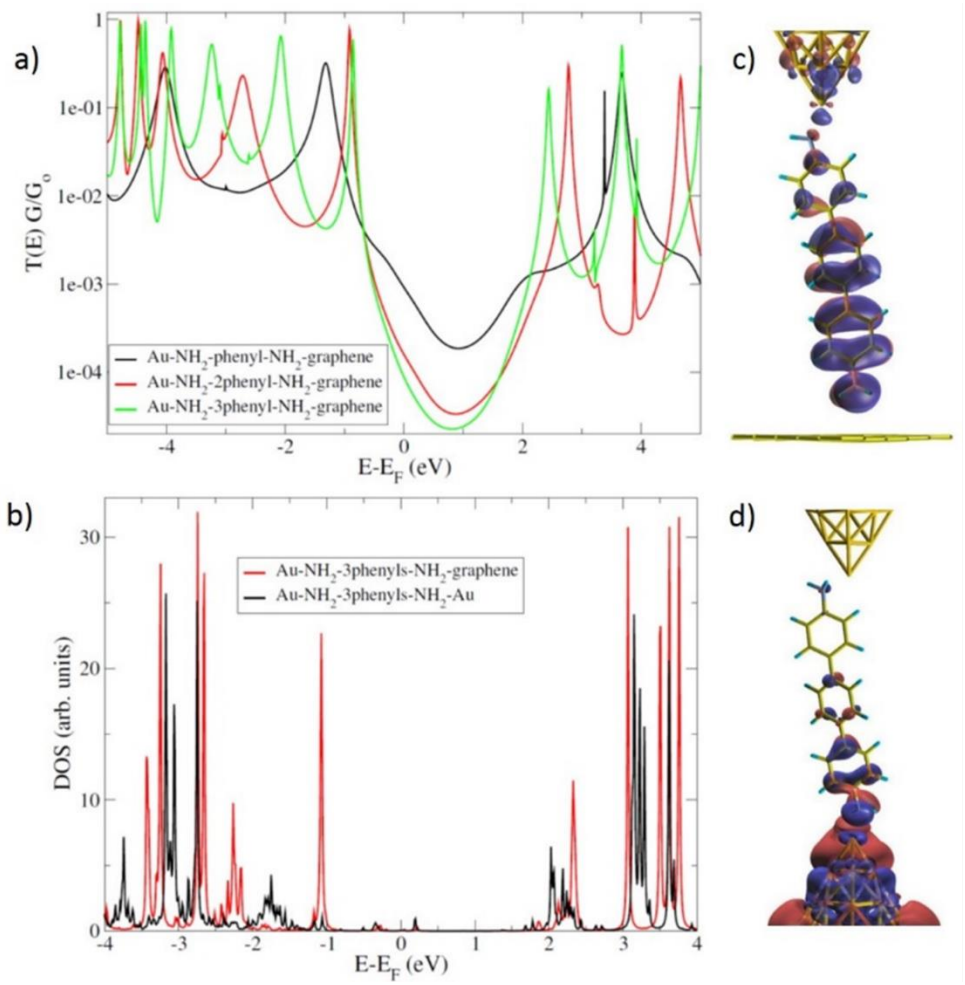

Figure 27: (a) Calculated transmissions for the Au/(amine terminated PPP)/graphene junctions (n=1, 2 and 3). (b) DOS comparison for Au/3b/Au and Au/3b/graphene junctions. (c) and (d) representation of the Au/3b/graphene and Au/3b/Au junctions, showing the respective HOMO wavefunctions.

In order to understand the similarities in the attenuation factors between gold-gold and gold-graphene junctions for the PPP based junctions, we have calculated the Density of States (DOS) for the three-phenyl chains in both gold-gold and gold-graphene junction configurations. The results are presented in Figure 26b for the dithiol case and Figure 27b for the diamine case. As is shown, the DOS are very similar for gold-gold or gold-graphene junctions for both types of anchoring groups, in particular around the energy gap. In the case of amine groups, very small differences in the positions of the molecular levels can be observed, with however very little impact on the electronic transport properties of the junction, in agreement with the experimental data. This peculiar behaviour explains why the attenuation factors β remains the same

for both types of electrodes, since β mainly depends on the molecular electronic structure. Note that this result is very different from what has been obtained previously with alkane chains in the junctions,[76,77] where the introduction of the graphene electrode resulted in a symmetry breaking in the junctions. Indeed, for the thiol groups, a global shift of the molecular electronic structure has been observed, whereas a splitting of the HOMO level occurred for the amine groups. In both cases, this symmetry breaking induced by the weak coupling of the graphene electrode with respect to the strong coupling of the gold electrode yielded importantly a reduction of the attenuation factor. Here the introduction of the graphene electrode does not bring the same symmetry breaking despite a weak coupling at the corresponding interface. This feature is further illustrated through calculations and corresponding visualisations of the HOMO isoelectronic DOS for both junctions. These are presented in Figure 26c and 26d for the dithiol and Figure 27c and 27d for the diamine. For the different electrode types, namely gold and graphene, and both thiol and amine anchoring groups, the HOMO orbital presents the same out of plane π-symmetry which propagates well along the molecular backbone. In this respect, the electrodes and anchoring groups couple well with the molecular backbone orbital, ensuring the electronic propagation and a constant attenuation factor. This situation is rather different from the one observed in alkane chains where the coupling to the molecular chain of thiol or amine was notably different.[76]

2.6. Conclusion

Using the STM-*I*(*s*) method, we have determined the electronic conductance and attenuation factor of the current in phenyl chain based molecular junctions, with both thiol or amine anchoring groups, using gold-gold or gold-graphene electrodes. Summarizing the experimental results detailed above, the following general observations can be made:

(1) Both amine- and thiol-terminated PPP systems can form junctions with a graphene contact on one side and with gold as the other contact.

(2) Conductance values for the Au/Au systems are much higher than the corresponding Au/graphene systems.

(3) Conductance value for BDT is much higher than BDMT in both of Au/Au and Au/graphene contacts.

(4) Au/(thiol-terminated PPP)/graphene junctions have slightly higher conductances than the corresponding Au/(amine-terminated PPP)/graphene systems.

(5) The conductance attenuation with molecular length (β value) is broadly similar for Au/Au and Au/graphene systems, irrespective of whether amine or thiol terminated analogues are used.

This contrasts with previous studies with unsaturated molecular chains (“alkane”) where the introduction of a graphene electrode drastically reduced the attenuation factor. These results are confirmed by DFT calculations, which show very little modification of the electronic DOS using gold-gold or gold-graphene electrodes. This result is explained by the π-symmetry of the HOMO orbital which couples well with all the anchoring groups and electrodes ensuring a propagation along the molecular backbone with consistently the same attenuation factor. As a consequence, the transport in phenyl chains is dominated by the intrinsic molecular properties and remains almost unaffected by the coupling to the electrode or the anchoring group.

3 Chapter 3: The conductance variation discussion of molecular junction based on an unsupervised data analysis approach.

3.1. Preface

Based on the research of Chapter 2, we found despite many advanced developments made to date, there is ongoing discrepancy on the measured conductance value for the same molecular junction system. Among our studies and many previous studies showed that different techniques or a slight changed in the experimental conditions, it can lead to a dramatic difference in the obtained conductance value. Especially, 1,4-benzene dithiol (BDT) with Au/Au contacts, Sergueev et al.[33] have concluded that the conductance of the BDT junction depends strongly on both the separation between the contacts and the trapping configuration of the BDT molecule, and the stretching of the junction results from pulling the gold atom out of the electrode accompanied by a sudden rise in the conductance. Recently, Zheng et al.[59] have measured the conductance of BDT with a combined mechanically controllable break junction (MCBJ) and in-situ surface enhanced Raman spectroscopy (SERS) method, they stated that the disulfide mediated dimerization (forming of S-S bond) of BDT contributed to the low conductance (10^{-4} G_0) feature. These data strongly suggested that there is more than one possible configuration of the forming of Au/BDT/Au junction, resulting in distinct variation in the conductance value. The various conductance behavior of Au/thiol terminated poly (p-phenyl) (PPP)/Au system has been considered arisen from not only the nature of linked molecule but also the complex contact between the thiol anchoring group and gold electrode.[125-128] In the measurement of the conductance behavior of an individual molecules, an accurate observation of the stochastic nature of the electronic properties of (single) molecular junctions requires collection of large data sets to obtain the full detail of a molecular system. The process of manual data selection greatly limits the data size. Here, an unsupervised MATLAB algorithm was introduced and further used to select and analysis the *I*(s) data.

3.2. Introduction

For sulfur-gold contact in (single) molecular junctions, isothiocyanate (-S=C=N) has the advantage of possessing a π-conjugated double-bond moiety that presumably exhibits a relatively smaller impedance when it used as a anchoring group. Same as thiol group, isothiocyanate is also a high-affinity anchoring group to bind with gold.[129] Fu et al.[130] has reported that the single-molecule conductance of Au/n-butanediisothiocyanate/Au is an order of magnitude bigger than the conductance of Au/n-octanedithiol/Au. Similar as Au/PPP/Au system, multiple conductance behavior has been reported in previous research that two conductance sets were found for alkanediisothiocyanates in both of experimental[130] and theoretical[131] insights. The relative multiple conductances were ascribed by their different Au/SCN(CH_2)nNCS/Au binding geometries.

3.2.1. The idea of unsupervised data analysis

The variability of conductance in molecular junction systems makes it especially meaningful to repeatedly record large amount of conductance data from the molecular junctions. The bigger of the data capacity means the more detail of the molecular junctions could be discovered. Fu et al.[130] have reported the 1D conductance histograms from 1000 traces without any preselection (as shown in Figure 28a) and from 274 traces preselected by removing noisy traces (as shown in Figure 28b) for Au/SCN(CH_2)$_4$NCS/Au junctions. The conductance peak was clearly identified after data selection. However, this manual selection limited the volume of *I*(s) data enormously, especially for the measurements using STM-*I*(s) technique. Because the STM-*I*(s) is a non-contact technique, compared with other break junction methods, the possibility of successful forming (single) molecular junction was relatively lower. In our STM-*I*(s) experimental set-up, the frequency for collecting the plateau traces was about 10%. In addition, it difficult to avoid conscious bias completely in manual selection process. In the actual measurements, analysing such datasets (around 10 000 traces) is full of challenging, especially when we started with a little-studied molecular system or when there exists an undesirable prior expectation.

Here, a statistical method is suggested to analyze the possible molecular junction configuration by plotting one dimensional (1D) conductance histogram. In the simplest case, a single peak in a 1D conductance histogram resulting from plateau featured traces is usually taken to represent molecule junction formation and the most probable conductance value. Such a statistical analysis has been underpinning for obtaining the conductivity of single molecular junctions. However, for some complex systems, it is very hard to obtain an unambiguous single peak in 1D conductance histogram as mentioned previously. Therefore, the data selection became especially crucial for the conductance measurements.

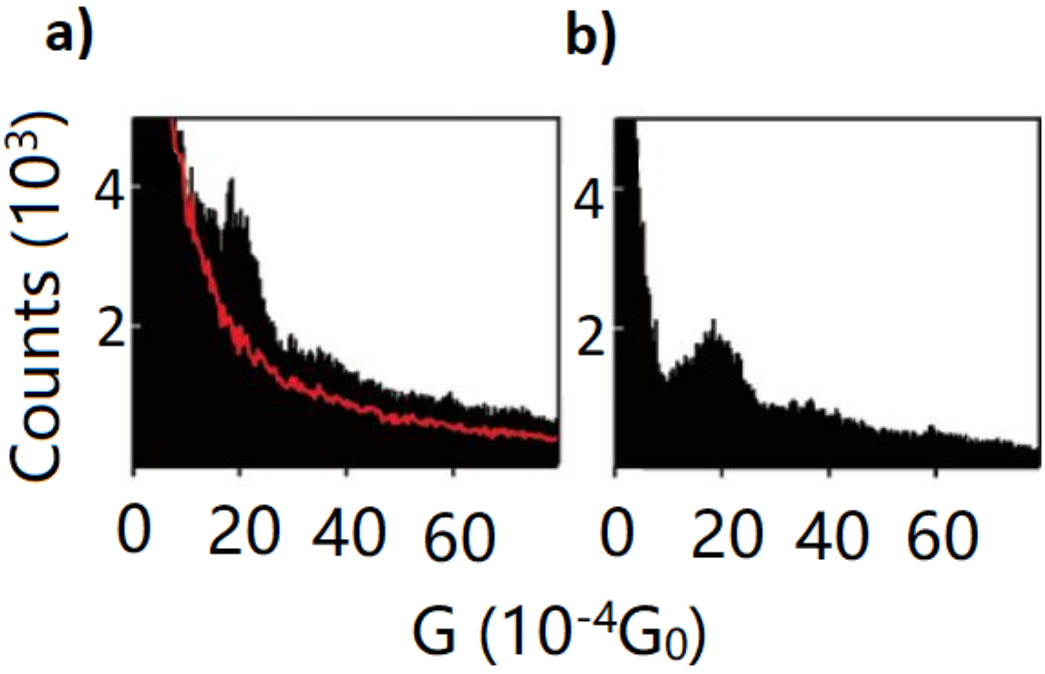

Figure 28: The 1D conductance histograms for Au/SCN$(CH_2)_4$NCS/Au from a) 1000 traces without any preselection, b) 274 traces preselected by removing noisy traces. [Copyright, American Chemical Society, Ref. 130]

3.2.2. The reported algorithm

In molecular electronics, the flourish of the automatic computer technologies offers new insights to data selection and contributed to scalability of the analysis of charge transport in (single) molecular junctions. There is a realizing in measuring single molecular junctions that the formation of (single) molecular junction at room temperature is a stochastic event and is subject to fluctuations. Therefore, the interpretation of data and the statistical analysis method are extremely critical to obtain the conductance value of molecular junctions. The idea of unsupervised data analysis was proposed by Jang et al. in 2006.[132] They have measured the conductance behavior of series of thiolalkanes with STM technique. For data analysis, they believed that the manual selection would leaded bias. They reported a new last-step analysis (LSA) method to clarify the contribution of these effects. In LSA method, only the last rapid drops parr of a conductance trace was used to plot the conductance histogram, and it does not require any manual data preselection, making the results less subjective and more reproducible. They compared the 1D histograms of Au/1,6-hexanedithiol/Au that obtained by LSA method (Figure 29a) and conventional method (Figure 29b). They further explained the difference of these two data selection methods that LAS method could avoid the influence of the background tunneling current, and present visible conductance peak.

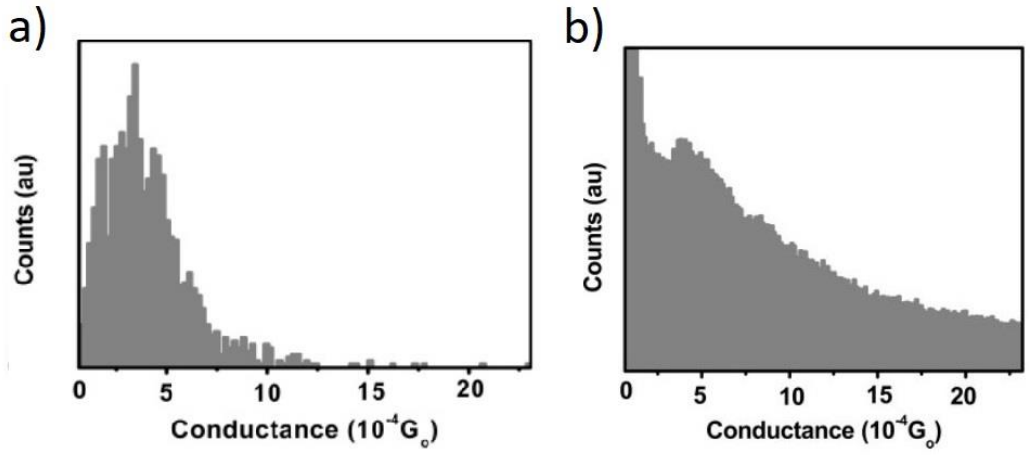

Figure 29: The conductance histogram of Au/1,6-hexanedithiol/Au that plotted by a) LSA method, b) conventional method. [Copyright, American Chemical Society, Ref. 132]

Till now, there are many well applied unsupervised data selection algorithm, which have been reported in previous studies.[133,134] Lemmer et al. have introduced a basic philosophy of unsupervised data analysis compared with conventional data selection process, as shown in Figure 30a, and reported a new multiparameter vector-based classification (MPVC) algorithm.[133] Their algorithm could separate the conductance traces in to different clusters relied on its plateau shape as shown in Figure 30b. Based on this algorithm, conductance traces could be divided into many groups on the 2D conductance mapping.

More recently, the Deep Learning methodologies also has been applied in the molecular conductance analysis to help researcher to discover and identify hidden signals in (single) molecule charge transport data.[134]

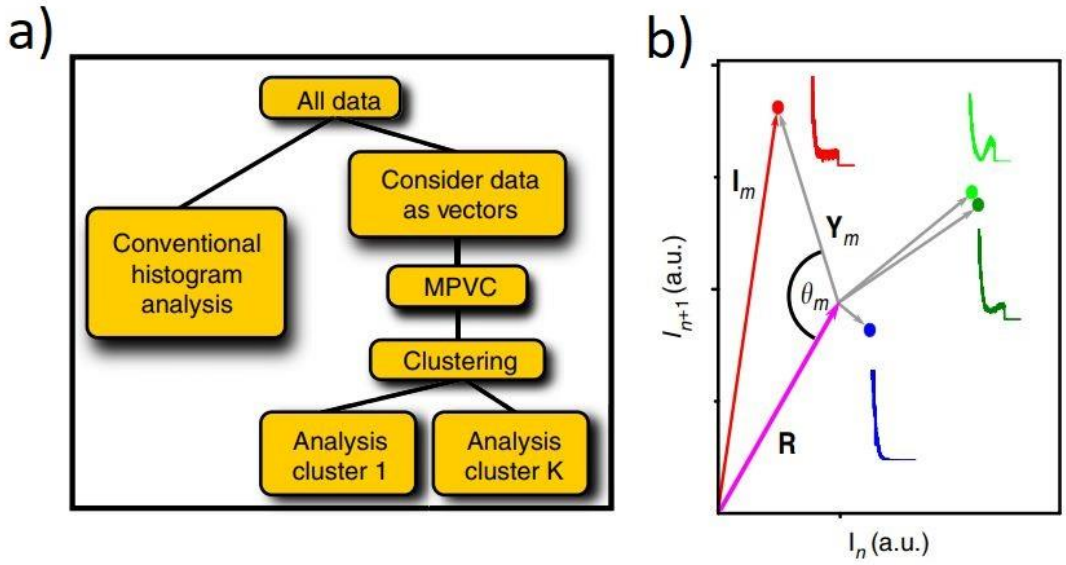

Figure 30: (a) Flowchart of conventional and unsupervised data analysis process. (b) Vector representation of the different shape of *I*(s) traces. [Copyright, Springer Nature, Ref. 133]

In 2018, our group also reported an efficient data sorting algorithm which is used specifically for the STM-*I*(s) measurement data.[135] The idea of this algorithm, as shown in Figure 31a, was removing the noisy traces by three main process: X-filter, Y-filter and peak-filter. This algorithm has been validated by the measuring of Au/ 1,8-octanedithiol/Au system, which shows the effectiveness to remove the noisy signal and capture the complexity of the conductance behavior. As shown in Figure 31b, the collected *I*(s) traces contributed a 1D histogram with obvious conductance peak that located at 3.67nS after the unsupervised data selection. The description of this algorithm will be briefly introduced in the later section of this Chapter and it forms an important tool to do the analysis work.

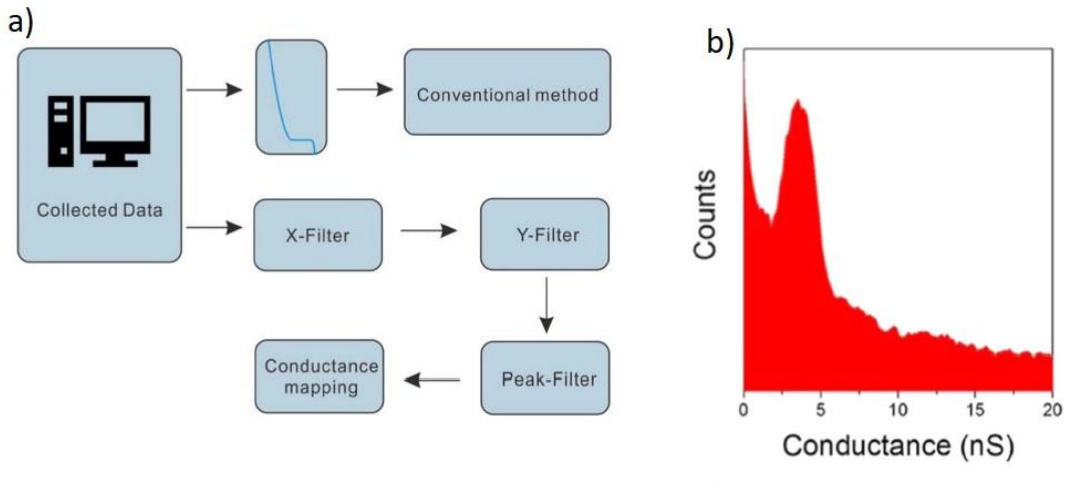

Figure 31: a) Flowchart of conventional and the unsupervised data analysis method. b) Conductance histogram of Au/ 1,8-octanedithiol/Au based on the unsupervised data selection method. [Copyright, Institute of Physics Science, Ref 135]

3.3. Research aim

In the last chapter we have discussed the effect of a series of intrinsic factors, such as anchoring group, electrode materials, and conjugated degree to the conductivity of (single) molecular junctions. Then we realized that an accurate measurement of the stochastic nature of the electronic properties of (single) molecular junctions requires collection of large data sets to obtain the full detail of a molecular system. In this chapter, two series of molecules, with chain shape and phenyl ring units each, are measured by STM-*I*(s) technique. In addition, an unsupervised MATLAB algorithm was used to select and analysis the *I*(s) data.

3.4. Experimental section

3.4.1. Conductance measurements

In this research, two groups of molecules were selected. The first group was chain-like molecules in increasing methylene groups terminated by isothiocyanate and methyl, including 6-(methylthio) hexyl isothiocyanate (6MHI) and 8-(methylthio) octyl isothiocyanate (8MOI). The second group was probed with ring-like molecules terminated by symmetric thiol groups, including biphenyl-4,4'-dithiol (DBDT) and p-terphenyl-4,4''-dithiol (TBDT). Their molecular structures are shown in Figure 32. The selected molecules have relatively similar molecular length, the distance between two sulfur atoms in each of molecular structure have been calculated by the Chemdraw 3D with minimized energy. The length of molecules is 1.05 nm for DBDT, 1.47 nm for TBDT, 1.12 nm for 6MHI, and 1.36 nm for 8MOI.

The conductance measurements were using STM-*I*(s) method in Au/Au contacts. 1 mM solution of the targeted molecule in mesitylene (99%) was prepared for each case. Other parameters were identical to the ones reported in Chapter 2.3.4, unless specifically stated. All these used molecules are commercially obtained, before the conductance measurements ^{1}HNMR spectrum was used to check the sample quality.

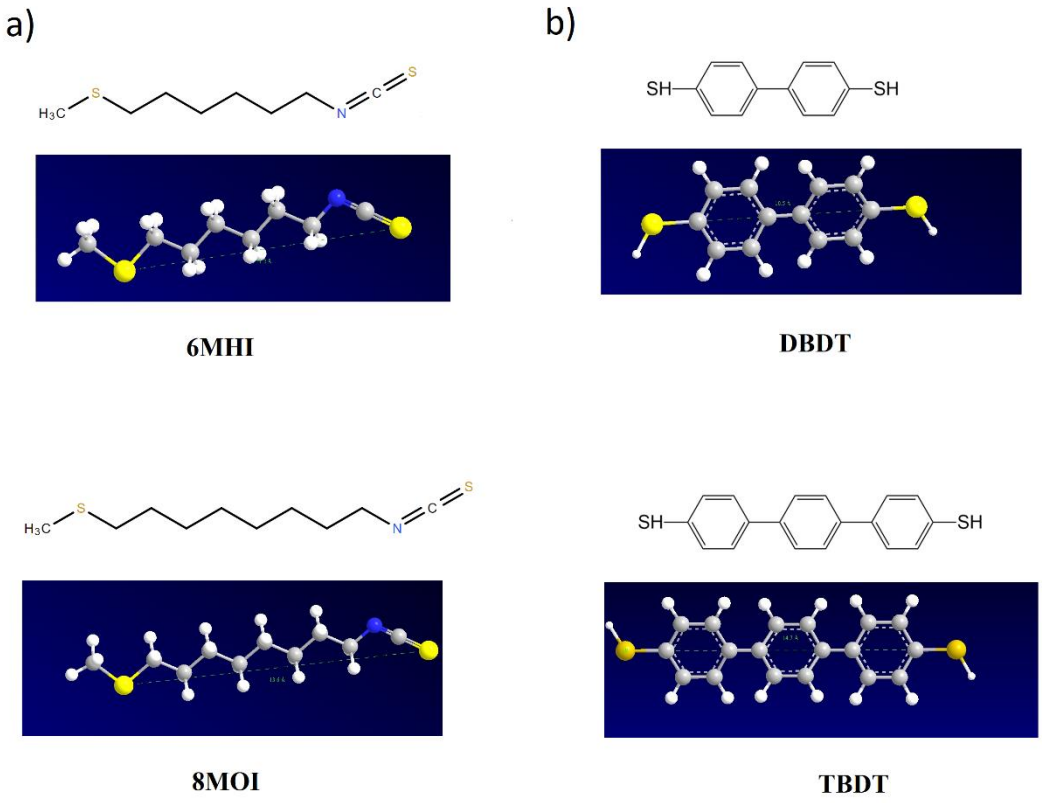

Figure 32: Molecular formula and relative 3D structure of measured molecules, a) 6MHI and 8MOL and b) DBDT and TBDT. For each of molecules, the molecular length was recorded as the distance between two sulfur atoms in terminal group.

3.4.2. The measurements of break-off distance

To further analyze the construction of molecular junctions, an estimated total break off distance S_{tatol} can be calculated by the equation 13.[12] S_{tatol} is usually compared to the length of the fully extended molecule. If a comparable value is achieved, which indicates a molecule successfully bridging the gap between two electrodes.

$$S_{tatol} = S_0 + \Delta S \qquad (13)$$

In this equation, ΔS represents the distance travelled by the tip from the set point current to junction break-off point, where the plateau returns to exponential decay as shown in Figure 33 (i.e. the intersect of two dotted lines). ΔS could be calculated for each molecular system by a statistic analysis using about 300 current-distance curves.

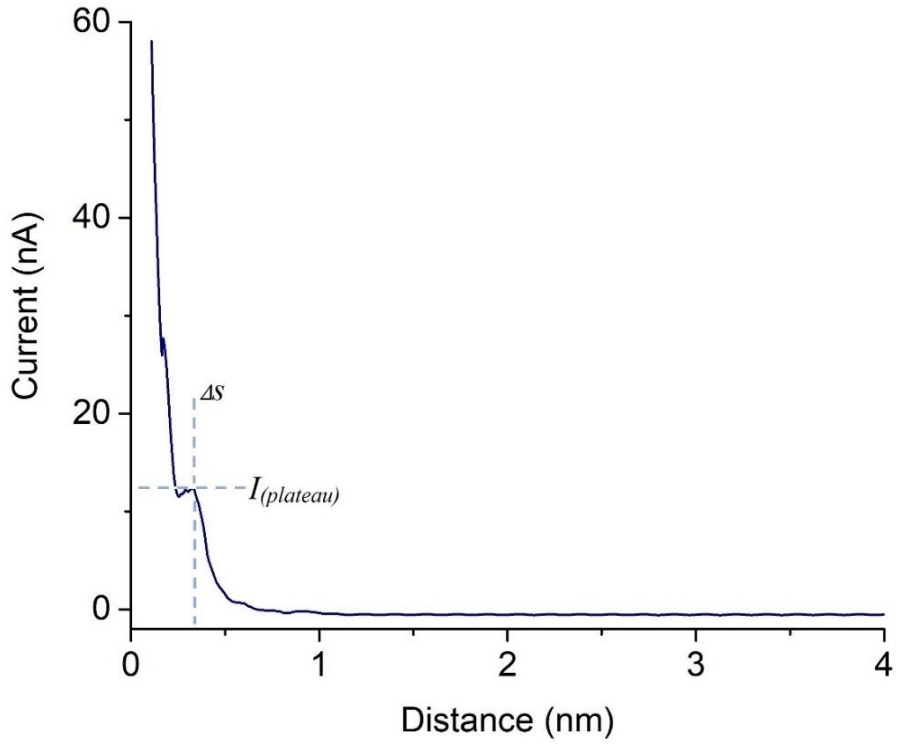

Figure 33: Plateau characteristic *I*(s) trace for Au/DBDT/Au.

While S_0 is the distance between the STM tip and substrate at a predetermined set point current (I_0). $S_0$was calculated by the following equation:

$$S_0 = \frac{\ln\left(G_0 \times \frac{V_{bias}}{I_0}\right)}{\frac{d\ln(I)}{ds}} \qquad (14)$$

Where $G_0 = 77400nS$, V bias is the applied voltage between tip and substrate, I_0 is the set point current in the experiment. $\frac{dln(I)}{ds}$ can be obtained as the slop of ln(I) versus distance (which I(s) trace with the evidence that no molecule linked between electrodes). After a linear fitting, we can obtain the slop value, as shown in Figure 34. After calculated the $\frac{dln(I)}{ds}$ value of 30 I(s) traces in each of molecular junction and took the average, the S_0 data were recorded as 0.38nm for Au/DBDT/Au, 0.41nm for Au/TBDT/Au, 0.34nm for Au/6MHI/Au isothiocyanate, and 0.36nm for Au/8MOI/Au molecular junctions.

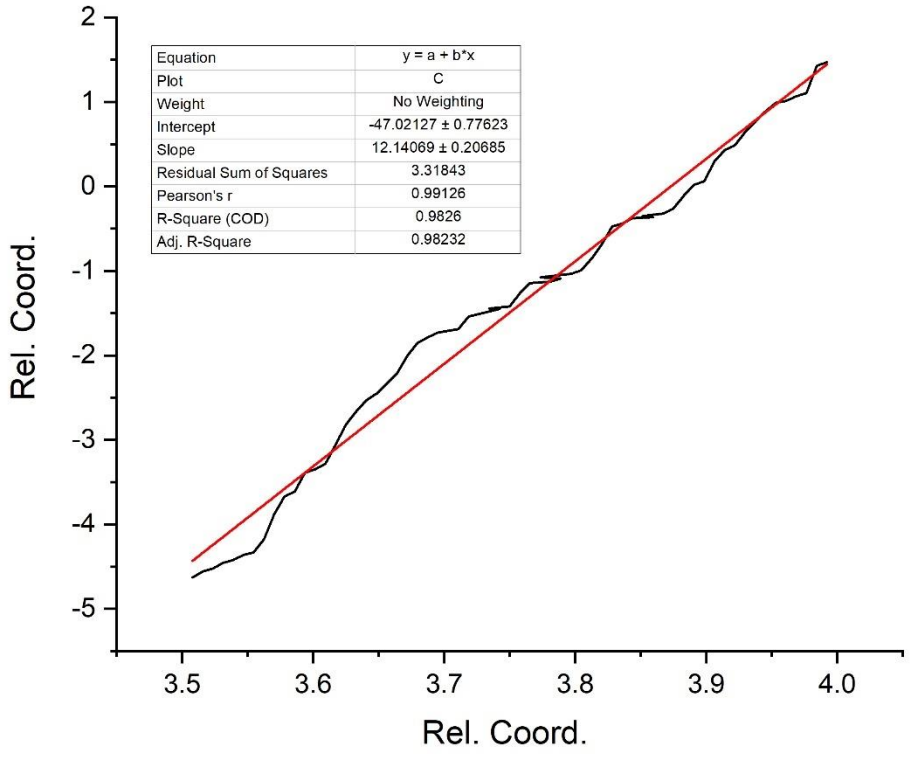

Figure 34: An example for obtaining the $\frac{dln(I)}{ds}$ value.

3.4.3. Unsupervised data analysis approach

Based on the data sorting routine reported by our group previously,[135] the *I*(s) data is sent through a series of filters to remove any noisy signals caused by, for instance, contamination of the electrodes, passivation of the STM tip, fluctuations of the molecular junctions and so on. The *I*(s) trace obtained from STM equipment can be explored into one ASCII documentary, which consisted of distance and current signals in *n* rows as shown in Figure 35a. For each target molecule, over 30 000 *I*(s) traces were measured and collected. This algorithm firstly removes noisy *I*(s) traces. Figure 33b shows typical *I*(s) traces. The green lines exhibit the plateau featuring trace, indicating the formation of molecular junction. The blue lines showed a direct current decay with no molecular junction formed. The red lines in Figure 35b showed three types of noisy traces, which would be filtered out by the X-filter, Y-filter, and peak-filter algorithm respectively. X-filter algorithm removes the noisy leaded the abnormal decay of the current. Y-filter algorithm removes the *I*(s) traces exhibiting an oscillating or excessively noisy signal at the beginning of the current decay, which may arise from poorly contacted molecules, contaminated tips or multiple interacting molecules in the junction. The peak-filter algorithm helps to remove the undesired noisy trace causing an unexpected broad peak in 1D conductance histogram.

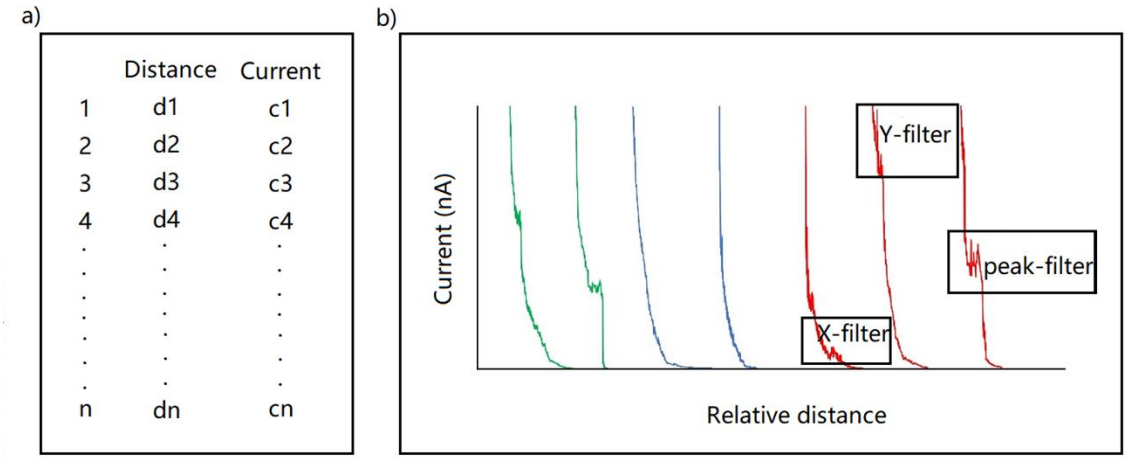

Figure 35: (a) Data structure of *I*(s) data. (b) green: plateau featuring *I*(s) traces; blue: decay traces without molecular junction formation, red: noisy traces which would be removed by X-filter, Y-filter and Peak-filter algorithm.

We then applied conductance mapping algorithm to the experimental data. Here, the measurement result of Au/ 6MHI /Au molecular junction was used as an example to explain this conductance mapping mechanism. We use a conductance mapping process to obtain the most dominant conductance value for a given molecular target. For a single *I*(s) trace the Y-axis (current axis) was simply divided int o many steps (bins). In each bin, the counts of the data points are different, and the plateau region will always have a larger bin count than those adjacent bins. In Figure 36a, we first selected all plateaus featuring *I*(s) traces, then identified the region of the plateaus. From the initial observations in Figure 36a, it is seems that the plateaus distributed in few different groups. The conductance map is then divided into three regions based on the plateau counts.

As shown in Figure 36b, group 1 (red) was deemed to correspond to the decay region without any plateau featured curves included, group 2 (green) reflected the *I*(s) curves with short plateau or small noisy peaks, and the group 3 (blue) is related to the plateau region with expected plateau curves of sufficient extension. Based on the conductance mapping function, we next obtained the optimized plateau distribution mapping. As shown in Figure 36c, for Au/ 6MHI /Au molecular junction, there are four separable plateau distribution regions, which were separated by different color.

This algorithm then plotted a 1D current histogram for each of conductance region automatically, as shown in Figure 36d-g. Figure 36d corresponds to the region 1 (red) in Figure 36c. Figure 36e corresponds to the region 2 (green) in Figure 36c. Figure 36f corresponds to region 3 (black) in Figure 36c, and Figure 36e corresponds to the region 4 (navy) in Figure 36c. The region having the most data values is considered as the most possible (dominated) conductance region, while the other region would be considered as the sub-group. In this measurement, region 1 contains 1021 *I*(s) curves, region 2 contains 1401 *I*(s) curves, region 3 contains 126 *I*(s) curves, and reion4 contains 28 *I*(s) curves. Herein, the Au/6MHI/Au molecular junction, the region 2 (green) in Figure 36c was the dominated conductance region.

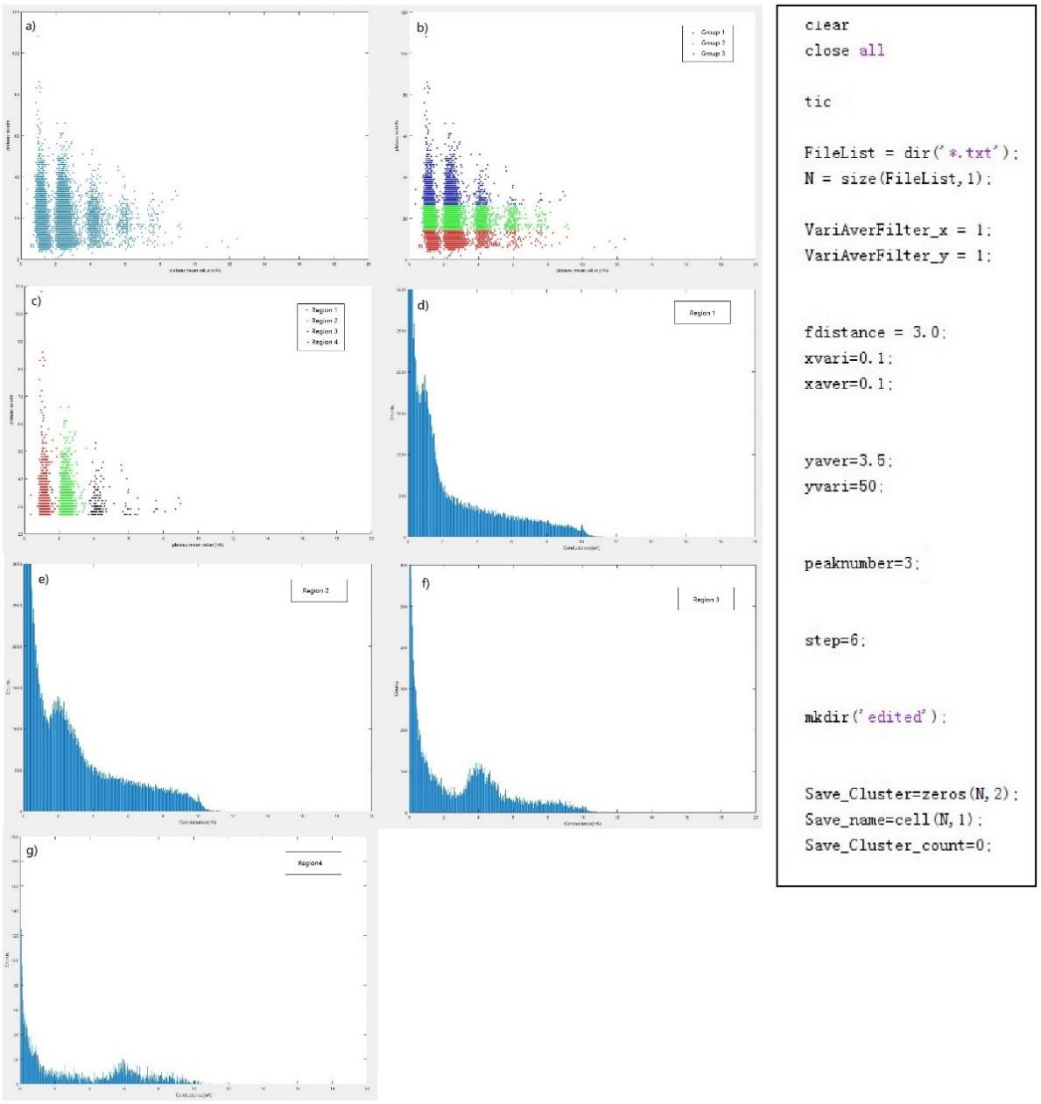

Figure 36: Automatically generated by algorithm (a) Conductance mapping grouped in five regions to get insights in the most dominant conductance peak. (b) Conductance mapping for Au/ 6MHI/Au molecular junction molecular junctions with color-coded grouping into three main regions based on the plateau counts. (c) Conductance mapping of the ideal plateau region, four refined regions were grouped to examine the most dominant conductance peak and sub-groups. (d) 1D current histogram plotted by *I*(s) traces from the region 1 (red) in Figure c, (e) 1D current histogram plotted by *I*(s) traces from the region 2 (green) in Figure c, (f) 1D current histogram plotted by *I*(s) traces from the region 3 (black) in Figure c, (g) 1D current histogram plotted by *I*(s) traces from the region 4 (navy) in Figure c. After determining the dominated current region, the relative conductance could be obtained by $G = \frac{I}{V_{bias}}$. The right inset is the used MATLAB algorithm parameters.

3.5. Conductance results

The 1D conductance histogram plotted by the *I*(*s*) traces from the dominated region is shown in Figure 37a, where the peak position indicated the conductance value is 6.55 nS for Au/6MHI/Au molecular junctions. Figure 37b shows the distribution of ΔS for all the measurements, the average experimental break off value was found to be 0.60 nm, the relative S_{total} could be obtained as 0.94 nm which agrees well to the molecular size.

To provide further insight into the experimental results, we plotted the conductance histogram of second most data contained region 1 of Au/6MHI/Au, as shown in Figure 37c. The conductance value reported by region 1 of Au/6MHI/Au molecular junctions is 3.20nS. The relative break-off distance was found to 0.65nS, while the S_{total} could be obtained as 0.99 nm which also agrees well to the molecular size. We notice that similar S_{total} were recorded in region 1 and region 2. This phenomenon identified that the difference conductance value between region 1 and region 2 could lead by the difference binding geometry of molecule/electrode, rather than various numbers of bridged molecules.

We subsequently plotted the conductance histogram that obtained from region 3. There are only 126 valid *I*(s) curves are contained in region 3. Compared with region 1 and region 2, the data volume of region 3 is dramatically reduced. The 1D conductance histogram of region 3 was shown in Figure 37e, the peak position indicated a relative higher conductance value, in which is 13.3nS. The break-off distance calculation revealed more details of the molecular junctions in region 3. As shown in Figure 37f, the average experimental break off value obtained from region 3 is 0.39nm, as well as the S_{total} is 0.73nm. remarkably, this S_{total} value is smaller than the 6MHI molecular size. If the bridged 6MHI is leaning on the gold substrate, the break-off distance would be decrease. In addition, in this kind of configuration, electrons could transport through the molecular junction without having to transport all this molecular backbone, which could effectively reduce the resistance. This experimental finding supports that the higher conductivity of molecular junction could be leaded by the tilt of the bridged molecules.

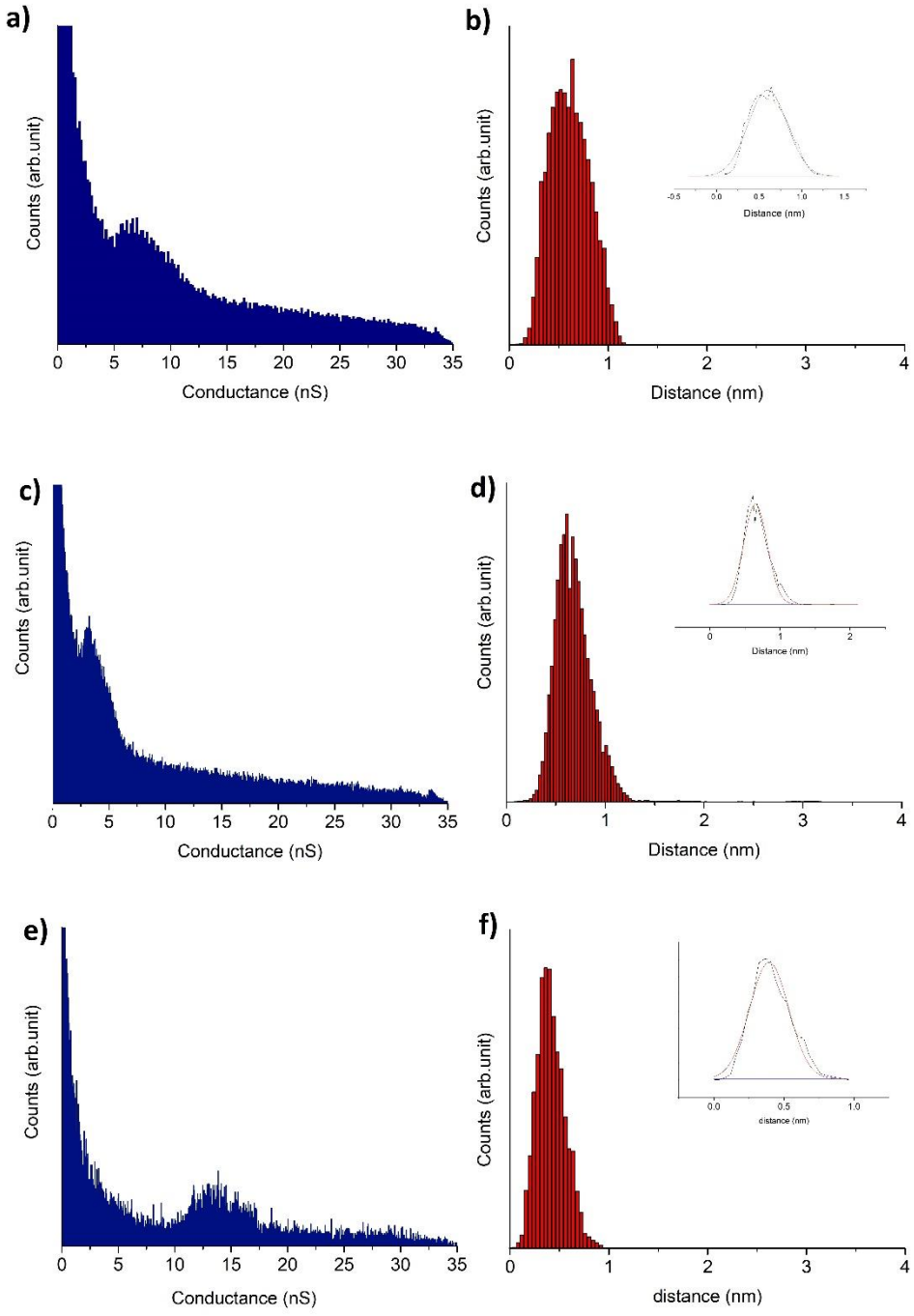

Figure 37: (a) The 1D conductance histogram of Au/6MHI/Au (region 2, dominated region), (b) the break of distance of relative molecular junctions, where the inset is the Gauss peak fitting. (c) The 1D conductance histogram of Au/6MHI/Au (region 1), (d) the break of distance of relative molecular junctions; (e) The 1D conductance histogram of Au/6MHI/Au (region 3), (f) the break of distance of relative molecular junctions.

The mapping results that automatically generated by algorithm of Au/8MOI/Au molecular junctions are shown in Figure 38a, b. There are four distinct conductance regions are recognized as shown in Figure 38b, where the region 1(red) is the dominated region. The relative 1D conductance histogram is shown in Figure 38c, where the peak position indicated the conductance value is 2.16 nS. Figure 38b shows the distribution of ΔS for all the measurements, the average experimental break off value was found to be 0.43 nm, the relative S_{total} could be obtained as 0.79 nm. The measured break-off distance is smaller than the molecular size of 8-(methylthio) octyl isothiocyanate (1.36 nm). This result indicates an unexpected tilt of the bridged molecules between the STM tip and substrate. This kind of tilt of bridged molecule could lead to a higher measurement value. We further compared this asymmetry $\mathrm{Au/CH_3SH-(CH_2)_n-NCS/Au}$ molecular junction to the previous reported symmetric $\mathrm{Au/NCS-(CH)_2-NCS/Au}$ junction.[130] The conductance values have been reported as 15.48 nS ($2\times10^{-4}G_0$) $\mathrm{Au-NCS-(CH_2)_6-NCS-Au}$, and 2.63 nS ($0.34\times10^{-4}G_0$). Through the comparison, we found that the asymmetry anchoring group will decrease the conductance value. It is worth noting that for the asymmetry anchoring group system, the conductance decreases with the increasing molecular length, but the attenuation trend is slower than the $\mathrm{Au-NCS-(CH_2)_6-NCS-Au}$. This conductivity decreasing due to asymmetry molecular junction had been reported in our previous research,[76] which has been rationalized by the breaking of junction symmetry, the variation of electrode/molecule coupling and the further energy level alignment.

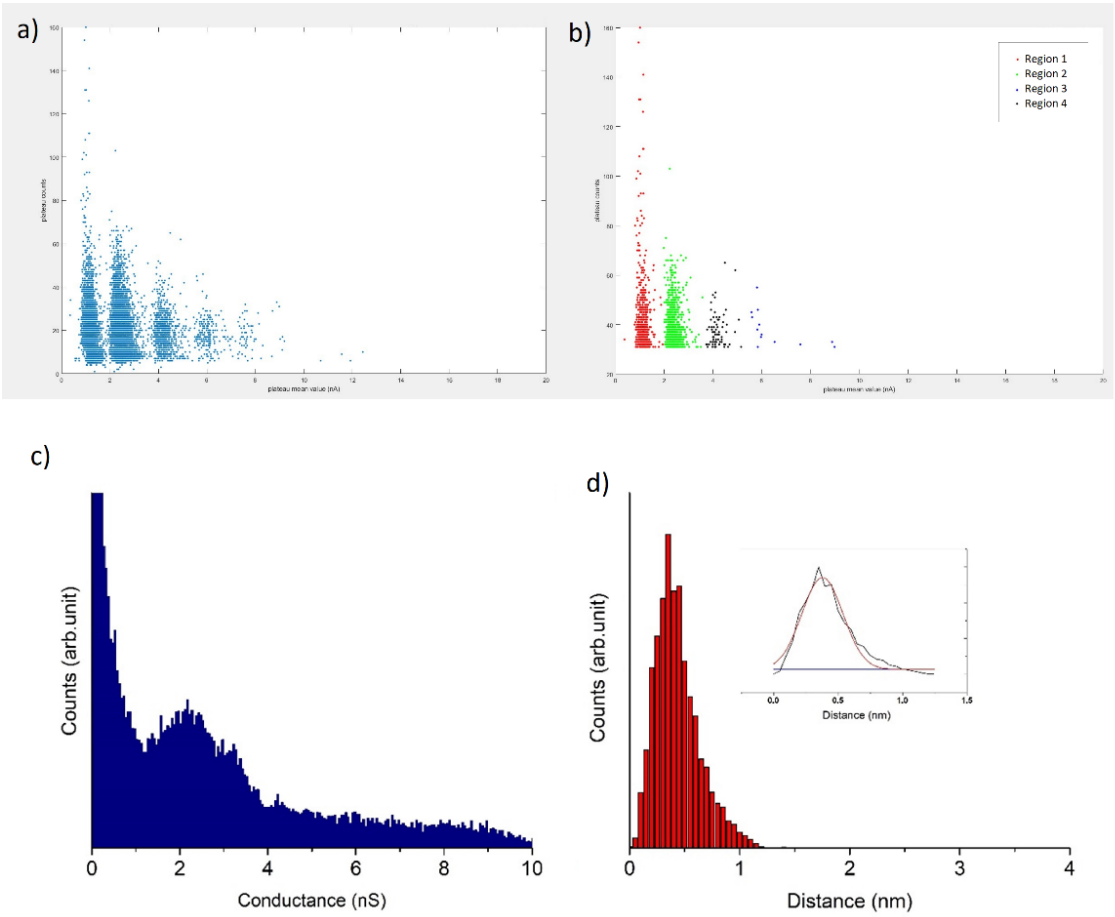

Figure 38: Automatically generated by algorithm (a) Conductance mapping for of Au/8MOI /Au molecular junctions grouping into few regions after removing the noisy *I*(s) traces. (b) Conductance mapping of the ideal plateau region, three refined regions were grouped to examine the most dominant conductance peak and sub-groups, where region (1) red is the most possible conductance region. (c) The 1D conductance histogram plotted by the *I*(s) traces that came from region 1 in Figure b, (d) the break of distance of relative molecular junctions, where the inset is the Gauss peak fitting.

The mapping results that automatically generated by algorithm of Au/DBDT/Au and Au/TBDT/Au junctions are shown in Figure 39. For Au/BDBT/Au junction, there are three main distinct conductance groups, where the region 1 (Figure 39b) represented the dominated conductance group. The conductance behavior of Au/TBDT/Au junctions seems more complex. It showed five conductance groups in Figure 39d, where region 2 (navy) is the dominated conductance group among these five conductance regions.

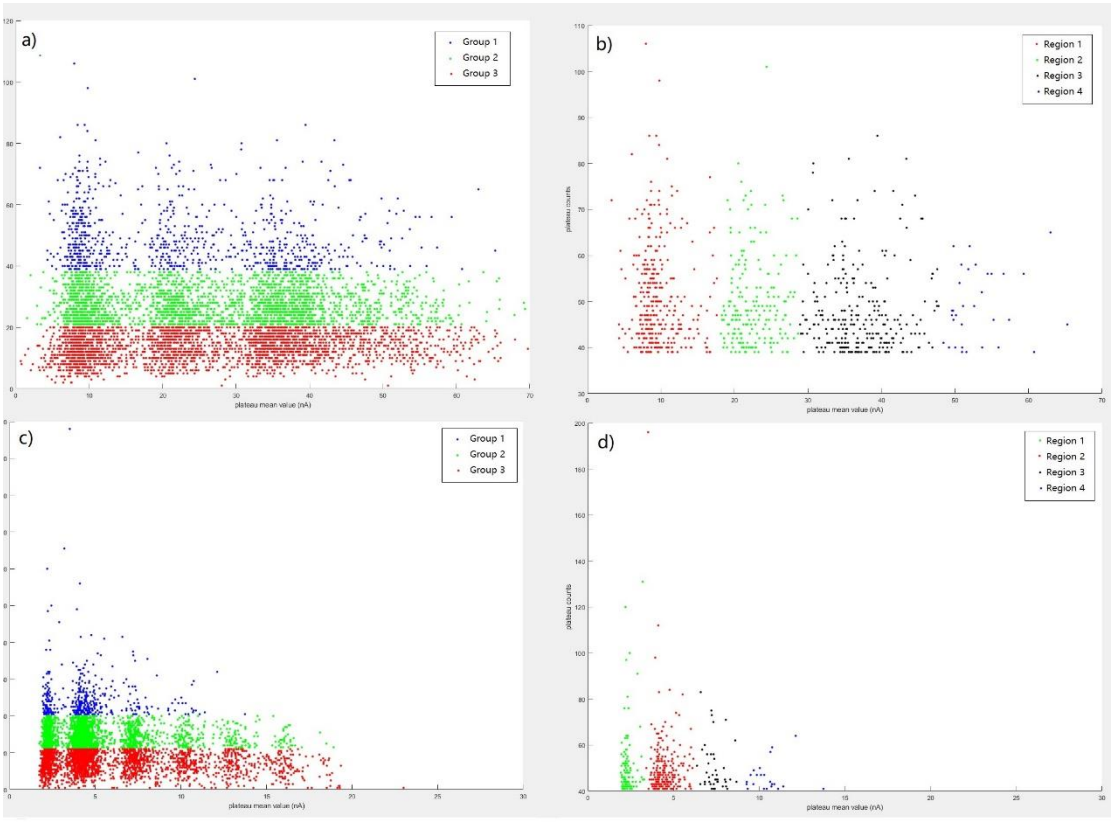

Figure 39: Automatically generated by algorithm (a) Conductance mapping for Au/DBDT/Au molecular junctions with color-coded grouping into three main regions based on the plateau counts. (b) Conductance mapping of the ideal plateau region, three refined regions were grouped to examine the most dominant conductance peak and sub-groups, where region 1 is the dominated conductance region. (c) Conductance mapping for Au/TBDT/Au molecular junctions with color-coded grouping into three main regions based on the plateau counts. (d) Conductance mapping of the ideal plateau region, five refined regions were grouped to examine the most dominant conductance peak and sub-groups, where region 2 is the dominated region.

The dominated 1D conductance histogram of Au/DBDT/Au, as shown in Figure 40a, was plotted by the *I*(s) traces from region 2 in Figure 39b, where the conductance was recoded at 117.5 nS through a Gauss peak fitting. Figure 40b shows the distribution of ΔS for all the measurements, the peak position is 0.88 nm, so the relative S_{total} is obtained as 1.26 nm, which agrees well to the molecular size. However, the maximum of ΔS reaches 1.83 nm, which is much longer than the molecular size. Therefore, some unexpected junction formation, such as two bridged molecules, may have been occurred in the measurements. The details of the configuration of these molecular junctions need to be further validated prospectively.

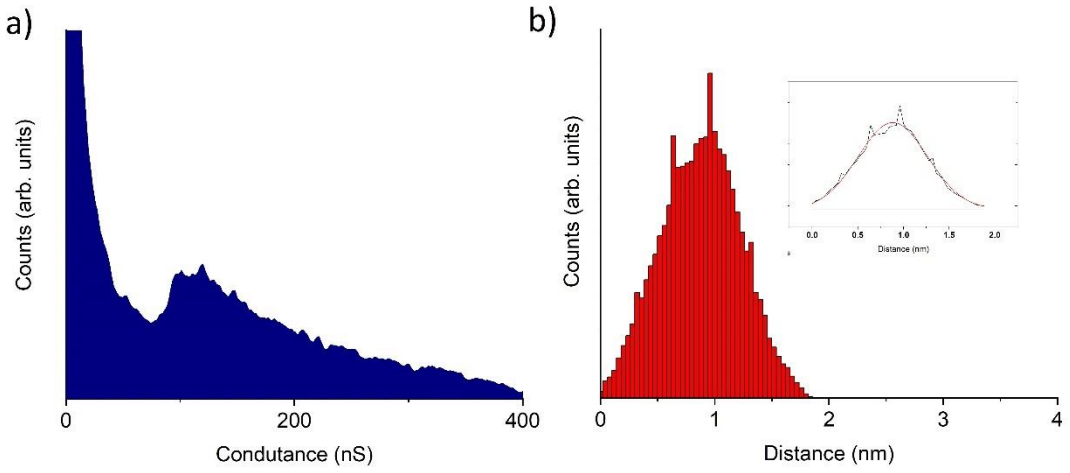

Figure 40: The 1D conductance histogram of Au/DBDT/Au, (b) the molecular junction break-off distance of relative molecular junctions, where the inset is the Gauss peak fitting.

The dominated 1D conductance histogram of Au/TBDT/Au, as shown in Figure 41a), was plotted by the *I*(s) traces from region 2 in Figure 39d, where the conductance was recoded at 32.1nS after a Gauss peak fitting. Figure 41b shows the distribution of ΔS in measurement, the peak position is 0.72 nm, so the relative S_{total} could be obtained as 1.13nm, which is slightly smaller than the molecular size of TBDT. This result could indicate an unexpected tilt of the bridged TDBT between the STM tip and substrate. In addition, we found that, the conductance values (117.5nS and 32.1nS) of Au/DBDT/Au and Au/TDBT/Au obtained using the unsupervised MATLAB algorithm

are basically coinciding with the manual selected conductance value we reported in Chapter 2, which are 126nS and 23.2nS, suggesting the robust and reliable features of this unsupervised data selection algorithm.

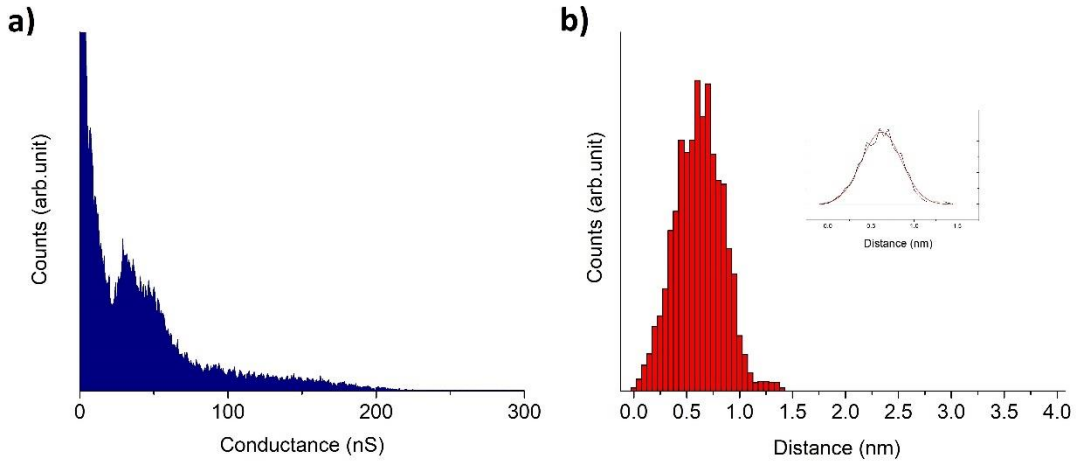

Figure 41: The 1D conductance histogram of Au/TBDT/Au, (b) the molecular junction break-off distance of relative molecular junctions, where the inset is the Gauss peak fitting.

The specific conductance value of Au/6MHI/Au, AU/8MOI/Au, Au/DBDT/Au and Au/TBDT/Au were recorded in Table 3. By comparing the electronic properties of these chain shape and phenyl ring bridged molecular junction within Au/Au contacts, the conductance of phenyl ring based molecular junction is significantly greater than the chain shape molecular junction even they possess similar molecular length. This finding is explained by the conjugated electrons located in phenyl ring-based molecule could increase the overall conductance performance.

Table 3: The conductance value and break-off distance of Au/6MHI/Au, AU/8MOI/Au, Au/DBDT/Au and Au/TBDT/Au systems based on unsupervised data analysis.

Molecule	Molecular length (nm)	Conductance (nS)	Average break-off distance (nm)
6MHI	1.12	6.55	0.94
8MOI	1.36	2.16	0.79
DBDT	1.05	117.5	1.26
TBDT	1.47	32.1	1.13

3.6. Conclusion

In this study, we have investigated the conductivity of four molecular junctions with Au/Au contacts using STM-*I*(s) technique. A fully automated and unsupervised data sorting algorithm was used to analyze the most dominant conductance groups. Summarizing the experimental results detailed above, the following general observations can be made:

1. This unsupervised MATLAB algorithm has been successfully applied to analyse the conductance behavior for Au/6MHI/Au, Au/8MOI/Au, Au/DBDT/Au and Au/TBDT/Au systems.

2. The conductance of phenyl ring based molecular junction is significantly greater than the chain shape molecular junction even they possess similar molecular length.

3.The measured break-off distance value of Au/8MOI/Au and Au/TBDT/Au are shorter than their respective molecular length, which indicated a possible tilt configuration of the bridged molecules.

4 Chapter 4: Measurement of redox active molecular junction

4.1. Preface

This research was carried out in collaboration with the theoretical calculation by Dr. Yannic J. Dappe (CEA, CNRS, France). I will present my experimental work on the molecular synthesis, and the further conductance measurements.

The single-molecular conductance of a redox active viologen molecular bridge between Au/graphene electrodes has been studied in an electrochemical gating configuration in an ionic liquid medium. A clear "off-on-off" conductance switching behavior was achieved through gating of the redox state when the electrochemical potential is swept. Au/viologen/graphene junctions showed a single-molecule conductance maximum centered close to the equilibrium redox potential. A simple gating model within Density Functional Theory (DFT) revealing the charge state evolution of the molecule supports this result. This work opens perspective for graphene-based molecular transistors.

4.2. Introduction

4.2.1. Gating of molecular junction

Using a single molecule to work as a simple wire to connect electrodes and transport electrons is the fundamental aspect of molecular electronics. After understanding the principle of the construction of (single) molecular junction, the attempts were made to a higher goal of molecular electronics, namely using a single molecule to work as an active electronic component, such as molecular switch and molecular diode, to perform a series controllable functions. In molecular electronics, a technical deliverables three-terminal molecular device relies on external modulation of molecular orbitals, has been the prominent challenge.[4]

Many methods have been studied to control the conductivity of the individual molecular junction, such as the solid-state gating,[136-139] optical gating,[140] pH value gating,[141] temperature gating,[114,142] and electrochemical gating,[143-149] opening a way for the use of molecular electronics more than just carrying the charge. A striking development recently is to achieve single-molecule transistor, an analogue of field

effect transistors in solid-state devices. In this configuration, a single molecule is tethered between two contacting electrodes (source and drain), while a third electrode is modulated, acting as a gate bias to control the conductance across multiple redox states of the target molecule.

For a solid-state device, the major challenge in technique that the effective gating requires the positioning of the third electrodes in extremely proximity of the linked molecule. An alternative approach to achieve the third terminal gating effect of molecular junctions is to use an electrochemical gate. This is typically achieved by an electrochemical scanning tunnelling microscope (EC-STM) technique. Operating the molecular junctions in electrochemical condition presents the advantage that two potential differences can be controlled separately, namely the bias voltage between STM tip and substrate (source and drain electrodes), and the gating potential between each working electrode and a reference electrode.

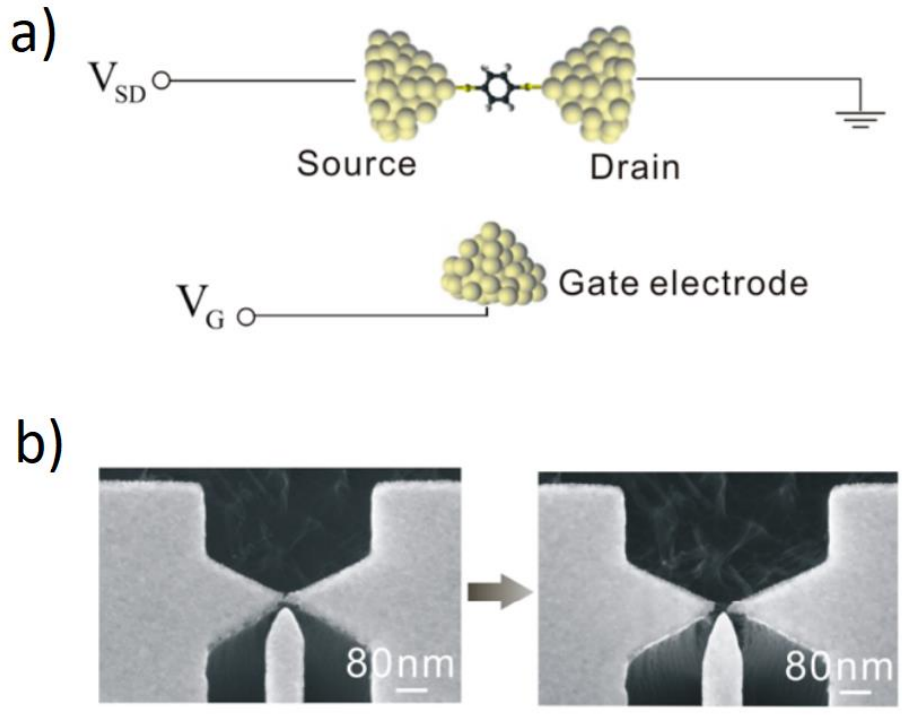

Figure 42: (a) Schematic illustrating a three terminal molecular device, the gate electrode was used to provide the gating effect. (b) SEM) image of a microfabricated MCBJ with a third gating electrode. [Copyright, American Chemical Society, Ref.136]

Comparing with other gating configuration, electrochemical gating method shows obvious advantages, for instance relative easy fabrication while producing high and stable gate efficiencies. The implementation of electrochemical gating follows the progress of nanoelectrochemical technique, which is commonly realized using a four-electrode bipotentiostatic electrochemical scanning tunnelling microscope (EC-STM) technique.[144-149] This technique can provide (single) molecular junctions a controllable electrochemical environment and measure the electronic properties at the meantime.

4.2.2. Redox active molecular junction

Viologens, 1,1'-disubstituted-4,4'-dipyridinium dications have been widely studied concerning the kinetics and mechanism of their redox reactions. The special electrochemical behavior of viologen which possess multiple electroactive sites has been the subject of early researches.[150,151] The interest of "viologen" compound lies in a two-step redox reaction of the 4,4'-bipyridinium (V^{2+}) moiety being electrochemically reduced to its radical cation form $V^{+\cdot}$ and further reduced to V^{0}, "Viologen" molecular wire started to enter the vision of molecular electronics at the beginning of the twentieth century. A Liverpool group have studied the electron transport properties of molecule wire containing the viologen core moiety bound symmetrically between a gold STM tip and a gold substrate.[12] They described a successful gating of gold/viologen/gold system when applied a negative electrochemical gating potential could resulted in an obvious increase in the molecular junction conductance. Based on these impressing finding, Wandlowski group further studied an Au/viologen core unit/Au molecular junction formed with gold STM tip, N-hexyl-N'-(6-thiohexyl)-4,4'-bipyridinium bromide and gold (111) substrate in an electrochemical environment.[152] In general, viologen based molecule wires have been the most widely investigated electrochemical molecular junction system, with a focus on the electron transfer properties, electrochemical gating, electrolyte effect, molecular structure effect, counter-anion dynamics.[144,152-155] The results of electrochemical viologen molecular junction showed the redox center of linked molecule could be reduced and oxidized reversibly to produce different conductance states, making them ideal candidates to molecular transistor.

Since then, varied redox active molecules have wildly used in three-terminal molecular devices. Liao et al.[156] have investigate the conductance behavior of a redox-active dithiolated tetrathiafulvalene derivatives (TTFdT) which has been bridged in two-dimensional nanoparticle arrays. The target TTFdT molecule could undergo a reversible two electron redox reaction as shown in Figure 43. They reported d a conductance increase of the TTFdT by up to 1 order of magnitude when it has been oxidized to its dication state.

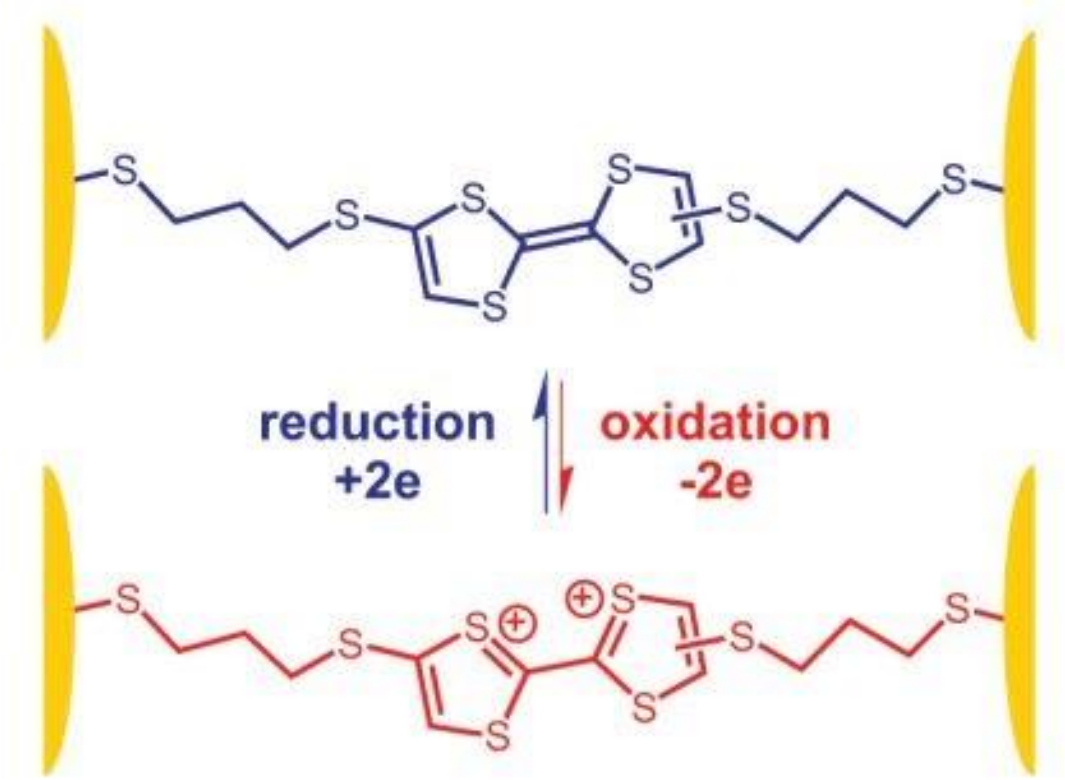

Figure 43: The redox-active dithiolated tetrathiafulvalene (TTFdT) studied by EC-STM technique. [Copyright, American Chemical Society, Ref.156]

Transition metal complexes have also been considered as potential redox active molecules in building three-terminal devices.[98, 157-160] As early as 2002, Park et al. have dominated that the Co ion bonded to polypyridyl ligands can act as a single molecular transistor.[158] Electrochemically gating effect also been realized to achieve conductivity modulation of metal complexes. Chappell et al. presented evidence that, for redox-active metal complexes, an off-on-off conductance behavior could be achieved via electrochemical gating, as shown in Figure 44. They also suggested that the hopping mechanism may be a significant factor for the relative electron transport.[98]

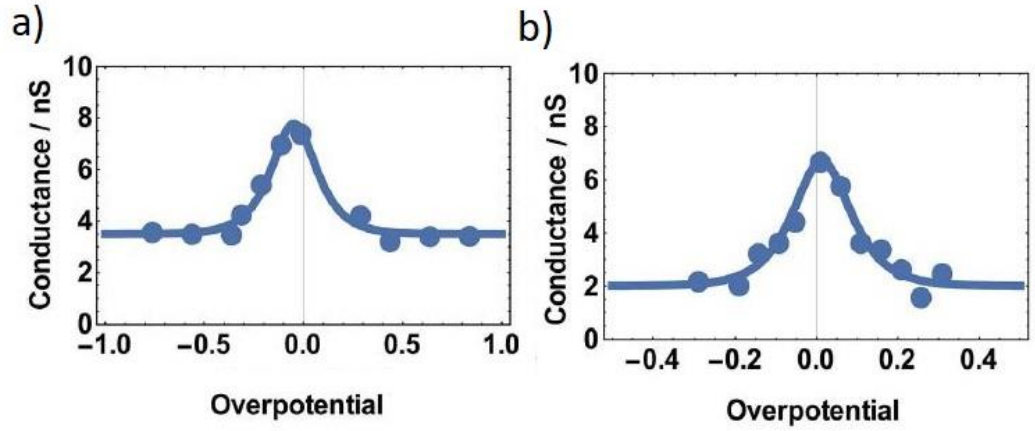

Figure 44: Conductance as a function of overpotential plots for (a) $[Co(pyterpy)_2]^{2+/3+}$ and (b) $[Fe(pyterpy)_2]^{2+/3+}$ in ionic liquid. [Copyright, The Royal Society of Chemistry, Ref. 98]

4.2.3. Ionic liquid

In the studies of electrochemical gating molecular devices, ionic liquid play an important role that act as a good electrolyte.[98, 144] Ionic liquids (ILs) are considered a novel 'green solvents' which almost composed entirely of anions and cations but exist in the liquid state at ambient conditions. Ionic liquid is very similar composition to salt, so ionic liquid had been called room temperature molten salt at the early stage of the study. However, with the further research, people considered the definition of room temperature molten is too narrow. Recently, Ionic liquids are considered as low melting point molten salts, with those that exist as liquid-form under 100℃ and are chemical stable upon exposure to ambient condition.

Interest in ILs are also led by the unique solvent ability to tune the solvent properties of the ILs by variation in the structure and composition of the cation and anion. ILs are characterized by weak interactions, leading by the combination of a large cation and a charge-delocalized anion.[161] This results in a low tendency to crystallize due to flexibility (anion) and dissymmetry (cation). For ILs, the cation regulates the melting point,[162] electrochemical window[163] and the viscosity of solvent.[164] while the anion could tune the solubility,[162] solvating ability,[165] thermal ability[165] and also the electrochemical window.[163] Comparing with traditional organic solvent, ILs possess many promising properties such as high ionic conductivity, low vapor pressure, wide liquid range, and high thermal stability.[166] For example, the melting point of ILs can drop as low as $-90℃$ the liquid rang can achieve 200℃, the electrochemical widow even can spanning up to 6V in some case, vapor pressure can be up to ~300–400℃. while the decomposition temperature can be reach 400℃.[167,168] Throughout the recent decade or so, ILs have been widely used in many areas of chemistry including organic, and inorganic synthesis, biphasic catalysis, separations processes and electrochemistry and electrodeposition due to their unique and useful properties.

ILs also have the potential to be the basis of important approaches in electrochemical conductance gating of single molecular junctions. The first study of single molecular junctions in ILs was reported in 2006. Albrecht et al. have investigated an Os bisterpyridine complex (Ossac) monolayer on Au(111) surface in 1-butyl-3-methylimidazoliumhexafluorophosphate (BMIM-PF_6) electrolyte by STM.[169] They compared the CV data of Ossac measured in aqueous solution and ionic liquid as shown in Figure 45, the redox peak showed a slight shift in these two different solution. Then thy reported that Ossac system showed an imposing 50 fold increase in tunnel current from the off state to the on state, demonstrating the potential of ILs as environments for single molecular electrochemical gating.

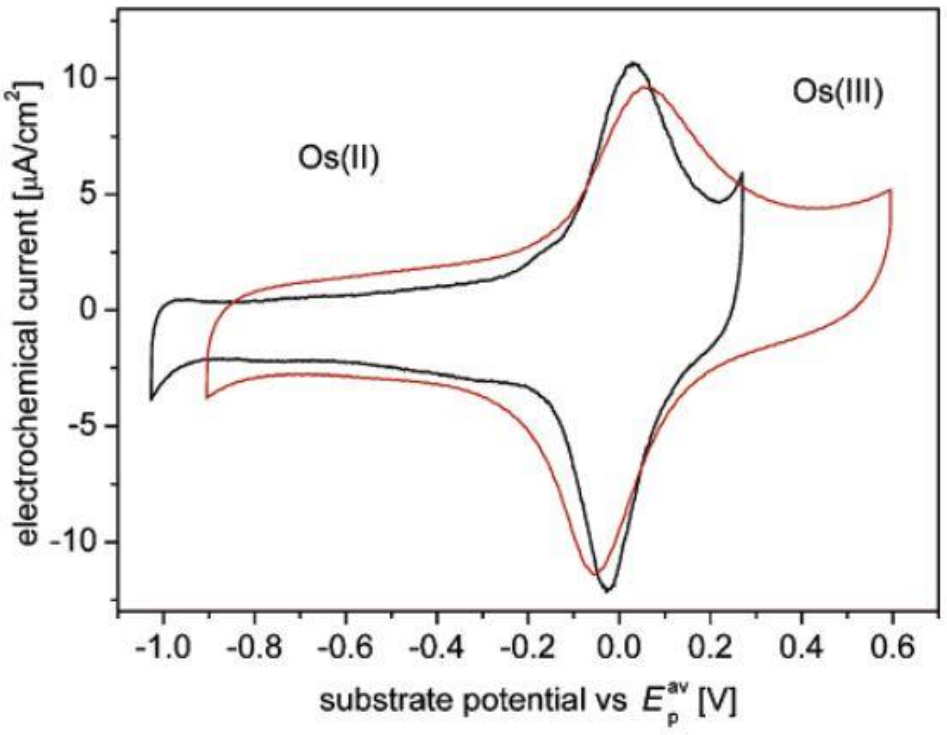

Figure 45: CV recorded for Ossac in (black) aqueous solution, and (red) ionic liquid. [Copyright, American Chemical Society, Ref. 169]

As research continues, scientists found that there are good reasons for using ILs electrolytes in the electrochemical single molecule studies. The most attractive advantage is an ability (wide electrochemical widow) to address redox states that are not accessible in aqueous electrolyte systems.[19] For example, previous study shows that the pyrrolo-TTF molecular wires only presented the first oxidation in aqueous electrolyte,[171] but three redox states could be reached in ILs.[172] So far, there are many studies demonstrated that ionic liquid electrochemical gating of single-molecule conductance is far more effective than gating that is generally achieved in solid-state three-terminal platforms or gating with aqueous electrolyte.

4.3. Research aim

This work utilizes EC-STM technique to realize a controllable three terminal molecular devices. In this research, ILs was used as the electrolyte to provide a stable measurement environment. The main aim of this study was to investigate the

conductance of a redox active 6V6 molecules with both Au/graphene and Au/Au contacts. The conductance of Au/6V6/graphene and Au/6V6/Au junctions are recorded as a function of the variation of the electrochemical potentials to elucidate the effect of third terminal gating effects.

4.4. Method

4.4.1 Synthesis of *N*,*N*'-Di-(6-(thioacetyl)hexyl)-4,4'-bipyridinium bis(hexafluorophosphate)

The used N,N'-Di-(6-(thioacetyl)hexyl)-4,4'-bipyridinium bis(hexafluorophosphate) (6V6) molecule was synthesized by a three-step reactions, which was reported in previous literature.[144] The specific synthetic route was shown in Figure 46. All other reagents were commercially available and used as received.

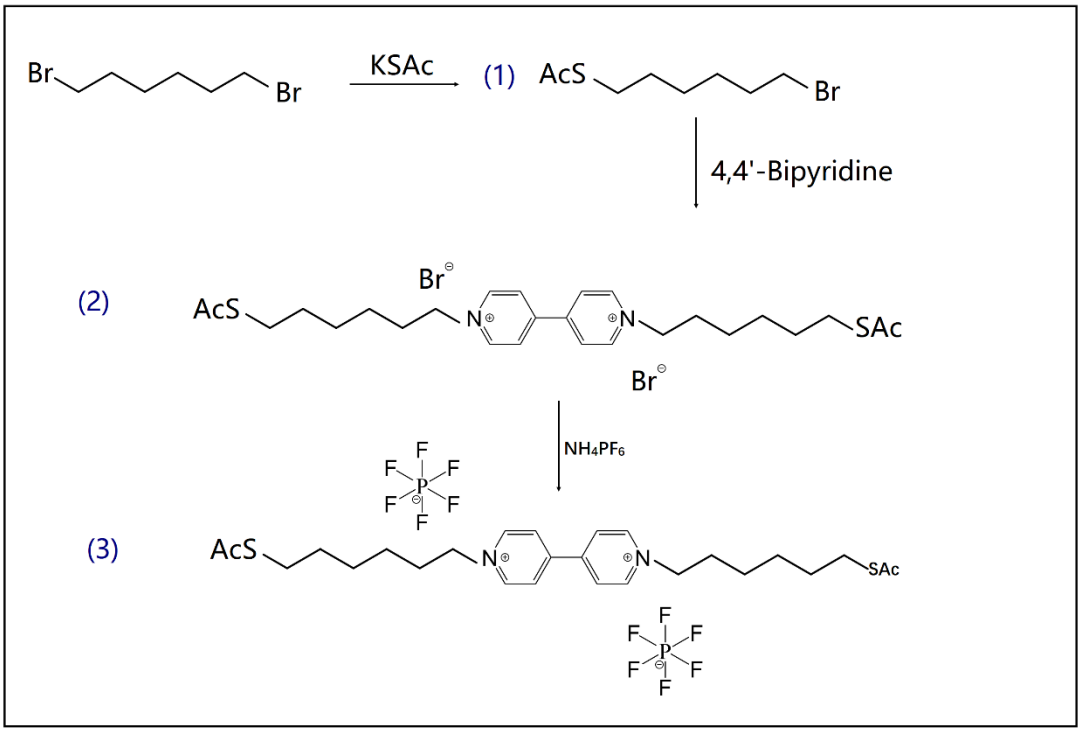

Figure 46: Synthetic route of target 6V6 molecule.

(1) Thioacetic acid S-(6-bromohexyl) Ester. A 250mL round-bottom flask was charged with 50ml THF. Add 1,6-dibromohexane (10.68 g, 43.8 mmol) into flask. An addition funnel containing potassium thioacetate (2.50g, 21.9mmol) in THF was attached to the flask, then the whole apparatus was protected by nitrogen. Then potassium thioacetate solution was added to the 1,6-dibromohexane solution at a rate of roughly 1 drop per second. After the addition was complete, the mixture was stirred for 24h at room temperature (21℃). During the reaction, TLC plate was used to identify the reaction with R_f=hexane: CH_2Cl_2=10:1, while $KMnO_4$ was used as the color developing agent. The ideal reaction is a monosubstitution reaction, the TLC plate showed two product points, the one of more point identified the unexpected disubstituted product. Then the solvent was removed in vacuo. CH_2Cl_2 was added, the org. soln. washed with deionized water. The mixture was then poured into separatory funnel, and the layer were separated. Then the organic phase solution was collected and dried with $MgSO_4$ and evaporated. The crude product purified by column chromatography (hexane: CH_2Cl=10:1) to provided 3.16g, 13.2mmol (60.3%). ^{1}H NMR (400 MHz, $CDCl_3$): δ=3.36 (t, J=6.5Hz, 2H); 2.83 (t, J=7.2Hz, 2H); 2.29 (s, 3H), 1.82(m,2H); 1.55(m, 2H); 1.38(m, 4H) ppm.

(2) N-N'-Di-(6-(thioacetyl)hexyl)-4,4'-bipyridinium dibromide. A 100mL round-bottom flask was charged with 15mL acetonitrile, 1.50g product 1, and 0.25g 4,4'-bioyridine. A condenser-west tube was attached to the flask, the whole apparatus was protected by nitrogen. All the mixture was heated with oil bath to reflux for 30h. After reaction, the mixture was cool to the room temperature (21℃). Then the mixture was sonicated 10 minutes. Then the mixture was filtered by Buchner funnel to get the crude product. Then washed the crude product with cold diethyl ether (40 mL). Then the crude product was purified by recrystallization form boiling EtOH to provide 0.75g product in yield 77%. ^{1}H NMR (400 Hz, methanol-d4): δ=9.37 (d, J=7.2Hz, 4H); 8.87 (d, J=5.6Hz, 4H); 4.87 (t, J=7.2Hz, 4H); 2.77(t, J=7.2Hz, 4H); 2.23 (s, 6H), 2.01 (m, 4H), 1.37 (m, 4H); 1.17 (m, 8H) ppm.

(3) N, N'-Di-(6-(thioacetyl)hexyl)-4,4'-bipyridinium bis (hexafluorophosphate) 6V6. 0.45g product 3 was added into 40mL DI water. Then added 1.16g ammonium hexafluorophosphate into the solution. We can observe the forming of white precipitate immediately. Then filtered the mixture to get white crude product. Then washed the crude product with DI water, then dried the product in vacuo to provided 0.436g final product 6V6 in yield 81.4%. ^{1}H NMR (400Hz, Acetone-d_6), δ=9.47 (d, J=6.8Hz, 4H); 8.86 (d, J=6.4Hz, 4H), 4.99 (t, J=7.6Hz, 4H), 2.85(t, J=4.4Hz,4H); 2.41(s, 6H); 2.22(m, 4H), 1.58-1.46(m, 12H) ppm. ^{13}C NMR (100 MHz, Methanol-d_4, 4096 times scan): 196.32, 145.65, 129.45, 61.83, 30.87, 29.43, 29.20, 29.02, 27.54, 25.10 ppm. HRMS showed intensity peak at 619.202$[PF_6]^+$. The relative ^{1}H NMR, ^{13}C NMR and HRMS are shown in Figure 47.

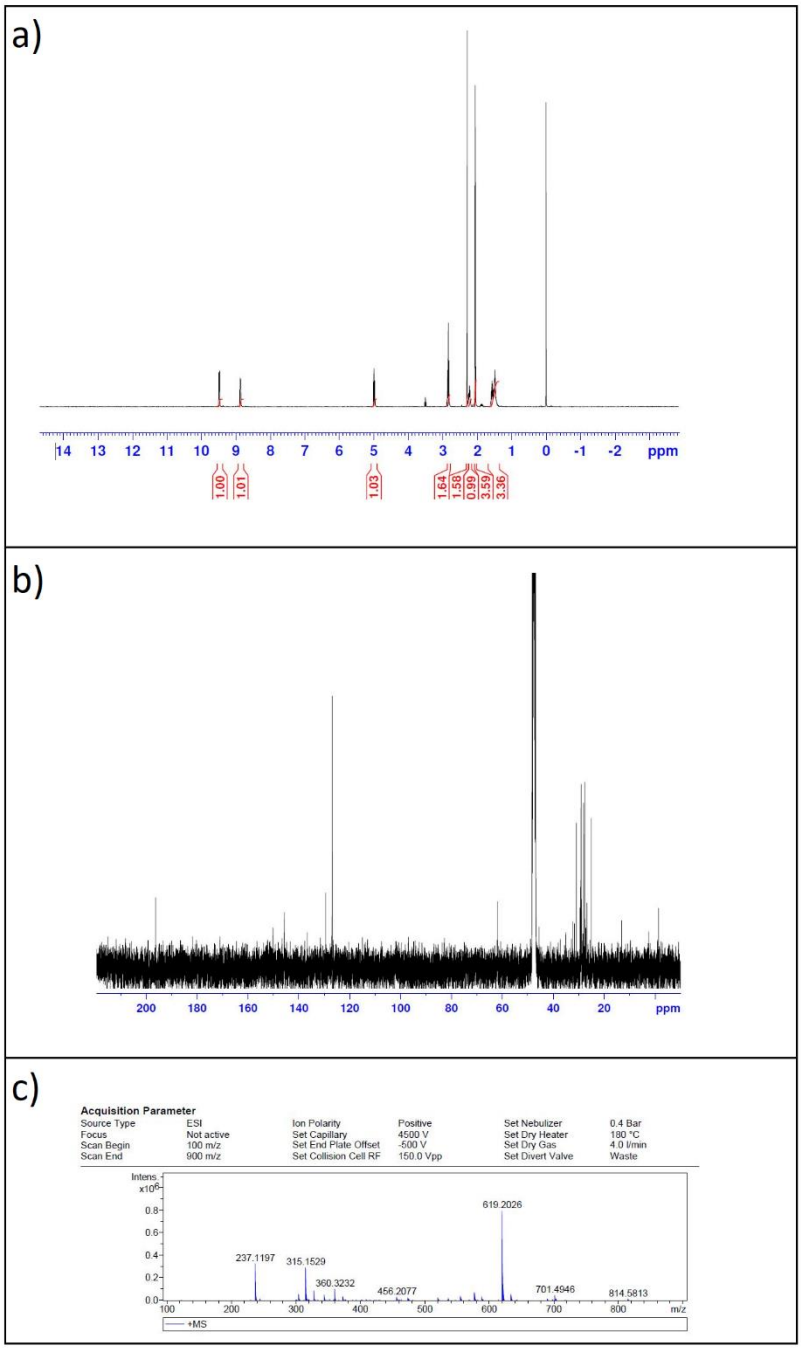

Figure 47: (a) ^{1}H NMR, (b)^{13}C NMR, and (c)HRMS spectrum for synthesized N, N'-Di-(6-(thioacetyl) hexyl)-4,4'-bipyridinium bis (hexafluorophosphate).

4.4.2 Cyclic Voltammetry measurements

A cyclic voltammetry (CV) experiment involves applying a potential to the working electrode, which changes with time. The current flowing through the working electrode is recorded as a function of the applied potential, resulting in a voltammogram of current vs. potential. The cyclic voltammetry experiments were completed using an CHI660E electrochemical workstation. For all experiments, a three-electrode set up was employed.

Here, the cyclic voltammograms were recorded using 99% 1-Butyl-3-methylimidazolium triflate (BMIM-OTf) as the electrolyte solution, which was dried for 24 h to use (80 °C) in air and then degassed by bubbling with nitrogen gas. Measurements were carried out in dried BMIM-OTf with 6V6 (5 mM) solution for graphene working electrode ($1cm^2$) and gold (111) working electrode ($1cm^2$) respectively. All voltammetric measurements were carried out at room temperature. When graphene working as the working electrode, in order to obtain clear CV spectra, a freshly prepared Ag/AgCl (Saturated silver chloride) electrode was served as reference and Pt net as the counter electrode. The potential difference between Ag/AgCl and Pt was calibrated as -0.423V.

4.4.3 Single molecule conductance measurement with electrochemical gating

The gold STM tips were fabricated by the electrochemical etching technique. To minimize the faradic current that generates from the charge transport through the electrolyte at the working electrode (STM tip), the gold STM tips were coated by nonconductive resin material. The coating process is shown in Figure 48a, a resin bar was heated by direct fire till it begins to melt, then move the sharp STM tip into the melt resin. The coated gold STM tip was tested by SEM technique. The top of the gold tip should be carefully coated while only tiny gold sticking out from the tip top as shown in Figure 48c.

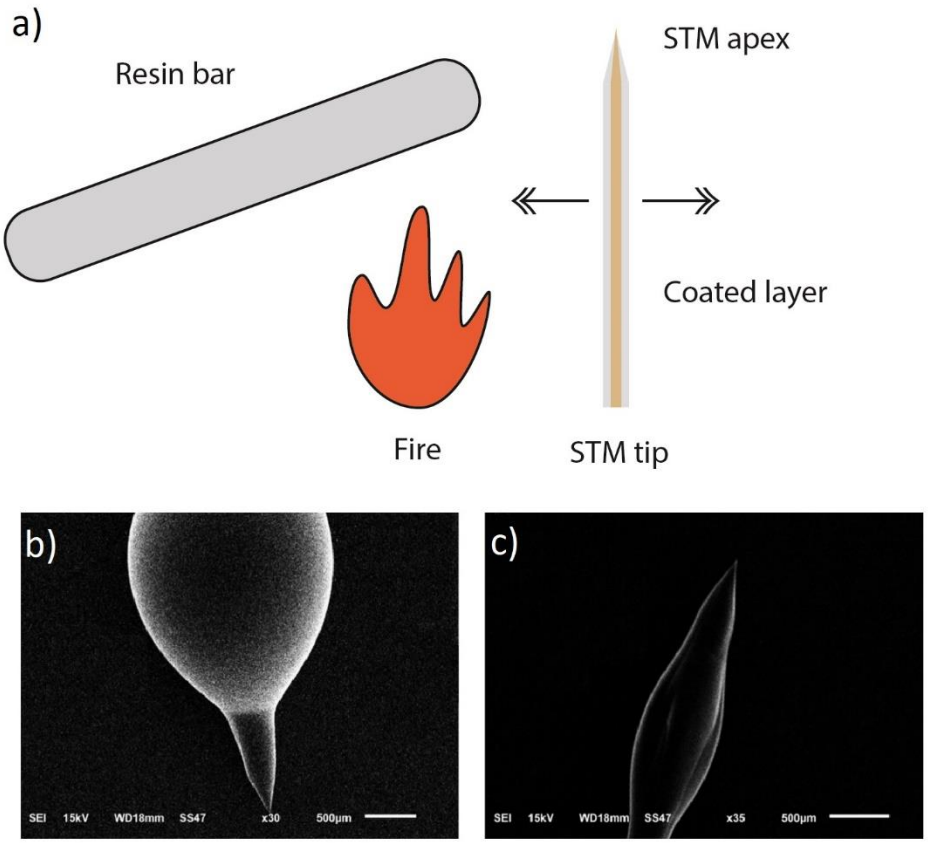

Figure 48: (a) Illustrating of the STM tip coating process. The SEM images of (b) poorly coated gold STM tip, (c) well coated gold STM tip.

In this study, a new electrochemical workstation has been applied to the original STM equipment. A liquid cell, as shown in Figure 49a, was used to provide a liquid environment for forming molecular junctions. The four electrodes EC-STM set-up was used in this measurement, including two working electrodes (STM tip and substrate), a counter Pt electrode, and a carefully calibrated reference Pt electrode. This four-electrode bipotentiostat configuration allows independent electrochemical potential control and the bias voltage between STM tip and substrate, provided that no contact occurs between them. In electrochemical potential set-up, where $E=V_{Sample}-V_{Reference}$. The bias voltage applied to the molecular junction was fixed to + 0.3V and ionic liquid BMIM-OTf was used as the electrolyte for all the measurements (5mM 6V6 in BMIM-OTf). In experiments, the electrochemical gating is considered as the "electrolyte gating" which relies on the formation of electrochemical double layers along the STM tip-substrate channel. The EC-STM method could be considered as a combination of STM *I*(s) method with the electrochemical control, which is utilized by Bruker STM instrument (Multimode 8, USA) with a Fluid cell (ECM-2) here. The overall EC-STM-set-up was shown in Figure 49b, two special wire (where the purple wire linked with counter electrode, and the yellow wire linked with reference electrode) were used to connected the electrodes to the electrochemical workstation.

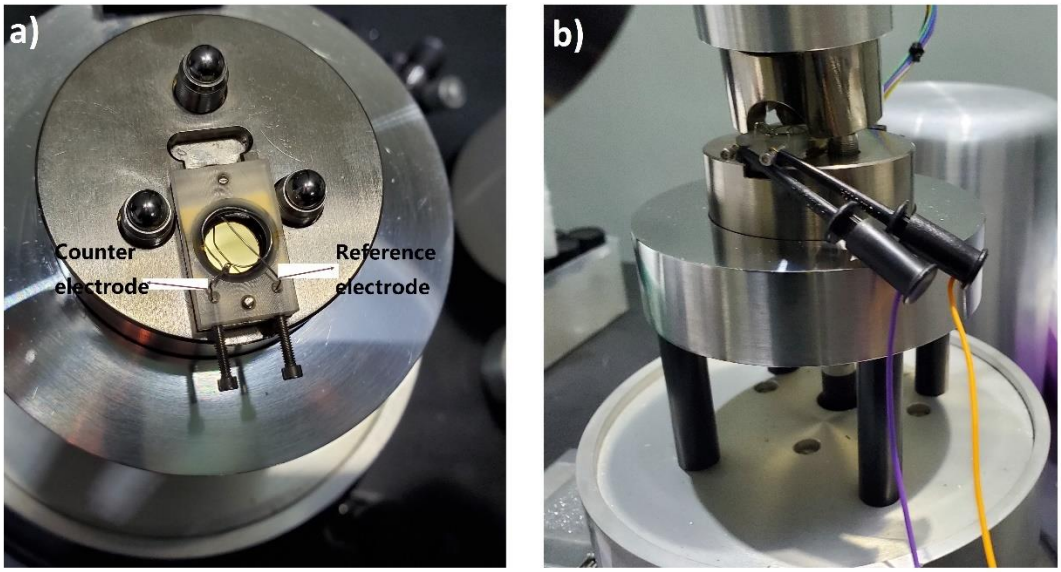

Figure 49: a) Counter electrode and reference electrode set up in EC-STM liquid cell, where a Pt ring are work as the counter electrode and a Pt wire are working as the reference electrode. The counter and reference electrode should avoid contacting with the substrate, at the meantime, these two electrodes should avoid contacting each other. b) The overall set up for EC-STM, where the purple wire contact with counter electrode, while yellow wire linked with reference electrode.

4.5. Results and discussion

4.5.1 Cyclic voltammogram

We firstly examined the electron transfer behavior of 6V6 molecular bridge with graphene as working electrode in BMIM-OTf solution using cyclic voltammetry. Here, Ag/AgCl was used as the reference electrode, because the electrochemical potential of Pt is instable, while the potential difference between Ag/AgCl and Pt was calibrated as -0.415V. The redox active molecular 6V6 exhibits two reversible redox reaction as shown in Figure 50. It undergo a two-electron transfer process, namely $V^{2+} + e^{-} \rightarrow V^{+\bullet}$ and $V^{+\bullet} + e^{-} \rightarrow V^{0}$, with V = viologen. Because of the larger electrochemical window in BMIM-OTf, both electron transfer curves are apparent. It's worth noting that this measured CV shows a sloped baseline, particularly apparent at the second redox wave ($V^{+\bullet} + e^{-} \rightarrow V^{0}$). With the viologens if the ionic liquid is not dry enough the second redox wave cannot be measured, therefore while this slope may be due to a minute amount of residual water, it is unlikely the underlying cause. For the first redox couple ($V^{2+} + e^{-} \rightarrow V^{+\bullet}$) is around 145mV at low scan rate which shows a quasi-reversible electrochemical process.[173] The average $E_{1/2}$ was measured as -0.25V versus Ag/AgCl. Based on Randles-Sevcik equation:

$$i_p = 0.4463nFAC\left(\frac{nFvD}{RT}\right)^{\frac{1}{2}} \qquad (15)$$

Where the i_p is the current maximum in amps, A is the electrode surface area in cm^2, n is the number of electrons transferred in the redox event, C is the concentration in mol/cm^3, D is the diffusion coefficient. The diffusion coefficient $V^{2+} + e^{-} \rightarrow V^{+\bullet}$ process in BMIM-OTf was calculated as $D = 2.79 \times 10^{-8}\ cm^2 s^{-1}$.

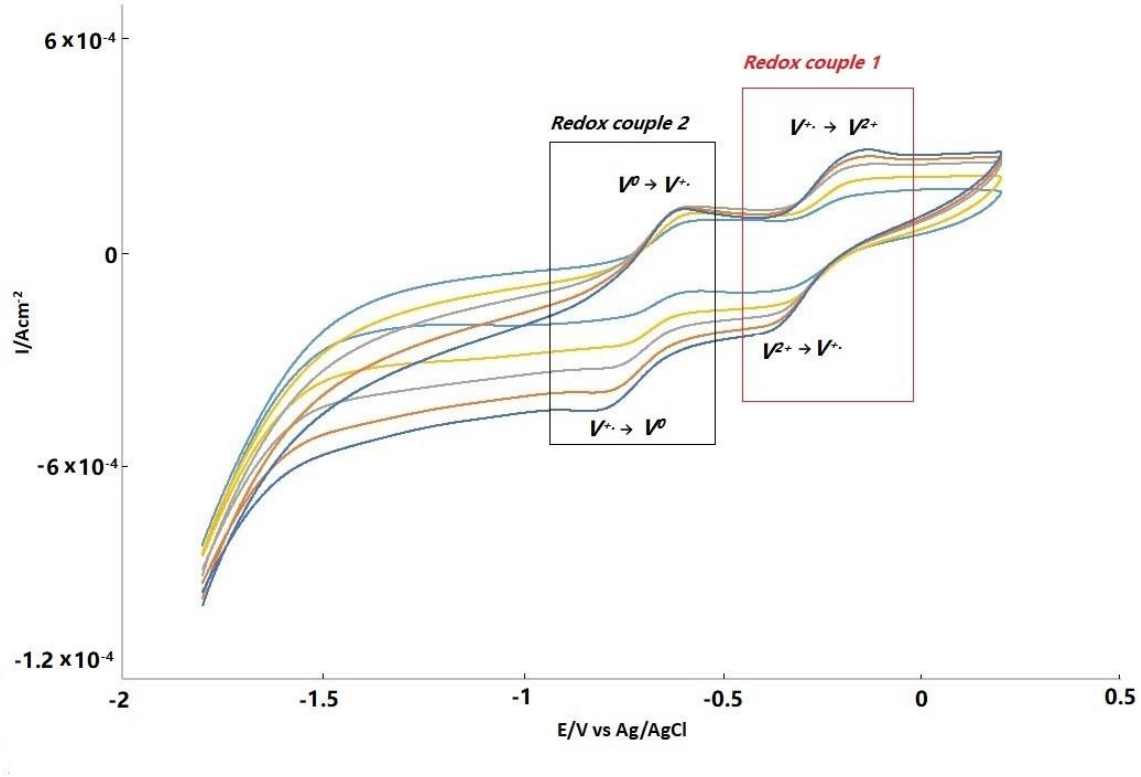

Figure 50: CV recorded for the reduction of 6V6 (5 mM) in BMIM-OTf. The system was referenced against an Ag/AgCl reference. The CVs were run at 0.2 V/s to 1V/s with graphene working electrode, Pt counter electrode and Ag/AgCl reference electrode.

4.5.2 Conductance results

These conductance histograms were recorded for the marked electrochemical potentials and for a constant bias voltage of +300mV. The molecular junctions are formed by the non-contact STM *I*(s) method as same as our previous researches. At first, the tip is brought close to the substrate within tunneling distance by a predetermined current. Then, the tip was retracted while the tunnelling current reached the set maximum current. If there is a failure of the formation of molecular junction, a pure decay *I*(s) decay trace could be found. As well as, if the molecular junction was formed successfully, obvious plateaus could be found in the *I*(s) trace. The current information easily converted to the molecular conductance value (G), by the equation:

$$G = \frac{I}{V_{bias}} \qquad (16)$$

Figure 51 shows the typic conductance versus distance curves. When there is no molecule present between STM tip and graphene substrate, the pure exponential decay could be observed as shown in the yellow curves. While the plateau characteristic *I*(s) traces are shown in green and blue lines which measured with -0.45V -0.35Velectrochemical potentials respectively.

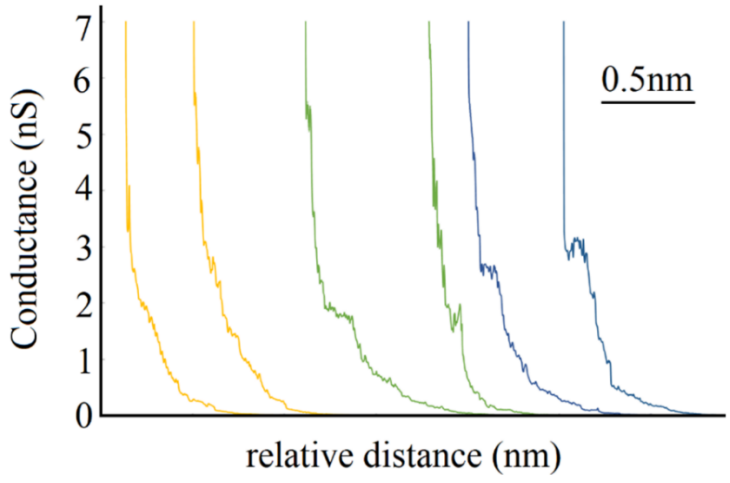

Figure 51: The direct decay *I*(s) trace (yellow). The plateau contained *I*(s) traces of Au/6V6/graphene versus electrochemical potential as a function of the marked electrochemical potential (versus Ag/AgCl), where green: -0.45V, blue: -0.35V.

As a reference for the graphene electrode measurements, the conductance of Au/6V6/Au junctions are measured by STM *I*(s) technique in air atmosphere without electrochemical gating. The sketch of Au/6V6/Au junction was shown in Figure 52a. The conductance of Au/6V6/Au under air atmosphere without external electrochemical gating was measured as 2.16nS, Figure 52b shows the relative 1D conductance histogram.

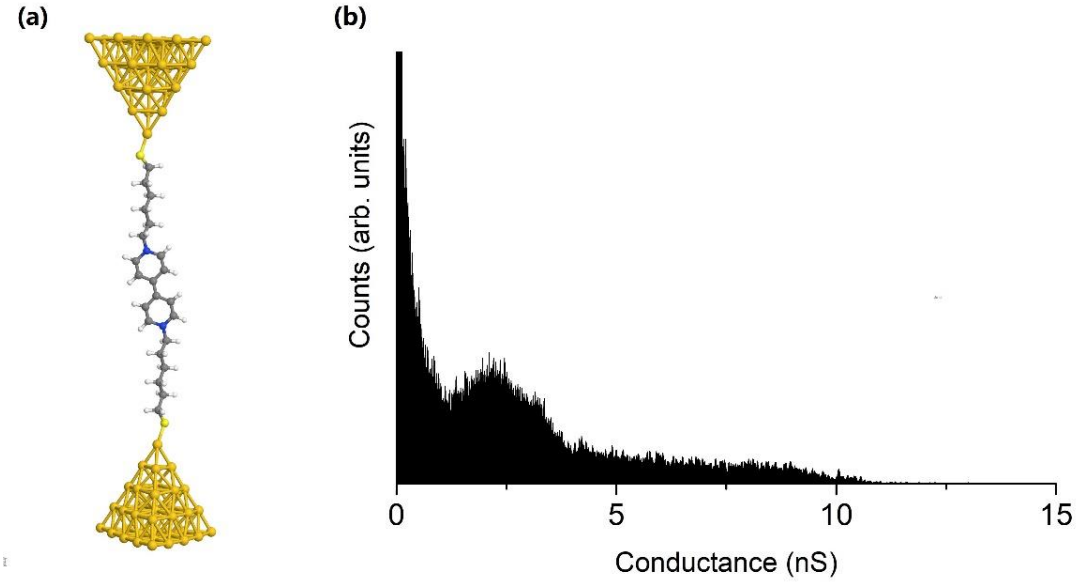

Figure 52: (a) Sketch of Au/6V6/Au junction. (b) The 1D conductance histogram of Au/6V6/Au which has been measured under air atmosphere.

Many studies reported the electrochemistry of viologen moieties attached to Au by alkyl thiol linkers in aqueous electrolytes.[35-37] Here, we move one-step further by using a graphene electrode in IL media. We measured the conductance value of Au/6V6/graphene junction using the EC-STM *I*(s) technique. For each of the molecular junction, which is formed under one specified electrochemical potential, we collected more than 300 plateaus feature *I*(s) curves, then plotted the conductance 1D histograms. Here we presented eight 1D conductance histograms that measured under different electrochemical gating potential, as shown in Figure 53a-h. For each of the 1D conductance histogram, a clear peak is observed, indicating the most prevalent junction configurations and the probable conductance value of the molecular junctions. For these eight 1D conductance histograms, an obvious peak shift with the change of electrochemical gating potential could be observed. The minimum conductance value was recorded as 1.74nS that measured under -0.95V25V (versus Ag/AgCl) electrochemical potential, while the maximum conductance value was recorded as 5.86nS that measured under -0.25V (versus Ag/AgCl) electrochemical potential. In addition, it is noticeable that there is a “shoulder” or “tail” appeared in some of the 1D conductance histograms. These phenomena might arise from the variation of the molecular junction.

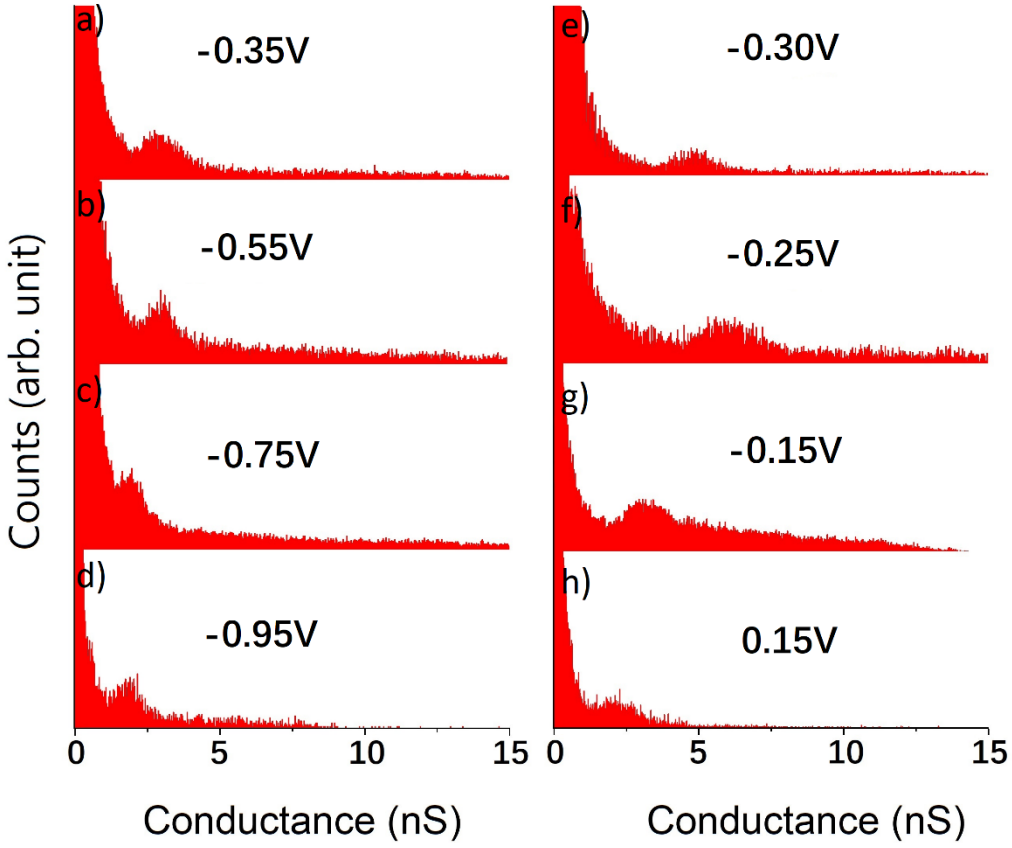

Figure 53: One-dimensional (1D) histogram representations of Au/6V6/graphene conductance behavior record at the electrochemical potentials of -0.95V, -0.75V,-0.55V,-0.35V, -0.30V, -0.25V, -0.15V, 0.15V (versus Ag/AgCl) measured in ionic liquid.

When plotted electrochemically gated single molecule conductance data (taken from the histogram peaks of current plateau values) for fourteen different electrochemical potentials, a bell-shaped profile is observed. As show in Figure 54. we plotted the conductance value obtained for Au/6V6/graphene over the range of electrochemical potential combination with cyclic voltammogram. The error bar was calculated as FWHM of the Gauss peak fitting of the relative 1D conductance histograms. The conductance maximum of around 5.6nS was observed which occurred at around the redox equilibrium potential of first redox reaction $V^{2+} + e^{-} \rightarrow V^{+\bullet}$. As the electrode potential is swept, the system follows a "off-on-off" conductance switching behavior. The experimental data of Au/6V6/graphene system show the maximum molecular conductance close to the $V^{2+}/V^{+\cdot}$ reversible potential, which is similarly to

the well-known Au/Au system . The conductance behavior of Au/6V6/Au system has been reported in aqueous media[106] and ionic liquid media[144] contrastively. The previous research showed that the conductance of Au/6V6/Au shows a monotone increasing with the negative electrochemical gating in aqueous media, while the same Au/6V6/Au system showed a "bell shape" conductance variation in ionic liquid media. In addition, there is a slight increasing of conductance which appeared around -0.55V. This conductance increasing could be considered as a response to the second redox reaction $V^{+\bullet}/V^{0}$, but this phenomenon is not as clear as the first conductance peak. The specific conductance value of Au/6V6/graphene measured under 14 different electrochemical potential were listed in Table 4.

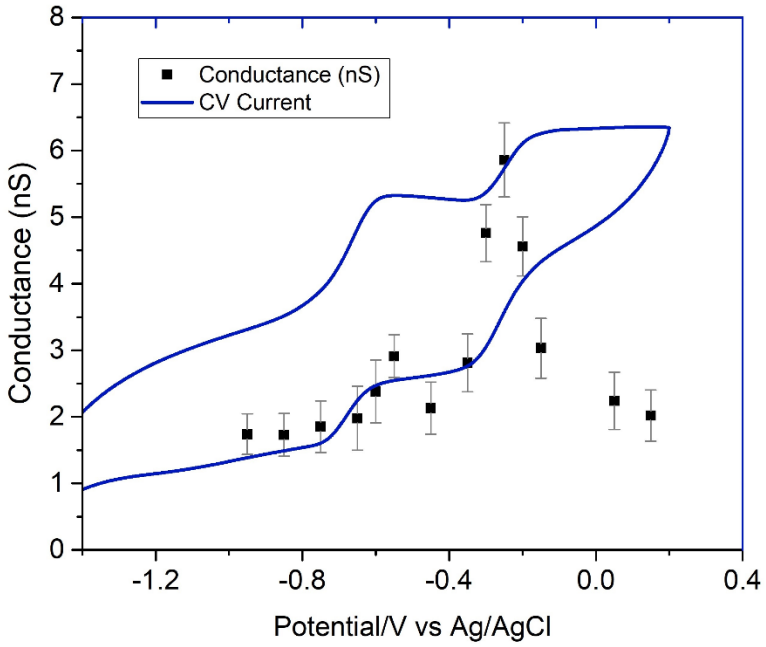

Figure 54: The plot conductance of Au/6V6/graphene against the sample electrochemical potential overlaid with a cyclic voltammogram (blue line) of 6V6 in BMIM-OTf.

This phenomenon could be interpreted in terms of a two-step electron transfer mechanism proposed by Ulstrup and Kuznetzov.[174] The process of electrochemically "gated" electron tunnelling involves the electron transfer from the left contact onto the reduced redox group (step 1), followed by the molecule and surrounding electrolyte partially relaxing (step 2), finally the electron transfer from the redox group (oxidation) onto the right contact (step 3). By gating the potential, the redox state of the molecular wire can be modulated. Around the redox potential of the molecule, it is more favorable for electrons to traverse the molecule, resulting in a large increase in the conductance.

Table 4: The conductance of Au/6V6/graphene system versus gating potentials.

Gating potential (mV) Versus Ag/AgCl	**Conductance (nS)**	**FWHM (Error Bar)**
-950mV	1.74	0.30656
-850mV	1.73	0.32234
-750mV	1.85	0.38901
-650mV	1.98	0.48339
-600mV	2.38	0.47043
-550mV	2.91	0.32268
-450mV	2.13	0.39243
-350mV	2.81	0.43448
-300mV	4.76	0.43026
-250mV	5.86	0.55626
-200mV	4.56	0.44231
-150mV	3.03	0.45015
50mV	2.24	0.42982
150mV	2.02	0.38448

As a comparing, the conductance behavior of Au/6v6/Au system with electrochemical controlling was recorded. The specific 1D conductance histograms of Au/6V6/Au junctions measured in ILs as shown in Figure 55a. These conductance histograms were recorded for the marked electrochemical potentials (versus $Ag/AgCl$). each of the histograms showed a clear peak where the peak position indicated the conductance value of the corresponding molecular junction. The specific conductance value of Au/6V6/Au versus seven different electrochemical potentials are listed in Table 5. The conductance of 6V6 measured in ILs is varied from 2.64nS to 3.40 nS with the change of electrochemical potentials. We notice that even the minimum conductance value measured in ILs is still greater than when it measured in air atmosphere (2.16nS). We also plotted the conductance value obtained for Au/6V6/Au overlapped with its cyclic voltammogram, as shown Figure 55b. The plotted conductance data shows a "bell" shape which could prove the effect electrochemical gating. These results are also in good agreement with the results presented by Osorio et al.[144] In the early study, Haiss et al. have reported the gating effect of Au/6V6/Au junction with aqueous electrolyte which showed the conductance solely increases as overpotential changed from positive to negative.[106] Noted here, the behavior observed using ionic liquid electrolyte is very different from previously reported for aqueous electrolyte. This demonstrates the effectiveness of ionic liquids for single molecule electrolyte gating, presenting a special electrochemical environment for investigations not possible in aqueous electrolytes.

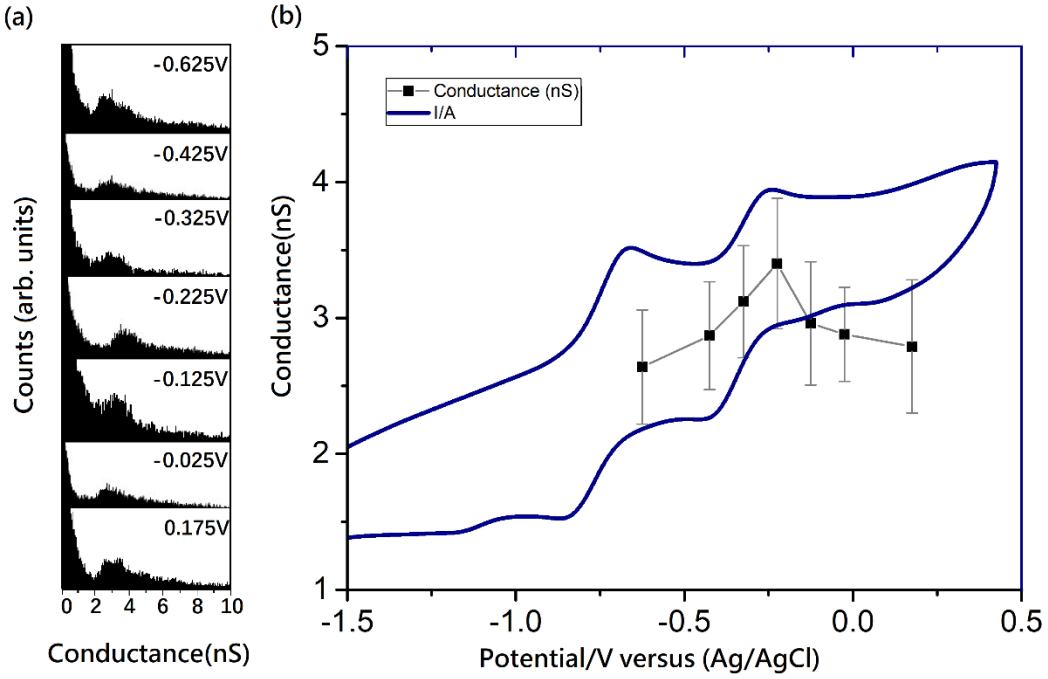

Figure 55: (a) The 1D conductance histograms of Au/6V6/Au junctions. (b) The plot conductance of Au/6V6/Au with error bar against the sample electrochemical potential overlaid with a cyclic voltammogram (blue line) of 6V6 in BMIM-OTf.

Table 5: The conductance of Au/6V6/Au system versus gating potentials

Gating potential (mV) Versus Ag/AgCl	**Conductance (nS)**	**FWHM (Error Bar)**
-0.625mV	2.64	0.41924
-0.425mV	2.87	0.39791
-0.325mV	3.12	0.41214
-0.225mV	3.40	0.47955
-0.125mV	2.96	0.45321
-0.025mV	2.88	0.34595
0.175mV	2.79	0.48981

In order to fully characterize the mechanism underlying the molecular gating, and in particular the evolution of the charge state of the molecule, we have performed DFT calculations of the junction with different molecular charges (by adding or removing electrons to the full system). The unit cell used for the calculations, namely the molecule between the gold and graphene electrode, plus the two PF_6^- ions, is represented in Figure 56 a). The corresponding transmissions calculated for molecular charges ranging from -2.71 to -1.71 electrons are represented in Figure 56b). Note that the equilibrium state of the system corresponds to a molecular charge of -2.13 electrons, namely very close to the V^{2+} state of the molecule.

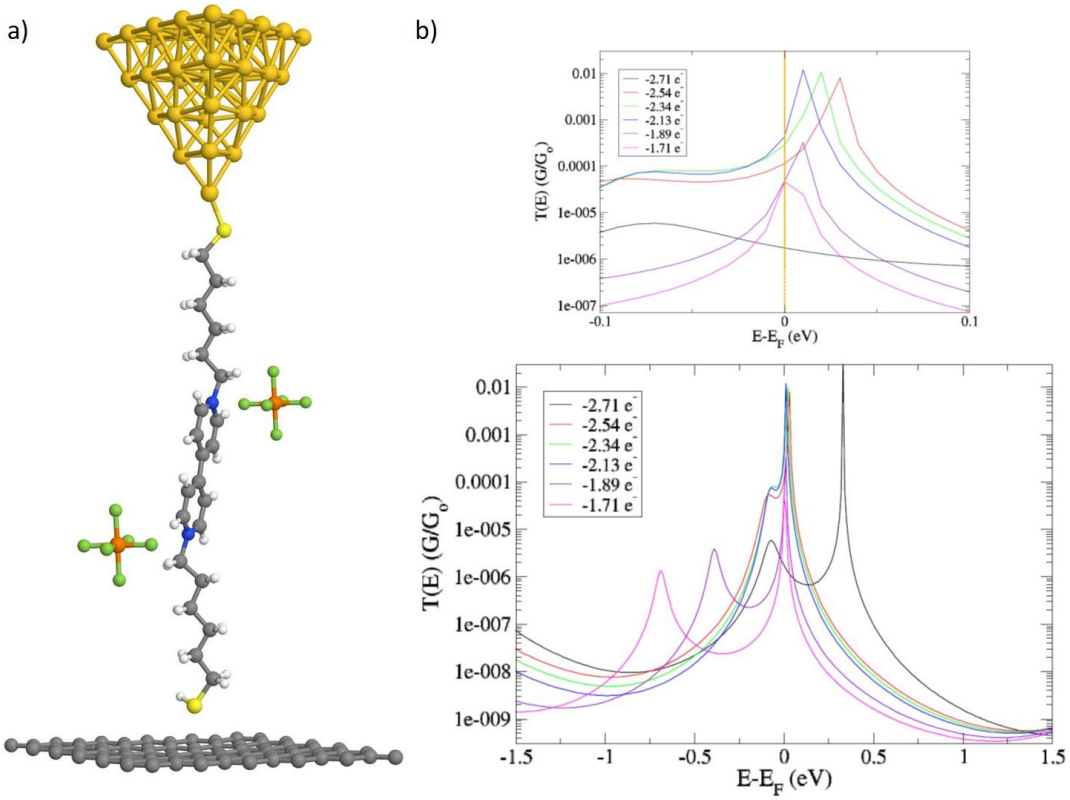

Figure 56: (a) Atomistic representation of the molecular junction and its two PF6 ions used for the DFT calculations. (b) Corresponding calculated electronic transmissions for different molecular charge states. In inset, a zoom of the transmissions near the Fermi level, showing the evolution of the conductance with the molecular charge.

As a main feature, one can observe a strong resonance near the Fermi level for almost all the transmissions. This is related to the oxidized state of the molecule with about two electrons left, reaching the full resonance exactly at the V^{2+} state. However, with the charging of the molecule, from -2.71 electrons to -1.71 electrons (gaining one electron), one can see a shift of the transmission spectra to the negative energies, similarly to what happens in a semiconductor based transistor when applying a gate potential.[175] Hence, the application of a gate potential in our experiments will modify the molecular charge around the V^{2+} state, and the measured conductance will be maximum at that resonance.

The evolution of the calculated conductance as a function of the molecular charge is represented in Figure 57. A reduction of the molecular charge corresponds here to the application of a negative gating potential experimentally, giving electrons to the molecule. A strong resonance is observed in the neighborhood of the V^{2+} state, similarly to what is measured experimentally where the highest conductance is observed for zero gating. Further charging of the molecule would therefore yield a second resonance, related to the V^{+} state, where the charge state of the molecule would be around -1 electron.

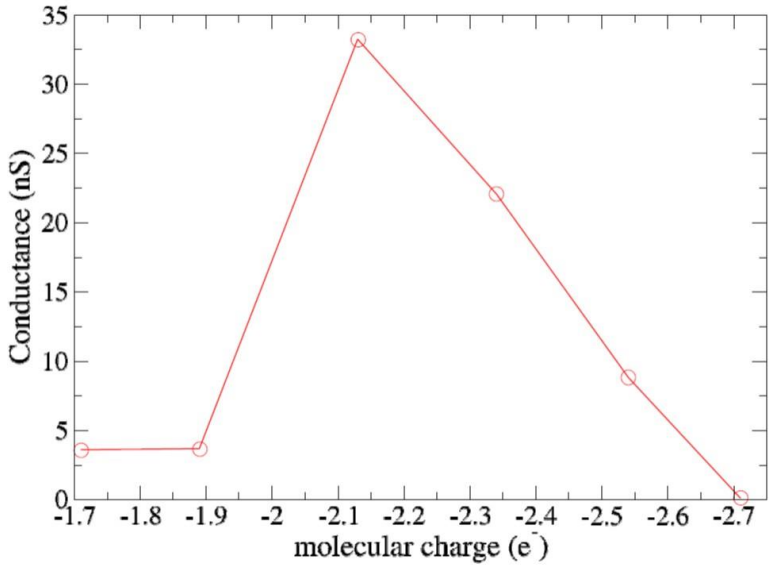

Figure 57: Evolution of the calculated conductance as a function of the molecular charge.

Obviously, a quantitative comparison between the DFT and the experimental results is complicated to obtain. Indeed, DFT is a theory of the fundamental state and here we are dealing with excited states, since we charge the molecule, which might induce small inaccuracies in the calculated resonances. Moreover, we extract the conductance from calculations in the neighborhood of mathematical resonances, leading to high maxima, which are of course not observed in the experimental conditions. Consequently, the theoretical gating curve presents a higher maximum than what is observed experimentally. However, the physical behavior of the molecular junction is well captured by the gating model we use here, and the observed resonance is clearly attributed to the V^{2+} state of the molecule.

Finally, comparison with the pure gold-gold junction leads to very similar results, either theoretically or experimentally. The main difference lies in the initial charge state of the molecule that drives the amplitude of the gate potential to be applied to reach the maximum of resonance. Regarding the similar conductance values, it can be attributed to the decoupling of the active molecular part with the alkyl chains, reducing the role of the electrodes. This feature is illustrated for the Au/6V6/Au junction through the isoelectronic Density of States calculation shown in Figure 58. The electronic density is localized near the red-ox active part, with no contribution along the alkyl chains.

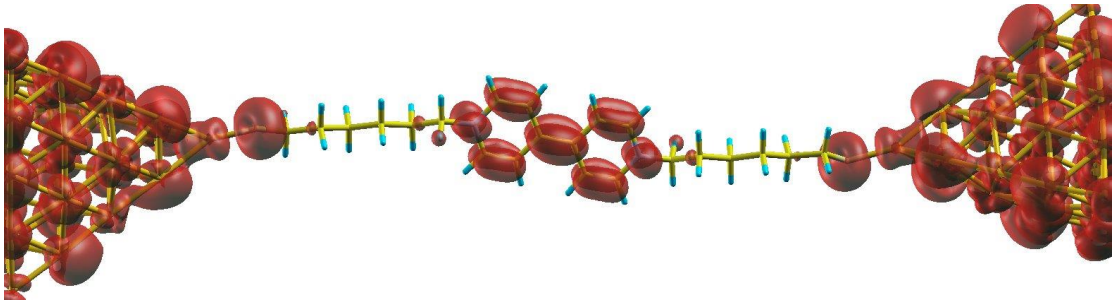

Figure 58: DFT calculated isoelectronic density of states of the Au/6V6/Au HOMO level, showing the decoupling of the central part with respect to the electrodes, due to the alkyl chains.

4.6. Conclusion

In this research, the electrochemical gating has been successfully applied to modulate the conductance behavior of (single) molecular junction. Based on the EC-STM technique, we have measured the electronic conductance of 6V6 based molecular junctions as a function of a gating potential in an ionic liquid. Summarizing the experimental results detailed above, the following general observations can be made:

1. Ionic liquid is a good electrolyte to perform the electrochemical gating to (single) molecular junctions.
2. Based on ionic liquid electrolyte, a clear resonance associated to the well-known V^{+}/V^{2+} redox transition in the viologen molecule was observed.
3. As the electrode potential is swept, the system follows a "off-on-off" conductance switching behaviors were observed in both of Au/6v6/graphene and Au/6V6/Au system.
4. The "off-on-off" behavior is more obvious in Au/6V6/graphene compared with Au/6V6/Au.

5 Conclusion and future work

In this project, we have researched the effect of electrode material, anchoring group, conjugation degree of bridged molecules, data analysis method, environments, and external electrochemical gating on the conductivity of a (single) molecular junction using STM-I(s) technique and EC-STM technique. The experimental results showed that all these factors are important for the (single) molecular conductance.

We have systematically studied the single-conductance of poly(p-phenylene) molecular wires bound either between Au/Au and Au/graphene contacts by STM-*I*(s) technique. The experimental results showed that the junction formed with Au/Au electrodes have higher conductance than those formed with Au/graphene electrodes. The measured conductance decays exponentially with an increase in the number of phenyl rings, giving a decay constant that is similar for thiol (1.31 per phenyl ring) and amine (1.40 per phenyl ring) terminated molecular junctions with Au/graphene contact. This work reveals that poly(p-phenylene) chains are similarly coupled to either gold or graphene electrodes, independently of the anchoring group, and that the transport properties are essentially dominated by the intrinsic molecular properties.

We next studied the conductance value and break-off distance of Au/6MHI/Au, AU/8MOI/Au, Au/DBDT/Au and Au/TBDT/Au systems by STM-*I*(s) technique. In this research, an unsupervised MATLAB data selection algorithm has been successfully applied to analyze the multiple conductance behavior of these four molecular systems. The dominated conductance of phenyl ring based molecular junction (Au/DBDT/Au and Au/TBDT/Au) is significantly greater than the chain shape molecular junctions (Au/6MHI/Au, AU/8MOI/Au), even they possess similar molecular length.

We further synthesized a redox active molecule (6V6), then measured its electrochemical properties with CV, and its conductance with EC-STM method. The conductance of Au/6V6/graphene has been investigated as a function of 14 different electrochemical potential in an ionic liquid medium. The conductance of Au/6V6/Au has been investigated as a function of 7 different electrochemical potential in an ILs electrolyte. A clear “off-on-off” conductance switching behavior was achieved through

gating of the redox state when the electrochemical potential was swept with both of Au/Au and Au/graphene contact. Both Au/6V6/graphene and Au/6V6/Au showed a single-molecule conductance maximum centered close to its equilibrium redox potential. In addition, the Au/6V6/graphene system presented the more obvious "off-on-off" conductance switching behavior compared with Au/6V6/Au system. The responding of variation molecular conductance to the external electrochemical gating potential indicated the true three terminal molecular electronics could be realized base on our experimental equipment.

The experimental results showed in this thesis presented the promising feather of graphene electrode in building (single) molecular junctions, especially in three-terminal electrochemical gating system. The future work could extend the asymmetry Au/molecule/graphene junction to the symmetry graphene/molecule/graphene junction. In addition, we have already achieved the chemical gating effect by EC-STM technique. The other gating methods are also very attractive for the realizing true three terminal single molecular devices, such as temperature gating and PH value gating.

6 References

1. Moore, G. E., Progress in digital integrated electronics. *IEDM Tech. Digest* **1975,** 11.
2. Hippel, A. R., molecular engineering, *Science* **1956**, 123, 315.
3. Feynman, R. P., There's plenty of room at the bottom. *Engineering and Science,* **1960,** *23* (5), 22-36.
4. Aviram, A., Ratner, M. A. Molecular Rectifiers. *Chem. Phys. Lett.* **1974**, 29, 277–283.
5. Polymeropoulos, E. E., MnBius, D., Kuhn, H. Monolayer assemblies with functional units of sensitizing and conducting molecular components: photovoltage, dark conduction and photoconduction in systems with aluminium and barium electrodes. *Thin Solid Films,* **1980**, 68(1), 173-190.
6. Halbritter, J., Tunnel channels, spectroscopy and imaging in STM. *Appl. Phys. A*, **1998**, 66 (1), S181-S186.
7. Ritter, D., Hamm, R. A., Panish, M. B., Vandenberg, J. M., Gershoni, D., Gunapala, S. D., Metalorganic molecular beam epitaxial growth of inp/gainas multiquantum wells for infrared photodetection. *Appl. Phys. Lett.,***1991**, 59(5), 552-554.
8. Binnig, G., Rohrer, H., Gerber, C., Weible, E., Vacuum tunneling. *Physica B+C*, **1982**, 109-110, 2075-2077.
9. Binnig, G., Rohrer, H., In Touch with Atoms. *Rev. Mod. Phys.*, **1999**, 71(2), 324-327.
10. Reed, M. A., Zhou, C., Muller, C., Burgin, T., Tour, J., Conductance of a molecular junction. *Science*, **1997**, 278 (5336), 252-254.
11. Xu, B. Q., Tao, N. J., Measurement of Single-Molecule Resistance by Repeated Formation of Molecular Junctions. *Science*, **2003**, 301, 1221-1223.
12. Haiss, W., Van, Z. H., Higgins, S. J., Bethell, D., Höbenreich, H., Schiffrin, D. J., Nichols, R. J., Redox state dependence of single molecule conductivity. *J. Am. Chem. Soc.*, **2003**, 125,15294-15295.

13. Cui, X. D., Primak, A., Zarate, X., Tomfohr, J., Sankey, O. F., Moore, A. L., Moore, T. A., Gust, D., Harris, G.; Lindsay, S. M., Reproducible Measurement of Single-Molecule Conductivity. *Science*, **2001**, 294, 571-574.
14. Binnig, G., Rohrer, H., In Touch with Atoms. *Review of Modern Physics*, **1999**, 71(2), 324-327.
15. Wiesendanger, R., Scanning probe microscopy and spectroscopy, Cambridge University Press, UK, 2008.
16. Stroscio, J. A., Eigler, D. M., Atomic and molecular manipulation with the scanning tunneling microscope. *Science*, **1991**, 254(5036), 1319-1326.
17. Meyer, G., Zöphel, S., Rieder, K.H., Manipulation of atoms and molecules with a low temperature scanning tunneling microscope. *Appl. Phys. A*,**1996**, 63, 557–564.
18. Nichols, R. J., Haiss, W., Higgins, S. J., Leary, E., Martin, S., Bethell, D., The experimental determination of the conductance of single molecules. *Phys. Chem. Chem. Phys.,* **2010**, 12 (12):2801–2815.
19. Nichols, R. J., Higgins, S. J. Single molecule electrochemistry in nanoscale junctions. *Current Opinion in Electrochemistry*, **2017**,4, 98–104.
20. Muller, C., Van Ruitenbeek, J., De Jongh, L., Experimental observation of the transition from weak link to tunnel junction. *Physica C: Superconductivity,* **1992**, 191 (3), 485-504.
21. Tsutsui, M., Taniguchi, M., Single molecule electronics and devices. *Sensors*, **2012**, 12(6), 7259-729
22. Leatherman, G., Durantini, E. N., Gust, D., Moore, T. A., Moore, A. L., Stone, S., Carotene as a molecular wire: conducting atomic force microscopy. **1999**, *J. Phys. Chem. B*, 103(20), 4006-4010.
23. Cui, X. D., Reproducible measurement of single-molecule conductivity. *Science*, **2001**, 294(5542), 571-574.
24. Sharvin, Y. V., A Possible Method for Studying Fermi Surfaces. *Soviet Journal of Experimental & Theoretical Physics*, **1965**, 21(3):655.

25. Landauer, R., Spatial variation of currents and fields due to localized scatterers in metallic conduction (and comment). *Ibm Journal of Research & Development*, **1996**, 37(10), 5259-5268
26. Ulrich, J., Esrail, D., Pontius, W., Venkataraman, L., Millar, D., Doerrer, L. H., Variability of conductance in molecular junctions. *J. Phys. Chem. B*, **2006**, 110(6), 2462-2466.
27. Xiao, X. Y., Xu, B. Q., Tao, N. J., Measurement of Single Molecule Conductance: Benzenedithiol and Benzenedimethanethiol. *Nano Lett.,* **2004**, 4, 267-271.
28. Emberly, E. G., Kirczenow, G., Theoretical study of electrical conduction through a molecule connected to metallic nanocontacts. *Phys. Rev. B,* **1998**, 58(16), 10911-10920.
29. Tsutsui, M., Teramae, Y., Kurokawa, S., Sakai, A., High-conductance states of single benzenedithiol molecules. *Phys. Lett.,* **2006**, 89, 163111-163113.
30. Beebe, J. M., Engelkes, V. B., Liu, J., Gooding, J. J., Eggers, P. K., Jun, Y., Length dependence of charge transport in nanoscopic molecular junctions incorporating a series of rigid thiol-terminated norbornylogs. *J. Phys. Chem. B,* 2005, 109(11), 5207-5215.
31. Tan, A., Balachandran, J., Sadat, S., Gavini, V., Dunietz, B. D., Jang, S. Y., Effect of length and contact chemistry on the electronic structure and thermoelectric properties of molecular junctions. *J. Am. Chem. Soc.,* **2011**, 133(23), 8838-41.
32. Kim, Y., Pietsch, T., Erbe, A., Belzig, W., Scheer, E., Benzenedithiol: a broad-range single-channel molecular conductor. *Nano Lett*., **2011**, 11(9), 3734.
33. Sergueev, N., Tsetseris, L., Varga, K., Pantelides, S., Configuration and conductance evolution of benzene-dithiol molecular junctions under elongation. *Phys. Rev. B,* **2010**, *82*(7), 2365-2376.
34. Kim, Y., Hellmuth, T. J. , Burkle, M. , Pauly, F. , Scheer, E., Characteristics of amine-ended and thiol-ended alkane single-molecule junctions revealed by inelastic electron tunneling spectroscopy. *Acs Nano*, **2011**, 5(5), 4104-11.

35. Widawsky, J. R., Kamenetska, M., Klare, J., Nuckolls, C., Steigerwald, M. L., Hybertsen, M. S., Measurement of voltage-dependent electronic transport across amine-linked single-molecular-wire junctions. *Nanotechnology*, **2009**, 20(43), 18968-18972.

36. Li, Z., Kosov, D. S., Nature of well-defined conductance of amine anchored molecular junctions. *Phys. Rev. B*, **2007**, 76(3).

37. Li, Z., Smeu, M., Mark, A. Effect of Anchoring Groups on Single Molecule Charge Transport through Porphyrins. *J. Phys. Chem. C*, **2013**, 117(29): 14890-14898.

38. Chen, F., Li, X., Hihath, J., Huang, Z., Tao, N. J. Effect of anchoring groups on single-molecule conductance: comparative study of thiol-, amine-, and carboxylic-acid-terminated molecules. *J. Ame. Chem. Soc*., **2006**, 128(49), 15874-81.

39. Bala, S., Aithal, R. K., Derosa, P., Janes, D., Kuila, D., Molecular rectifying diodes based on an aluminum/4′-hydroxy-4-biphenyl carboxylic acid/p+-silicon junction. *J. Phys. Chem. C*, **2010**, *114*(48), 20877-20884.

40. Chen, F., Peng, L. L., Hong, Z. W., Mao, J. C., Zheng, J. F., Shao, Y., Comparative study on single-molecule junctions of alkane- and benzene-based molecules with carboxylic acid/aldehyde as the anchoring groups. *Nanoscale Research Letters*, **2016**, 11(1), 380.

41. Ahn, S., Aradhya, S. V., Klausen, R. S., Capozzi, B., Roy, X., Steigerwald, M. L., Electronic transport and mechanical stability of carboxyl linked single-molecule junctions. *Phys. Chem. Chem. Phys.,* **2012**, 14(40), 13841-13845.

42. Kim, B. S., Beebe, J. M., Jun, Y., Zhu, X. Y., Frisbie, C. D., Correlation between homo alignment and contact resistance in molecular junctions: aromatic thiols versus aromatic isocyanides. *J. Am. Chem. Soc*. **2006**, 128, 4970–4971.

43. Venkataraman, L., Klare, J. E., Tam, I. W., Nuckolls, C., Hybertsen, M. S., Steigerwald, M. L., Single-molecule circuits with well-defined molecular conductance. *Nano Lett*., **2006**, 6(3), 458.

44. Fan, F. R. F., Yao, Y., Cai, L., Cheng, L., Tour, J. M., Bard, A. J., Structure-dependent charge transport and storage in self-assembled monolayers of compounds of interest in molecular electronics: effects of tip material, headgroup, and surface concentration. *J. Am. Chem. Soc*., **2004**, *126*(12), 4035-4042.
45. Baldea, I. Quantifying the relative molecular orbital alignment for molecular junctions with similar chemical linkage to electrodes. *Nanotechnology*, **2015**, 25(45):455202.
46. Santiago, M., Yufit, D. S., Howard, J. A. K., Osorio, H. M., Víctor, M., Simplifying the conductance profiles of molecular junctions: the use of the trimethylsilylethynyl moiety as a molecule–gold contact. *Dalton Transactions*, **2012**, 42.
47. Kamenetska, M., Quek, S. Y., Whalley, A. C., Steigerwald, M. L., Choi, H. J., Louie, S. G., Nuckolls, C., Hybertsen, M. S., Neaton, J. B., Venkataraman, L., Conductance and geometry of pyridine-linked single-molecule junctions. *J. Am. Chem. Soc.* **2010**, 132, 6817–6821.
48. Ko, C. H., Huang, M. J., Fu, M. D., Chen, C. H., Superior contact for single-molecule conductance: electronic coupling of thiolate and isothiocyanate on Pt, Pd, and Au. *J. Am. Chem. Soc*. **2010**, 132, 756–764.
49. Park, Y. S., Whalley, A. C., Kamenetska, M., Steigerwald, M. L., Hybertsen, M. S., Nuckolls, C., Venkataraman, L., Contact chemistry and single-molecule conductance: a comparison of phosphines, methyl sulfides, and amines. *J. Am. Chem. Soc.* **2016**, 129(51), 15768–15769.
50. Nowak, A. M., Mccreery, R. L., In situ raman spectroscopy of bias-induced structural changes in nitroazobenzene molecular electronic junctions. *J. Am. Chem. Soc.*, **2004**, 126(50), 16621-31.
51. Huang, M. L., Zhang, F., Wang, C., Zheng, J. F., Mao, H. L., Xie, H. J., Side-group effect on electron transport of single molecular junctions. *Micromachines*, **2018**, 9(5), 234.

52. Miwa, K., Najarian, A. M., McCreery, R. L., Galperin, M., Hubbard Nonequilibrium Green's Function Analysis of Photocurrent in Nitroazobenzene Molecular Junction. *J. Phys. Chem. Lett.,* **2019**. 10(7), 1550-1557.

53. Yokota, K., Taniguchi, M., Tsutsui, M., Kawai, T. Molecule − Electrode Bonding Design for High Single-Molecule Conductance. *J. Am. Chem. Soc*., **2010**, 132, 17364 −17365.

54. Kaun, C. C., Jorn, R., Seideman, T., Spontaneous oscillation of current in fullerene molecular junctions. *Phys. Rev. B Condens. Matter*, **2006**, 74(4), p.045415.1-045415.9.

55. Martin, C. A., Ding, D., Sørensen, J. K., Bjørnholm, T., van Ruitenbeek, J. M., van der Zant, H. S. J., Fullerene-based anchoring groups for molecular electronics. *J. Am. Chem. Soc.,* **2008**, 130, 13198.

56. Markussen, T., Settnes, M., Thygesen, K. S., Robust conductance of dumbbell molecular junctions with fullerene anchoring groups. *J. Chem. Phys*., **2011**, 14;135(14), 144104.

57. Haiss, W., Martin, S., Leary, E., Zalinge, H. V., Higgins, S. J., Bouffier, L., Nichols, R. J., Impact of junction formation method and surface roughness on single molecule conductance. *J. Phys. Chem. C*, **2009**, 113(14), 5823-5833.

58. Wang, C., Batsanov, A. S., Bryce, M. R., Martin, S., Nichols, R. J., Higgins, S. J., Oligoyne single molecule wires. *J. Am. Chem. Soc.,* **2009**, 131(43), 15647-54.

59. Zheng, J., Liu, J., Zhuo, Y., Li, R., Jin, X., Yang, Y., Chen, Z., Shi, J., Xiao, Z., Hong, W., Tia, Z. Electrical and SERS detection of disulfide-mediated dimerization in single-molecule benzene-1,4-dithiol junctions. *Chem.Sci.* **2018**, 9.

60. Emberly, E. G.; Kirczenow, G., Theoretical Study of Electrical Conduction Through a Molecule Connected to Metallic Nanocontacts, *Phys. Rev. B* **1998**, 58, 10911-10920.

61. Leary, E., Zotti, L., A., Miguel, D., Márquez, I., The role of oligomeric gold-thiolate units in single-molecule junctions of thiol-anchored molecules. *J. Phys. Chem. C*, **2018**, 122(6): 3211-3218.
62. Peng, Z. L., Chen, Z. B., Zhou, X. Y., Sun, Y. Y., Liang, J. H., Single molecule conductance of carboxylic acids contacting Ag and Cu electrodes. *J. Phys. Chem. C,* **2012**, 116, 21699–705
63. Kim, T., Vázquez, H., Hybertsen, M. S., Venkataraman, L. Conductance of molecular junctions formed with silver electrodes. *Nano Lett.,* **2013**,13, 3358–3364
64. Parashar, S., Srivastava, P., Pattanaik, M., Jain, S. K., Electron transport in asymmetric biphenyl molecular junctions: effects of conformation and molecule-electrode distance. *European Physical Journal B*, **2014**, 87(9), 1-10.
65. Lee, S. K., Ohto, T., Yamada, R., Tada, H., Thermopower of benzenedithiol and c 60 molecular junctions with ni and au electrodes. *Nano Lett.,* **2014**, 14(9), 5276-5280.
66. Chen, F., Huang, Z., Tao, N. J., Forming single molecular junctions between indium tin oxide electrodes. *Appl. Phys. Lett*., **2007**, 91(16):277-245. (2007).
67. Cummings, C. Y., Wadhawan, J. D., Nakabayashi, T., Haga, M. A., Rassaei, L., Dale, S. E. C., Electron hopping rate measurements in ito junctions: charge diffusion in a layer-by-layer deposited ruthenium(ii)-bis(benzimidazolyl)pyridine-phosphonate–tio 2 film. *J. Electroanal. Chem.,* **2011**, 657(1-2), 196-201.
68. Vezzoli, A., Brooke, R. J., Ferri, N., Higgins, S. J., Schwarzacher, W., Nichols, R. J., Single-Molecule Transport at a Rectifying GaAs Contact. *Nano. Lett*., **2017**, 17, 1109-1115.
69. Vezzoli, A., Brooke, R. J., Higgins, S. J., Schwarzacher, W., Nichols, R. J., Single-Molecule Photocurrent at a Metal-Molecule-Semiconductor Junction. *Nano. Lett.,* **2017**, 17, 6702-6707.

70. Su, T. A., Widawsky, J. R., Li, H., Klausen, R. S., Leighton, J. L., Steigerwald, M. L., Silicon ring strain creates high-conductance pathways in single-molecule circuits. *J. Am. Chem. Soc.*, **2013**, 135(49), 18331-4.

71. Choi, J. K., Pham, H.T., Jeong, H. D., A comparative study of electron transport in benzene molecule covalently bonded to gold and silicon electrodes for pioneering the electron transport properties of silicon quantum dot-molecule hybrid polymers. *Curr. Appl. Phys*., **2015**, 15(8), 877-884.

72. Laurans, M., Francesca, K. D., Volatron, F., Izzet, G., Proust, A., Molecular signature of polyoxometalates in electron transport of silicon-based molecular junctions. *Nanoscale*, **2018**, 10(36).

73. Nozaki, D., Cuniberti, G. Silicon-based molecular switch junctions. *Nano Research*, **2009**, 2(8), 648-659.

74. Ricoeur, G., Lenfant, S., Guérin, D., Vuillaume, D., Molecule-electrode interface energetics in molecular junction: a transition voltage spectroscopy study. *J. Phys. Chem. C*, **2012**, 116(39), 20722-20730.

75. Guo, X. F., Small, J. P., Klare, J. E., Wang, Y. L., Purewal, M. S., Tam, I. W., Hong, B. H., Caldwell, R., Huang, L. M., O'Brien, S., Yan, J.M., Breslow, R., Wind, S. J., Hone, J., Kim, P., Nuckolls, C., Covalently bridging gaps in single-walled carbon nanotubes with conducting molecules. *Science,* **2006**, 311, 356-359.

76. Zhang, Q., Tao, S. H., Yi, R. W., He, C. H., Zhao, C. Z., Su, W., Smogunov, A. Dappe, Y. J., Nichols, R. J., Yang, L., Symmetry Effects on Attenuation Factors in Graphene-Based Molecular Junctions. *J. Phys. Chem. Lett.* **2017**, 8, 5987-5992.

77. Zhang, Q., Liu, L. L, Tao, S. H. , Wang, C., Zhao, C., Gonzalez, C.;Dappe, Y. J.; Nichols, R. J.; Yang, L.Graphene as a Promising Electrode for Low-Current Attenuation in Nonsymmetric Molecular Junctions . *Nano Lett.,* **2016**, 16, 6534-6540.

78. Liu, L., Zhang, Q., Tao, S. H., Zhao, C., Almutib, E., Galiby, Q., Bailey, S. W. D., Grace, L., Lambert, C. J., Du, J., Yang, L. Charge transport through

dicarboxylic-acid-terminated alkanes bound to graphene-gold nanogap electrodes. *Nanoscale*, **2016**, 8, 14507-14513.

79. Kim, T., Liu, Z., Lee, C., Neaton, J. B., Venkataraman, L., Charge transport and rectification in molecular junctions formed with carbon-based electrodes. *Proc. Natl. Acad. Sci.,* **2014**, 111,10928-10932.
80. Yang, C., Qin, A., Tang, Z., Guo.X. F. Fabrication and functions of graphene–molecule–graphene single-molecule junctions. *J. Chem. Phys*., **2020**, 152(12), 120902.
81. He, C., Zhang, Q., Gao, T., Liu, C., Chen, Z., Zhao, C., Charge transport in hybrid platinum/molecule/graphene single molecule junctions. *Phys. Chem. Chem. Phys.*,2020, 22.
82. Island, J. O., Holovchenko, A., Koole, M., Alkemade, P. F. A., Menelaou, M., Aliaga-Alcalde, N., Fabrication of hybrid molecular devices using multi-layer graphene break junctions. *J. Phys. Cond. Matt*., **2014**, 26(47), 474205.
83. Kroto, H. W., Heath, J. R., O'Brien, S. C., Curl, R. F., Smalley, R. E., C60: buckminsterfullerene. *Nature*, **1985**, 318(6042), 162-163.
84. Iijima, S., Helical microtubes of graphite carbon. *Nature*, **1991**, 354(6348), 56--58.
85. Novoselov, K. S., Geim, A. K., Morozov, S. V., Jiang, D., Zhang, Y., Dubonos, S. V., Grigorieva, I. V., Firsov, A. A., Electric field effect in atomically thin carbon films. *Science*, **2004**, 306: 666—669.
86. Chen, J. H., Jang, C., Xiao, S., Ishigami, M. Fuhrer, M. S., Intrinsic and extrinsic performance limits of graphene devices on SiO_2. *Nature Nanotechnol.*, **2008**, 3(4), 206-9.
87. Service, R. F., Carbon sheets an atom thick give rise to graphene dreams. *Science*, **2009**, 324, 875-877.
88. Balandin, A. A., Ghosh, S., Bao, W., Calizo, I., Teweldebrhan, D., Miao, F., Superior thermal conductivity of single-layer graphene. *Nano Lett.,* **2008**, 8(3), 902-907.

89. Novoselov, K. S., Jiang, Z., Zhang, Y., Morozov, S. V., Geim, A. K., Room-temperature quantum hall effect in graphene. *Science*, **2007**, 315(5817), 1379.

90. Wang, Y., Huang, Y., Song, Y., Zhang, X., Ma, Y., Liang, J., Room-temperature ferromagnetism of graphene. *Nano Lett.,* **2009**, 9(1), 220-224.

91. Aswal, D. K., Lenfant, S., Guerin, D., Yakhmi, J. V., Vuillaume, D. Self assembled monolayers on silicon for molecular electronics. *Analytica Chimica Acta*, **2006**, 568(1-2), 84-108.

92. Wang, W., Lee, T., Reed, M. A., Mechanism of electron conduction in self-assembled alkanethiol monolayer devices, *Phys. Rev. B,* **2003**, 68, 035416.

93. Chen, J., Calvet, L. C., Reed, M. A., Carr, D. W., Grubisha, D. S., Bennett. D. W., Electronic transport through metal–1,4-phenylene diisocyanide–metal junctions. *Chem. Phys. Lett*., **1999**, 313(5-6), 741-748.

94. Sharma, R. N., Lakshmikumar, S. T., Rastogi, A. C., Electrical behaviour of electron-beam-evaporated yttrium oxide thin films on silicon. *Thin Solid Films*, **1991**, 199(1), 1-8.

95. Simmons, J. G., Generalized formula for the electric tunnel effect between similar electrodes separated by a thin insulating film. *J. Appl. Phys.* **1963**, 34 (6), 1793-1803.

96. Engelkes, V. B., Beebe, J. M., Frisbie, C. D., Length-dependent transport in molecular junctions based on sams of alkanethiols and alkanedithiols: effect of metal work function and applied bias on tunneling efficiency and contact resistance. *J. Am. Chem. Soc*., **2004**, 126(43), 14287-96.

97. Albrecht, T., Moth-Poulsen, K., Christensen, J. B., Guckian, A., Bjørnholm, T., Vos, J. G., Ulstrup, J., In situ scanning tunnelling spectroscopy of inorganic transition metal complexes. *Faraday Discussions*, **2006**, 131, 265-279.

98. Chappell, S., Brooke, C., Nichols, R. J., Cook, L. J. K., Halcrow, M., Ulstrupc, J., Higgins, S. J., Evidence for a hopping mechanism in metal|single molecule|metal junctions involving conjugated metal–terpyridyl complexes; potential-dependent conductances of complexes $[M(pyterpy)_2]^{2+}$ (M = Co and

Fe; pyterpy = 4′-(pyridin-4-yl)-2,2′:6′,2′′-terpyridine) in ionic liquid. *Faraday Discussions*, **2016**, 193(0): 113-131.

99. Wohlgamuth, C. H., Mcwilliams, M. A., Slinker, J. D., DNA as a molecular wire: distance and sequence dependence. *Anal. Chem.,* **2013**, 85(18), 8634-8640.
100. Berlin, Y. A., Charge Hopping in DNA. *J. Am. Chem. Soc*., **2001**, 123(2): 260-268.
101. Lu, Q., Liu, K., Zhang, H., Du, Z., Wang, X., Wang, F., From tunneling to hopping: a comprehensive investigation of charge transport mechanism in molecular junctions based on oligo(p-phenylene ethynylene)s. *Acs Nano*, **2009**, 3(12), 3861-8.
102. Lee, S. K., Yamada, R., Ohto, T., Tanaka, S., Tada, H., Charge Transport Mechanisms in Oligothiophene Molecular Junctions Studied by Electrical Conductance and Thermopower Measurements. Springer International Publishing, 2017.
103. Lee, S. K., Yamada, R., Tanaka, S., Electrical Conductance of Single Oligothiophene Molecular Wires: Temperature Effect. *Mrs Proceedings*, 2011.
104. Hines, T., Diez-Perez, I., Hihath, J., Liu, H., Wang, Z. S., Zhao, J., Transition from tunneling to hopping in single molecular junctions by measuring length and temperature dependence. *J. Am. Chem. Soc*., **2010**, 132(33), 11658.
105. Zhao, X., Huang, C., Gulcur, M., Batsanov, A. S., Baghernejad, M., Hong, W., Oligo(aryleneethynylene)s with terminal pyridyl groups: synthesis and length dependence of the tunneling-to-hopping transition of single-molecule conductances. *Chemistry of Materials*, **2013**, 25(21), 4340-4347.
106. Haiss, W., Albrecht, T., Van Zalinge, H., Higgins, S. J., Bethell, D., Höbenreich, H., Schiffrin, D. J., Nichols, R. J., Kuznetsov, A. M., Zhang, J., Chi, Q., Ulstrup, J., Single-molecule conductance of redox molecules in electrochemical scanning tunneling microscopy. *J. Phys. Chem. B*, **2007**, 111(24), 6703–6712.

107. Kuznetsov, A. M., Ulstrup, J., Mechanisms of in situ scanning tunnelling microscopy of organized redox molecular assemblies, *J. Phys. Chem. A,* **2000**, 104, 11531.

108. Zhang, J., Kuznetsov, A. M., Medvedev, I. G., Chi, Q., Albrecht, T., Jensen, P. S., Ulstrup, J. Single-molecule electron transfer in electrochemical environments. *Chem. Rev*., **2008**, 108, 2737–2791.

109. Latha, V., Klare, J. E., Colin, N., Hybertsen, M. S., Steigerwald, M. L., Dependence of single-molecule junction conductance on molecular conformation. *Nature*, **2006**, 442, 904-907.

110. Chen, W., Widawsky, J. R., Vázquez, H., Schneebeli, S. T., Hybertsen, M. S., Breslow, R., Venkataraman, L., Highly conducting π-conjugated molecular junctions covalently bonded to gold electrodes. *J. Am. Chem. Soc*., **2011**, 133, 17160-17163.

111. Xu, B. Q., Li, X. L., Xiao, X. Y., Sakaguchi, H., Tao, N. J., Electromechanical and Conductance Switching Properties of Single Oligothiophene Molecules. *Nano Lett.*, **2005**, 5, 1491-1495.

112. Zhang, X., Chen, K., Long, M., He, J., Gao, Y., Effect of length and negative differential resistance behavior in conjugated molecular wire tetrathiafulvalene devices. *Mod. Phys. Lett. B*, **2015**, 29(20), 1550106.

113. Tao, N. J. Electron transport in molecular junctions. *Nat. Nano-technol.,* **2006**, 1, 173-181.

114. Selzer, Y., Cabassi, M. A., Mayer, T. S., Allara, D. L., Temperature effects on conduction through a molecular junction. *Nanotechnol.,* **2004**, 15(7), 483.

115. Nakazumi, T., Kaneko, S., Matsushita, R., Kiguchi, M., Electric conductance of single ethylene and acetylene molecules bridging between Pt electrodes. *J. Phys. Chem. C*, **2012**, 116, 18250–18255.

116. Ren, B., Picardi, G., Pettinger, B., Preparation of gold tips suitable for tip-enhanced Raman spectroscopy and light emission by electro-chemical etching. *Rev. Sci. Instrum.* 2004, 75, 837-841.

117. Malard, L. M., Pimenta, M. A., Dresselhaus, G., Dresselhaus, M. S., Raman spectroscopy in graphene. *Phys. Rep.*, **2009**, 473(5-6), 51-87.

118. Tang, B., Guoxin, H., Gao, H. Raman spectroscopic characterization of graphene. *Appl. Spectrosc. Rev.,* **2010**, 45(5), 369-407.

119. Wu, J., Xu, H., Zhang, J., Raman spectroscopy of graphene. *Acta Chimica Sinica*, **2014**, (3), 301–318.

120. Kaneko, S. , Murai, D. , Fujii, S., Kiguchi, M., Surface enhanced raman scattering of single 1,4-benzenedithiol molecular junction. *J. Mod. Phys. B,* **2016**, 1642010.

121. Kaneko, S., Nakamura, Y., Matsushita, R., Marqués-González, S., Kiguchi, M., Simultaneous measurement of electrical conductance and thermopower of single benzenedithiol molecular junctions. *Appl. Phys. Express*, **2015**, 8(6), 065201.1-065201.4.

122. Lin, L. L., Wang, C. K., Luo, Y., Inelastic electron tunneling spectroscopy of gold-benzenedithiol-gold junctions: accurate determination of molecular conformation. *Acs Nano*, **2011**, 5(3), 2257.

123. Horiguchi, K., Tsutsui, M., Kurokawa, S., Sakai, A., Electron transmission characteristics of au/1,4-benzenedithiol/au junctions. *Nanotechnology*, **2009**, 20(2), 025204.

124. Bürkle, M., Viljas, J. K., Mishchenko, A., Vonlanthen, D., Schön, G., Mayor, M., Wandlowski, T., Pauly, F., Conduction mechanisms in biphenyl-dithiol single-molecule junctions. *Phys. Rev. B*, **2012**, 85, 1123-1132.

125. Häkkinen, H., The gold–sulfur interface at the nanoscale. *Nature Chem*., **2012**, 4, 443–455.

126. Bain, C. D., Biebuyck, H. A. & Whitesides, G. M. Comparison of self-assembled monolayers on gold: Coadsorption of thiols and disulfides. *Langmuir,* **1989**, 5, 723–727.

127. Poirier, G. E. & Pylant, E. D. The Self-Assembly Mechanism of Alkanethiols on Au(111), *Science,* **1996**, 272, 1145–1148.

128. Inkpen, M. S., Liu, Z., Li, H., Campos, L., Neaton, J., Venkataraman, L., Non-chemisorbed gold–sulfur binding prevails in self-assembled monolayers. *Nature Chem.* **2019**, 11, 351–358.

129. Qian, X., Emory, S. R., Nie, S., Anchoring molecular chromophores to colloidal gold nanocrystals: surface-enhanced raman evidence for strong electronic coupling and irreversible structural locking. *J. Am. Chem. Soc.,* **2012**, 134(4), 2000-2003.

130. Fu, M. D., Chen, I. W. P., Lu, H. C., Kuo, C. T., Tseng, W. H., Chen, C. H., Conductance of alkanediisothiocyanates: effect of headgroupelectrode contacts. *J. Phys. Chem. C*, **2007**, 111(30), 11450-11455.

131. Luzhbin, D. A., Kaun, C. C., Origin of high- and low-conductance traces in alkanediisothiocyanate single-molecule contacts. *Phys. Rev. B*, **2010**, 81(3), 1718-1720.

132. Jang, S. Y., Reddy, P., Majumdar, A., Segalman, R. A., Interpretation of stochastic events in single molecule conductance measurements. *Nano Lett.,* **2006**, 6(10), 2362-2367.

133. Lemmer, M., Inkpen, M. S., Kornysheva, K., Unsupervised vector-based classification of single-molecule charge transport data, *Nature Commun.,* **2016**, 7, 12922.

134. Vladyka, A., Albrecht, T., Unsupervised classification of single-molecule data with autoencoders and transfer learning. *Machine Learning: Science and Technology*, **2020**, 1(3): 035013.

135. Zhang, Q., Liu, C., Tao, S. H., Yi, R. W., Su, W., Zhao, C., Zhao, C. Z., Dappe, Y. J., Nichols, R. J., Yang, L., Fast and straightforward analysis approach of charge transport data in single molecule junctions. *Nanotechnology*, **2018**, 29(32), 325701.

136. Xiang, D., Kim, D., Jeong, H., Lee, T., Mayer, D., Three-terminal single-molecule junctions formed by mechanically controllable break junctions with side gating. *Nano Lett*., **2013**, 13(6).

137. Kubatkin, S., Danilov, A., Hjort, M., Cornil, J., Bredas, J. L., Stuhr-Hansen, N., Single-electron transistor of a single organic molecule with access to several redox states. *Nature*, **2003**, 425(6959), 698-701.

138. Ghosh, A. W., Rakshit, T., Datta, S., Gating of a molecular transistor: electrostatic and conformational. *Nano Lett*., **2004**, 4(4), 565-568.

139. Song, H., Kim, Y., Jang, Y. H., Jeong, H., Reed, M. A., Lee, T., Observation of molecular orbital gating. *Nature*, **2009**, 462(7276), 1039-43.

140. Jia, C., Migliore, A., Xin, N., Huang, S., Wang, J., Yang, Q., Covalently bonded single-molecule junctions with stable and reversible photoswitched conductivity. *Science*, **2016**, 352(6292), 1443.

141. Brooke, R. J., Szumski, D. S., Vezzoli, A., Higgins, S. J., Nichols, R. J., Schwarzacher, W., Dual Control of Molecular Conductance through pH and Potential in Single-Molecule Devices. *Nano Lett*., **2018**, 18(2).

142. Lovat, G., Choi, B., Paley, D. W., Steigerwald, M. L., Venkataraman, L., Roy, X., Room-temperature current blockade in atomically defined single-cluster junctions, *Nature Nanotechnol.,* **2017**, 12(11).

143. Yin, X., Zang, Y., Zhu, L., Low, J. Z., Liu, Z. F., Cui, J., Neaton, J. B., Venkataraman, L., Campos, L. M., A reversible single-molecule switch based on activated antiaromaticity. *Sci Adv*., **2017**, 3(10), 2615.

144. Osorio, H. M., Catarelli, S., Cea, P., Gluyas, J. B. G., Hartl, F., Higgins, S. J., Nichols, R. J., Electrochemical single-molecule transistors with optimized gate coupling. Journal of the American Chemical Society, *J. Am. Chem. Soc.*, **2015**, 137(45), 14319.

145. Osorio, E. A., Bjornholm, T., Lehn, J. M., Ruben, M., van der Zant, H. S. J., Single-molecule transport in three-terminal devices. *J. Phys.: Condens. Matter*, **2008**, 20, 374121.

146. Osorio, E. A., O'Neill, K., Wegewijs, M., Stuhr-Hansen, N., Paaske, J., Bjornholm, T., van der Zant, H. S. Electronic excitations of a single molecule contacted in a three-terminal configuration. *Nano Lett.,* **2007**, 7.3336.

147. Nichols, R. J., Higgins, S. J., Single molecule nanoelectrochemistry in electrical junctions . *Acc Chem. Res.,* **2016**, 49 (11), 2640–2648.

148. Seo, K., Konchenko, A. V., Lee, J., Bang, G. S., Leeq, H., Molecular conductance switch-on of single ruthenium complex molecules. *J. Am. Chem. Soc.*, **2008**, 130(8), 2553-2259.

149. Brooke, R. J., Jin, C., Szumski, D. S., Nichols, R. J., Mao, B. W., Thygesen, K. S., Single-molecule electrochemical transistor utilizing a nickel-pyridyl spinterface. *Nano Lett*., **2014**, 15(1).

150. Ammar, F., Convolution potential sweep voltammetry ii. multistep nernstian waves. *Journal of Electroanalytical Chemistry*. **1973**, 47, 115.

151. Flanagan, J. B., Margel, S., Bard, A. J., Anson, F. C., Electron transfer to and from molecules containing multiple, noninteracting redox centers. electrochemical oxidation of poly(vinylferrocene). *J. Am. Chem. Soc.*, **1978**, 100(13), 2633-2639.

152. Pobelov, I. V., Li, Z., Wandlowski, T.,Electrolyte gating in redox-active tunneling junctions--an electrochemical STM approach. *J. Am. Chem. Soc.*, **2008**, 130(47), 16045.

153. Lee, N., Shin, H., Qian, D., Kwon, Y., Study on electrical conduction of viologen derivatives using scanning tunneling microscopy. *Thin Solid Films*, **2007**, 515(12), 5163-5166.

154. Li, Z., Han, B., Meszaros, G., Pobelov, I., Mayor, M., Two-dimensional assembly and local redox-activity of molecular hybrid structures in an electrochemical environment. *Faraday Discussions*, **2006**, 131.

155. Bodappa, N., 1, Fu, Y., Broekmann, P., Furrer, J., Zick, K., Vesztergom, S., Tahara, H., Sagara, T., Electron transfer controlled by solvent and counter anion dynamics in electrochemistry of viologen-type ionic liquid, *Electrochimica. Acta*., **2019**, 320, 134559.

156. Liao, J., Agustsson, J. S., Wu, S., SchonNenberger, C., Calame, M., Leroux, Y., Cyclic conductance switching in networks of redox-active molecular junctions. *Nano Lett.,* **2010**, 10(3), 759-764.

157. Liu, K. , Wang, X. , Wang, F., Probing charge transport of ruthenium-complex-based molecular wires at the single-molecule level. *Acs Nano*, **2008**, 2(11), 2315-2323.

158. Park, J., Pasupathy, A. N., Goldsmith, J. I., Chang, C., Yaish, Y., Petta, J. R., Coulomb blockade and the kondo effect in single-atom transistors. *Nature*, **2002**, 417(6890), 722-5.

159. Li, H., Garner, M. H., Shangguan, Z., Zheng, Q., Su, T. A., Neupane, M., Conformations of cyclopentasilane stereoisomers control molecular junction conductance. *Chem. Science*, **2006**, 7(9), 5657-5662.

160. Paul, N. D., Rana, U., Goswami, S., Mondal, T. K., Goswami, S., Azo anion radical complex of rhodium as a molecular memory switching device: isolation, characterization, and evaluation of current-voltage characteristics. *J. Am. Chem. Soc.*, **2012**, 134(15), 6520.

161. Armand, M., Endres, F., Macfarlane, D. R., Ohno, H., Scrosati, B., Ionic-liquid materials for the electrochemical challenges of the future. *Nature Materials*, **2009**, 8(8), 621.

162. Huddleston, J. G., Visser, A. E., Reichert, W. M., Willauer, H. D., Broker, G. A., Rogers, R. D. Characterization and comparison of hydrophilic and hydrophobic room temperature ionic liquids incorporating the imidazolium cation. *Green Chemistry*, **2001**, 3, 156-164.

163. Rogers, E. I., Šljukić, B., Hardacre, C., Compton, R. G. Electrochemistry in Room-Temperature Ionic Liquids: Potential Windows at Mercury Electrodes. *Journal of Chemical & Engineering Data,* **2009**, 54, 2049-2053.

164. Abbott, A. P., McKenzie, K. J., Application of ionic liquids to the electrodeposition of metals. *Phys. Chem. Chem. Phys*., **2006**, 8, 4265–4279.

165. Crowhurst, L., Mawdsley, P. R., Perez-Arlandis, J. M., Salter, P. A., Welton, T., Solvent–solute interactions in ionic liquids. *Phys. Chem. Chem. Phys*., **2003**, 5(13), 2790-2794.

166. Naushad, M., Alothman, Z. A., Khan, A. B., Ali, M., Effect of ionic liquid on activity, stability, and structure of enzymes: a review. *International Journal of Biological Macromolecules*, **2012**, 51(4), 555-560.

167. Wasserscheid, P., Welton, T., Ionic Liquids in Synthesis (Wiley-VCH, 2007).

168. Endres, F., Abbott, A., MacFarlane, D. R., Electrodeposition from Ionic Liquids (Wiley-VCH, 2008).

169. Albrecht, T., Moth-Poulsen, K., Christensen, J. B., Hjelm, J., Bjørnholm, T., Ulstrup, J. Scanning Tunneling Spectroscopy in an Ionic Liquid. *J. Am. Chem. Soc.*, **2006**, 128(20), 6574-6575.

170. Buzzeo, M. C. Evans, R. G.; Compton, R. G., Non-haloaluminate room‐temperature ionic liquids in electrochemistry-A review. *Chem. Phys. Chem*., **2004**, 5 (8), 1106-1120.

171. Leary, E., Higgins, S.J., van Zalinge, H., Haiss, W., Nichols, R. J., Nygaard, S., Jeppesen, J. O., Ulstrup, J., Structure-property relationships in redox-gated single molecule junctions - A comparison of pyrrolo-tetrathiafulvalene and viologen redox groups. *J. Am. Chem. Soc*., **2008**, 130 (37):12204–12205.

172. Kay, N.J., Higgins, S.J., J Jeppesen, J. O., Leary, E., Lycoops, J., Ulstrup, J., Nichols, R. J., Single-Molecule Electrochemical Gating in Ionic Liquids. *J. Am. Chem. Soc.* **2012**, 134 (40), 16817–16826.

173. Atkins, P. W., Physical chemistry. OXFORD UNIVERSITY PRESS, **1986**.

174. Zhang, J., Chi, Q., Kuznetsov, A. M., Hansen, A. G., Wackerbarth, H., Christensen, H. E. M., Andersen, J. E. T., Ulstrup, J., Electronic properties of functional biomolecules at metal/aqueous solution interfaces. *J. Phys. Chem. B*, 2002, 106(6), 1131-1152.

175. Di Felice, D., Dappe, Y. J., 2D vertical field effect transistor. *Nanotechnology*, **2018**, 29, 505708.